Isolation and Use of the *Aeromonas hydrophila* Secretin ExeD for Nanopore Analysis

A Thesis Submitted to the College of Graduate Studies and Research

In Partial Fulfillment of the Requirements for the

Degree of Masters of Science

In the Department of Biochemistry

University of Saskatchewan

Saskatoon

By

Christopher A. Christensen

PERMISSION TO USE

This thesis has been written as a requirement for a Master's of Science in Biochemistry. In submitting this work I acknowledge that the libraries of the University of Saskatchewan may make it freely available for use.

I also acknowledge that this work may be used in whole or in part by faculty in the Department of Biochemistry or the Dean of the College of my discipline. It is understood that no financial gain should be made off of this work without my express written permission, and that recognition should be given for any use of this work.

Requests for permission to use this work should be addressed to:

Head of the Department of Biochemistry

University of Saskatchewan

Saskatoon, SK

S7N 0W0

Abstract

Nanopore analysis is a technique for measuring single molecule interactions with an open pore in solution. Current progress in the field is hindered by the size of the most commonly used nanopore, α-hemolysin. The narrow vestibule of the pore doesn't allow proteins or peptide aggregates to pass through its channel. A larger pore, using the type II secretin of *Aeromonas hydrophila*, may be able to circumvent the size constraint of α-hemolysin and could allow research into larger molecules to be made. The goal of this project was to isolate and use the type II secretin ExeD in nanopore analysis. After this was accomplished, the ExeD pore would be inserted into a lipid bilayer in a patch clamp setup where observations could be made about the ability of ExeD to translocate small molecules and peptides. If ExeD could translocate larger peptides than α-hemolysin, nanopore analysis could be expanded to include these larger molecules. Nanopore research has previously been done using the ExeD homologues PulD and XpcQ, but results were unclear due to contaminant proteins and problems with measuring the molecular interactions. In the case of PulD, the tightly-bound lipoprotein PulS co-purified with PulD and could not be separated prior to the experiments. To avoid the presence of a similar lipoprotein co-purifying with ExeD, the gene was cloned from the bacteria *Aeromonas hydrophila* (which does not have a PulS homologue) and expressed in *E. coli*. The protein was then purified using a combination of detergents and chromatography. The resultant extract was shown to be free from contaminant proteins and capable of inserting into a planar lipid bilayer. Previous research using XpcQ were inconclusive due to both an ion-leak across the membrane and from having uncertain pore insertions. Our experiments showed that under specific conditions, pore insertions could be consistently repeated and easily identified, and that ion-leak would not occur. We further identified a new method in inserting ExeD into lipid bilayers.

Currently, membrane proteins often require proteoliposomes for inserting the pore into the lipid bilayer. Our research found that using an acetone precipitate of ExeD was preferable to forming liposomes due to both the ease of the protocol and the pore's ability to insert from a precipitate. During the course of the study it was found that when the *exeD* gene was highly expressed using elevated temperatures and high amounts of the transcriptional inducer IPTG, the self-assembling protein would produce unusual results in patch clamp. The gating and conductance of these pores were highly variable and difficult to reproduce across experiments. We concluded that these pores were non-native conformations of the multimer and had been incorrectly assembled. It was found that at low temperatures and low levels of IPTG, protein expression not only increased but the pores which were produced were uniform and had identical activity to one another. The conformation of the protein that most likely represents the native form was identified from both its prevalence across a range of expression conditions, from its behavioural similarity to PulD, and from its channel characteristics. We compared gating events and pore conductance at three different pH levels and several voltages. At pHs of 5 and 7.4 gating is rapid and the events fall into a characteristic pattern depending on the applied voltage. At a pH of 9.5 gating is far less frequent and the events produce a smaller blockade current with a unique distribution from those of pH 7.4 and 5. It was found that using a pH of 9.5 and a low applied voltage lowered the natural gating levels considerably, making DNA interactions distinguishable from naturally occurring gating events and producing a peak which we believe corresponds to translocation. A small α-helical peptide was also examined under similar conditions, but produced only bumping interactions, showing that peptides are unable to translocate. These results demonstrate that ExeD is likely capable of passing strands of DNA through its channel, but molecules the size of peptides or larger may require channel activation from additional proteins. In conclusion, we

have extensively studied the secretin ExeD and have found it is not suitable for studying peptides or proteins as it currently exists.

ACKNOWLEDGEMENTS

It’s been a long journey.

Thanks to everyone who has helped and aided me along the way.

LIST OF FIGURES

LIST OF ABBREVIATIONS

A10: Fmoc-$D_2A_{10}K_2$
CD: Circular Dichroism
DGCP: 1,2-diphytanoyl-sn-glycero-3-phosphocholine
ETEC: Enterotoxigenic *Escherichia coli*
Exe: Nomenclature denoting *Aeromonas hydrophila*
Gsp: General secretion pathway
HELP: HpaII Tiny Fragment Enrichment Ligation-mediated PCR
HR: Homology Region
IPTG: Isopropyl β-D-1-thiogalactopyranoside
MeDIP: Methylated DNA Immunoprecipitation
MspA: *Mycobacterium smegmatis* porin A
NMR: Nuclear magnetic resonance
PCR: Polymerase Chain Reaction
PMF: Proton Motive Force
pRNA: Bacteriophage RNA
qPCR: quantitative real-time PCR
SDS: Sodium Dodecyl Sulfate
Sec: General secretion route
SNP: Single Nucleotide Polymorphism
T2SS: Type II Secretion System
Tat: Twin-arginine translocation pathway
Zw 3-14: n-Tetradecyl-N,N-dimethyl-3-ammonio-1-propanesulfonate
α-HL: α-Hemolysin

Introduction

1.1 Nanopore Detection and Analysis

1.1.1 Principles and Methodology of Nanopore Detection

Nanopore analysis is an investigative method for single molecule detection. It requires two electrodes (commonly Ag/AgCl) to drive molecules electrophoretically through a nanometer scale opening (Jetha et al., 2009; Kasianowicz et al., 1996). Conventionally, a micron-sized pore is embedded within an otherwise impermeable Teflon wall. This opening is the only channel linking the two chambers housing the electrodes. In most forms of nanopore analysis, a lipid coating is applied across the micron-sized hole which can then be thinned to remove the excess lipids, leaving only single bilayer separating the chambers. A bacterial pore is added to the setup, wherein it spontaneously inserts into the bilayer. This creates a nanopore-sized channel through which molecules can flow into the adjacent compartment (Kasianowicz et al., 1996). The chambers containing both electrodes are filled with a salt buffer (typically KCl) and provide a source of ions for the apparatus (Smeets et al., 2006). When a potential difference is introduced at one electrode, the voltage causes ions to flow through the bacterial pore and creates a small but measurable current. This small current is amplified and eventually visualized as an electronic output. The entire setup is a derivation of a previously developed method called voltage clamp, which was used to measure membrane potential across excitable cells (Vandenberg and Waxman, 2012). This derivation, termed patch clamp, is used to measure ion flow through only one or a few membrane channels. The patch clamp setup is shown in Figure 1. By convention the compartment housing the AgCl electrode is termed the *cis* chamber. The opposite compartment, housing the grounding Ag electrode, is termed the *trans* chamber.

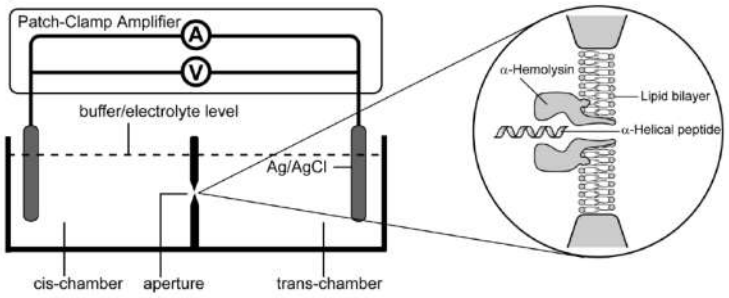

Figure 1: Patch Clamp Setup. Ag/AgCl electrodes measure conductivity of ions through an opening in an otherwise impermeable membrane. Ions are driven by an applied voltage which induces a current through the nanometer sized pore. The most common pore used is α-hemolysin.

Nanopore analysis is primarily used to study single molecule interactions with the pore, and conveys information about molecular size, shape, structure, and binding. When the patch clamp setup is assembled and a pore is inserted in the lipid bilayer, a molecule of interest can be added to the *cis* side of the chamber. It is then driven down its electrophoretic gradient towards the opening in the bilayer (Christensen et al., 2011). Upon interaction of the protein or peptide with the membranous pore, the molecule acts as a barrier and hinders the flow of Cl- ions. For a brief moment the current is interrupted. This alteration of current is then measured, recorded, and compiled using patch clamp software (Hamill et al., 1981). When several thousand of such events are compiled and graphed, the resulting plot of the current interruptions produces a representative distribution of all the forms of interactions that a molecule can have with the membrane opening. Each type of molecule produces a characteristic distribution that is unique to its size, charge, and structure (Almers et al., 1981) making nanopore analysis useful for distinguishing different proteins and peptides and their relative conformations.

1.1.2 Event Profiles for Pore-Molecule Interactions

Three types of events are possible in this system, with each type of event being distinguished based on both the average current blockade and the duration of interaction (Meng et al., 2010). The three event types are: 1) bumping events where the molecule approaches the pore but diffuses away before entering, 2) intercalation events where the molecule becomes

temporarily trapped in the vestibule of the pore but is ejected, and 3) translocation events where the molecule passes completely through the channel (Meng et al., 2010). These events are shown respectively in Figure 2, A-C. Bumping events are evident when the blockade current is small (typically less than 50 pA) and brief as the molecule spends little time near the membrane opening. Translocation events have a large amperage (often above 50 pA) and have a longer duration. In translocation events the peptide/protein passes through the opening of the pore and occupies the internal cavity. When the peptide blocks the internal cavity in these events, there is less ion flow across the membrane than when the peptide merely interferes with the outside of the pore as in bumping events. This principle reflects why translocation events produce larger changes in current than bumping events.

Intercalation events are more difficult to distinguish. In these types of interactions, molecules approach the pore but are unable to translocate due to either their size, conformation, or charge. Unlike bumping events however, the molecules do not immediately diffuse away. They are instead trapped in the opening by the applied voltage. They produce blockade currents which are larger than typical bumping events, but they are of a shorter duration than standard translocation interactions (Meng et al., 2010). In order to separate these from other event types, experiments are usually done at varying voltages. By changing the voltage it is possible to change the electrophoretic driving force of the peptide, resulting in differences between the time of interaction of the peptide/protein and the pore. What is normally seen in such experiments is that as the potential difference across the perfusion cup increases, the electrophoretic force also increases, which results in translocation and bumping times decreasing. This occurs because the molecule can pass through the pore quicker, but also forces faster diffusion away if the molecule cannot translocate (Christensen et al., 2011). Intercalation events however experience the opposite effect: instead of the potential difference moving the molecule more quickly through the

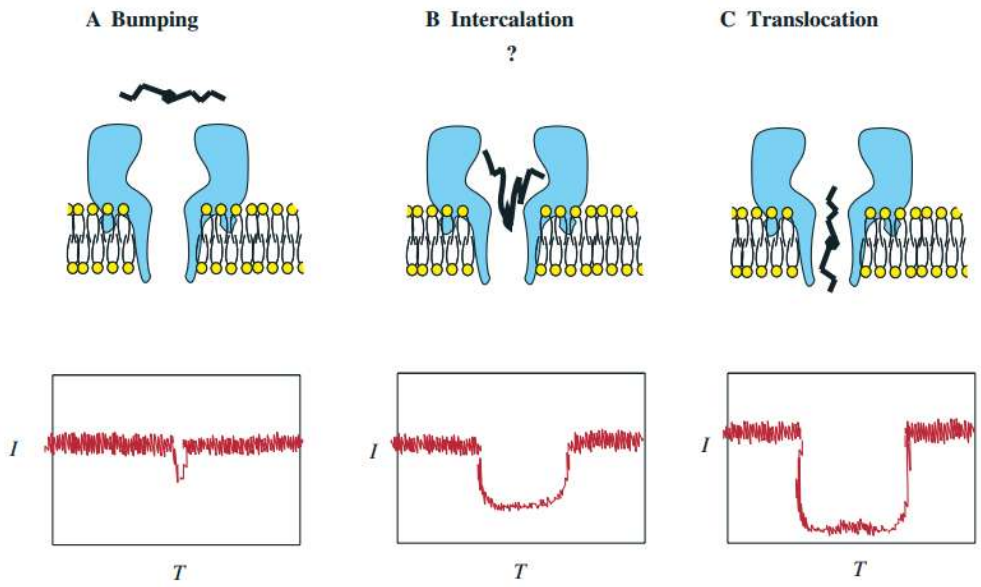

Figure 2: Types of Nanopore Events. A) In bumping interactions the molecule approaches the pore but does not pass through. The interruption in current is brief and small. B) Intercalation events occur when the molecule becomes briefly trapped in the cavity but diffuses away. Often this produces a larger amount of current which is impeded for a longer period of time. C) Translocation events happen when the molecule passes through the pore. This interaction produces the longest and highest current interruptions (from Meng et al., 2010; with permission).

pore, the molecules are forced into the vestibule and are unable to translocate. Instead they must diffuse away at a much slower rate than normal bumping events. Consequently, as voltage increases intercalation times also increase because the driving force becomes a hindrance.

1.1.3 α-Hemolysin: The Most Commonly Used Pore in Nanopore Analysis

The conventional pore used for nanopore experiments is α-hemolysin (Ashkenasy et al., 2005; Jetha et al., 2009), seen in Figure 3. This protein is produced by the bacterium *Staphylococcus aureus* and causes the lysis of red blood cells *in vivo* by forming openings in the erythrocyte's phospholipid bilayer (Song et al., 1996). Monomers of α-hemolysin migrate

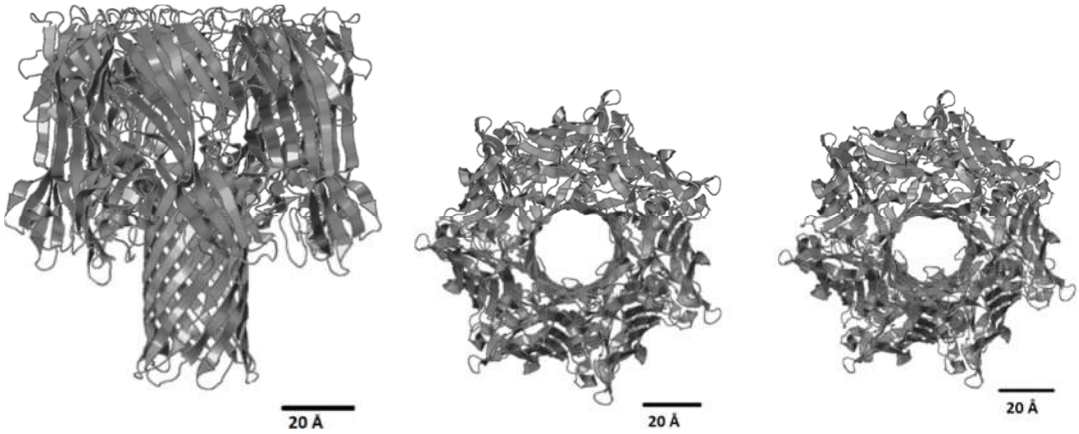

Figure 3: Shape and Structure α-Hemolysin. The structure of heptameric α-HL as seen from the side, bottom, and top (pictured left, middle, and right respectively). Note that the scale is set at 20 Å (from Song et al., 1996; with permission).

towards susceptible cells until they make contact with the lipid bilayer. Upon making contact, the monomers spontaneously oligomerize to produce a transmembrane heptameric pore with a hydrophilic interior cavity (Song et al., 1996). The hydrophilic interior allows ions to freely diffuse out of the erythrocyte. Consequently, upon infection with hemolysin, cells lose both their electrochemical potential and their osmotic balance, causing ATP production to cease and the cells to swell with an influx of water.

Upon assembly, the hemolysin structure adopts a mushroom-like shape with a total length of 100 Å as measured from the stem to the cap. The cap resides in the extramembrane space and spans 100 Å across its width. The pore has constricting dimensions of 26 Å at its entrance and a diameter of 14 Å at its narrowest internal point. The 14 Å channel is large enough to allow ions and small organic molecules to diffuse across the barrier of the cell, but any peptides or molecules larger than this are unable to pass through. When α-hemolysin is inserted into a planar lipid bilayer, channel formation can be detected based on discrete increases in conductivity as measured by a patch clamp apparatus. At 100 mV, each pore produces 100 pA of conductivity under normal experimental conditions (i.e. 1 M KCL, 22 ˚C, pH 7.4; Menestrina et al., 1996). High salt concentrations and neutral pH levels produce minimal background noise in the setup device and have become the standard for nanopore experiments (Smeets et al., 2006).

There are many properties of biological pores that make them useful for molecular analysis. One of the most beneficial aspects of α-hemolysin is that the channel opening is independent of voltage or ligand gating at a neutral pH (Kasianowicz et al., 1996). Consequently, when the pore is used to study polynucleotides or peptides, all observed current blockades can be only attributed to the molecule under investigation. A second useful property is that the transmembrane cavity formed by hemolysin is highly reproducible (Menestrina et al., 1996). Pores formed under the same conditions will almost always demonstrate the same electrical conductivity. Lastly, α-hemolysin is readily acquired commercially and is relatively simple to work with.

Biological pores have been used consistently for over two decades to study low concentrations of biochemicals. To date, α-HL has been used for both peptide discrimination and nucleic acid sequencing (Madampage et al., 2012; Feng et al., 2015). The reason α-HL works well for DNA sequencing is that the narrow channel is only slightly larger than single-stranded DNA, so when an ssDNA molecule passes through the channel, the small differences between base pairs are more easily read and can be used to determine the base pair order of the strand. α-HL can be further coupled to an exonuclease to cleave nucleotides from long chains of DNA, improving detection of single molecular components (specificity) and allowing longer sequences to be read (Manara et al., 2015). Although the small interior cavity of the pore is primarily suited for studying single-stranded DNA molecules (Kasianowicz et al., 1996), other groups have been able to study conformational changes in peptides using hemolysin (Tavassoly and Lee, 2012). In such experiments, event graphs of the peptide are generated before and after conformational changes and the results are compared.

Despite the benefits of using α-HL in these experiments, there are also drawbacks with the pore. Due to the relatively small channel, research into molecules larger than peptides becomes difficult. Double-stranded DNA and most proteins are too large to pass through the 14 Å channel (Meng et al., 2010). In these cases, the altered current will produce only bumping or intercalation events as the molecules can approach the pore but will not pass through. Consequently, the primary indicator of a molecule's size and structure - translocation events - cannot be observed (Meng et al., 2010). The heptameric structure of α-HL is also relatively

unstable. Although the pore is able to insert and remain open from pH 3 to pH 12 (Maglia et al., 2010), experiments lasting longer than a few hours are rarely able to be performed. After a few hours of exposure to the 100-150mV of applied voltage used in experiments, the transmembrane channel will often spontaneously eject. The cause of these ejections is still not entirely understood.

1.1.4 Other Biological Pores

A few other channel-forming proteins have been investigated for their use in single lipid-bilayer experiments. *Mycobacterium smegmatis* porin A (MspA) is the largest and most important porin in the bacterium *M. smegmatis* and regulates the exchange of hydrophilic solutes between the intermembrane space and the extracellular milieu. The shape and structure of the pore is shown in Figure 4.

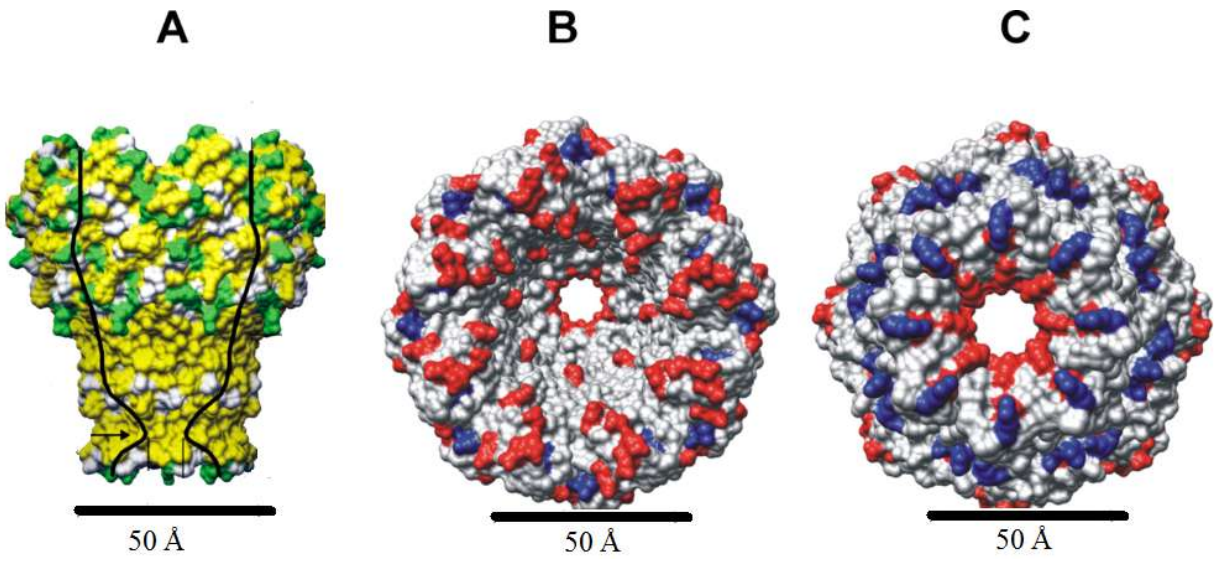

Figure 4: Shape and Structure MspA. The structure of homooctamer MspA as seen from the side, bottom, and top (pictured as A, B, and C respectively). Note that the scale is set at 50 *Angstroms* (from Butler et al., 2008; with permission).

MspA is an octameric porin extending 96 Å lengthwise, with only a 37 Å area composing the transmembrane domain. A globular rim approximately 65 Å in width surrounds the hydrophilic cap and extends into the extracellular region. The overall structure is conical with the narrowest point facing the interior of the cell (Butler et al., 2008).

MspA is not only large, it is also highly resilient. It retains its ability to form a channel between pH 0-14, or after being boiled for 30 minutes (Heinz et al., 2003). One of the major problems with the pore is its inner cavity. The wild-type octamer has a negative interior that prevents DNA or other negatively charged molecules from translocating, but in 2008 researchers produced a modified pore using site-directed mutagenesis (Butler et al., 2008). They changed three aspartic acid residues to asparagines, which conferred upon the channel the ability to translocate ssDNA.

MspA is narrower than α-HL, having a constriction point of less than 10 Å. However, this small constriction point has been shown to improve specificity for single nucleotides as there is much less room for strands to shift laterally while translocating. Results suggest that this narrow channel may make it ideal for ssDNA analysis. Yet the same feature that makes MspA useful for studying DNA would prevent the pore from giving meaningful information for peptides or proteins: the narrow opening prevents such molecules from passing through the channel and would likely yield only bumping events (Butler et al., 2008). Hence MspA's usefulness is primarily limited to studying single-stranded DNA.

Another biological pore with analytical potential is the phi29 DNA packaging-motor. Phi29 is different from the other biological pores previously discussed because unlike α-HL or MspA, phi29 is neither a membrane protein nor an ion-conducting channel. Instead it is a pore-forming polymerase used to translocate double-stranded DNA. The channel is driven by an ATP motor and allows between 2 and 2.5 base pairs of dsDNA to be packaged per ATP (Xiao et al., 2005). During viral maturation, DNA moves through phi29's small connector region into an adjacent procapsid where it awaits cell lysis (Figure 5). Phi29's ability to move dsDNA at a high rate through its channel makes the pore useful for nanopore research as it allows dsDNA analysis and reduces the amount of time necessary to run experiments.

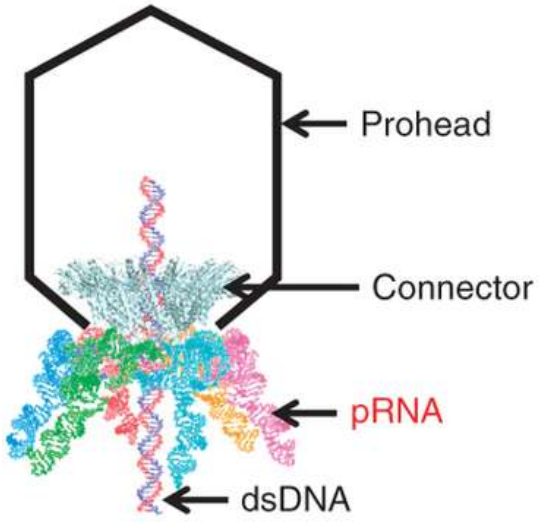

Figure 5: Phi29's Role in the Procapsid. Phi29 connects to an adjacent procapsid to facilitate dsDNA translocation through its channel. A connector protein facilitates linkage of the prohead and phi29 (from Shu et al., 2013; with permission).

The polymerase is shaped like a simple funnel with a width ranging from 36 Å to 60 Å (Berman et al., 2007). The pore is made up of 12 α-helical protein subunits powered by an adjacent ATP-driven hexameric ring. The hexameric ring is formed from a series of non-coding RNA elements used in regulating ribosomal RNA transcription (pRNA). The ring of pRNA attaches to the N-terminal of the proteins and extends to the outside of the procapsid. A central ring of the polymerase is extremely hydrophobic on its outer surface, and allows phi29 to insert into a lipid membrane. Flanking the hydrophobic ring on the N and C terminals are hydrophilic rings which allow the protein to function in a water-soluble environment.

Experiments using short lengths of DNA (131-bp and 35-bp) and long strands of linear plasmid DNA (5.5 kb) were previously performed by passing each strand through the opening of phi29 (Wendell et al., 2009). In all three cases the readings produced large blockade currents indicative of dsDNA translocating through the phi29 channel. Researchers confirmed passage of DNA through the channel by qPCR analysis of the *trans* compartment, and the results definitively proved that phi29 could be used in DNA analysis.

One of the major difficulties in working with phi29 is how quickly DNA moves through the channel. Some degree of speed is desired, but the rate at which phi29 can translocate DNA is rapid enough that it lowers the accuracy of base-pair readings. In its native form phi29 has such a low sensitivity of detection that the pore is unusable in nucleotide readings (Wendell et al., 2009).

In 2012, researchers fused phi29 to MspA and used the product to measure DNA readings in patch clamp (Manrao et al., 2012). They found that the phi29-MspA protein not only translocated dsDNA, but also had a specificity that exceeded either pore on its own. The phi29 motor was used to slow down DNA movement, and MspA read the DNA at the decreased speed. The result was a longer translocation time for individual base-pairs, which enhanced the distinction between each T A C or G.

1.1.5 Solid-State Pores

There are alternatives to having to use biological pores in the patch clamp setup. Solid-state pores are an attractive option for experiments needing to measure proteins larger than double-stranded DNA. As opposed to the Teflon setup used in biological pores wherein a lipid bilayer is painted over a micron-sized hole, solid-state pores create a nanoscale opening directly within the material. Lipids and biological pores are therefore not needed for the experimental setup. Solid-state pores can be made in a range of dimensions, using multiple materials, and the pores themselves can be used for longer periods of time in a single experiment (Dekker, 2007). Typically, the solid matrix material is silicon nitride, which is far more stable than the lipid matrix used in biological alternatives (Li et al., 2001).

Making an opening in the matrix with nanoscale precision and high reproducibility has been difficult. There are currently several ways researchers use to generate the opening. Most commonly, ion-beam drilling is performed. This method uses a focused Ar^{+} stream directed at a silicon nitride background to excavate an opening in the material. The focus of the beam is gradually diminished to create a precisely-sized opening, accurate to as low as 1 nm (Li et al., 2001). The resulting pore is narrowed to the correct size, but it is preferentially selective for

cations. An Al_2O_3 film can be deposited over the material to correct for cation bias, making the pore symmetrical in terms of its conductive characteristics (Venkatesan et al., 2010). At this point the pore is suitable for nanopore analysis.

A related method utilizes a transmission electron microscope and potassium hydroxide to etch a large (20 nm) hole into the SiO_2 matrix (Storm et al., 2003). The opening is slowly closed by thermal oxidation and a diffuse electron beam. The SiO_2 membrane melts during this process and creates an opening which is both symmetrical and without cation selectivity. Eventually the pore is scaled down to the desired size (to a minimum of 3 nm) within a 0.5 nm range of error. The major drawback to this method is that it is slow, laborious, and technically challenging.

Producing nanoscale openings such as these within the silicon material is possible but difficult, and subject to a great deal of mechanical error and operator failure (Dekker, 2007). Both ion-beam drilling and peroxide etching methods are expensive due to materials and equipment, have low success rates, and cannot be mass-produced through automation. It takes up to two days to test an individual pore, and the procedure for setting up the experiment is difficult to follow and reproduce (Venkatesan et al., 2010). A great deal of time and money can be lost attempting to perform a solid-state experiment, and there is no guarantee that any of the pores used will work.

Given the challenges faced by producing solid-state pores, recent research has focused on improving the way the openings are excavated. One of the most promising methods for creating solid-state nanopores involves “dielectric breakdown” wherein a high voltage is pulsed across a thin silicon nitride membrane (Briggs et al., 2014). At a determined threshold point, the material ruptures and produces a small (sub-nm) opening. The opening can be enlarged by increasing the applied voltage until the desired channel size is achieved. This setup is ideal because it requires most of the standard equipment already used in nanopore analysis: Ag/AgCl electrodes, a salt solution, and a voltage generator. This method has only started to be explored within the last year, though it appears to be considerably cheaper than conventional methods of creating a solid-state pore, has a higher likelihood of success, and is far less labour-intensive.

Other non-biological pores include graphene (Nam et al., 2014), gold-plated materials (Takale et al., 2014), organosilanes (Wanunu and Meller, 2007), and silica material covered with a thin lipid layer (Korman et al., 2013). Graphene has already been used to measure DNA translocation and can be coupled to a reader to allow high-speed discrimination (Nam et al., 2014). However, none of these materials have been tested extensively enough to replace the conventional solid-state channel, though progress is being made towards a generalized protocol.

1.1.6 Current Applications and Future Potential of Nanopore Technology

Nanopore sensing was initially conceived as a method for analyzing individual nucleotides in DNA and RNA strands, with the eventual goal of being able to sequence entire genomes using the technique (Kasianowicz et al., 1996). The scope of its ability has expanded to include looking at structures of peptides and proteins (Madampage et al., 2012), determining binding interactions with drugs and inorganic compounds (Tavassoly and Lee, 2012), and establishing the foundations of prion detectors (Madampage et al., 2010).

In 1996 Kasianowicz et al. laid the foundation for DNA sequencing with biological nanopores. They showed that α-HL is capable of not only detecting RNA, but it can be used to distinguish between the possible interactions of RNA with the biological pore. Kasianowicz found both translocation and bumping events for RNA in their experiments. Accordingly, the event histograms for RNA done by the researchers found separate peaks that could be assigned to both of the aforementioned types of interaction. The duration of these interactions was seen to range from 0.095 ms to 1.288 ms, and the interior cavity of α-HL had current blockades proportional to the size of the RNA. The peak with a longer duration of interaction (around 1.2-1.3 ms) was found to vary inversely with the applied voltage (expected with translocation events as opposed to intercalation). When the voltage was increased, the time-of-interaction for this peak decreased. The researchers attributed these events to be characteristic of RNA translocation through the biological pore. The other events were faster (typically less than 0.1 ms) and their rate of interaction was independent of the external voltage. This peak also blocked a smaller proportion of ionic movement through the interior cavity of α-HL. The researchers believed this event to be RNA colliding with the exterior of the opening and not going through – hence,

blocking events. In a similar experiment using DNA instead of RNA, Kasianowicz et al. (1996) confirmed the translocation of DNA through the pore by performing polymerase chain reactions (PCR) on samples taken from the *trans* side of the perfusion cup. PCR replication of translocated DNA proved that α-HL had passed the nucleic acids through its channel and into the *trans* compartment.

Almost 20 years from that initial experiment, nanopore analysis has developed to the point of near-commercial use in DNA sequencing. Startup companies such as Oxford Nanopore are currently fine-tuning the ability of α-HL to reliably sequence thousands of base-pairs at a time. A major problem in the fine-tuning process which remains to be solved is the low resolution of nucleotide sequencing (Benowitz, 2014). The fast rate of translocation prevents a perfect reading of the DNA in a single pass, so steps are taken to slow the rate of DNA movement and to improve nucleotide readings. Improved resolution has been accomplished by lowering the environmental temperatures to 4 °C, which causes translocation times to increase (Meller et al., 2000). Another approach incorporates hairpin structures into the ssDNA being read. These secondary structures are forced to unzip prior to translocating, which provides additional time for the molecule to interact with the pore (Vercoutere et al., 2003). However, these methods by themselves are not enough to alleviate the problem of rapid DNA movement through the membrane channels.

One alternative, shown in Figure 6, is to attach an exonuclease to α-HL so that nucleotides are cleaved prior to detection, greatly slowing the rate at which molecules enter the vestibule. The idea was first proposed in 2006 (Astier et al., 2006) and a working model has been developed and used by both Manara et al. (2015) and Oxford Nanopore Technologies (Benowitz, 2014). In this system, the exonuclease sits at the vestibule of the pore and binds to approaching ssDNA. Nucleotides are removed individually and are pushed towards the vestibule via the applied potential. This technique allows for α-HL to read each base separately as only one base resides in the pore at a time. A secondary method shown in Figure 7 uses a "ratcheting" system (Cherf et al., 2012). In this technique, the phi29 polymerase is used in conjunction with α-HL, essentially moving the DNA through two constriction points. The DNA to be sequenced is incubated alongside phi29 in the *cis* chamber. Blocking oligomers are used to ensure that the

DNA is not subject to uncontrolled extension in the presence of the polymerase. Phi29 binds to the DNA-oligomer complex, forming an inactive trimer. The trimer remains inactive until it reaches the α-HL pore. Upon reaching the pore, the blocked DNA strands are forced through α-HL via the applied negative voltage, causing the blocking oligomers to become unzipped. The motor function of phi29 continues to push the ssDNA through the pore, and the mechanical unzipping of the oligomer slows the rate of DNA translocation. If the ssDNA template "slips" backwards against the applied voltage, unbound nucleotides spontaneously reform the template into duplex DNA.

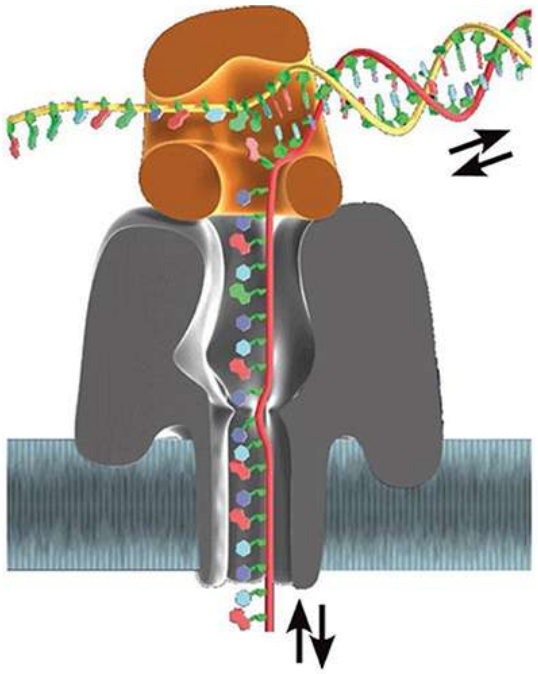

Figure 6: Exonuclease Bound to α-HL at the Vestibule. DNA is electrophoretically driven towards the vestibule of α-HL where it interacts with a covalently bound exonuclease. The enzyme cleaves individual nucleotides off the approaching strand and the nearby pore captures the mononucleotides before they diffuse away (from Schneider and Dekker, 2015; with permission).

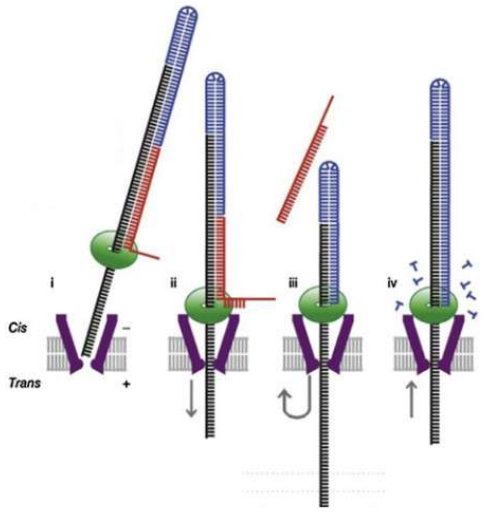

Figure 7: Ratcheting Method of DNA Analysis. i. A blocking oligomer (red and blue) binds to the ssDNA template to be read (black). ii. Upon reaching phi29, part of the oligomer is unwound to allow passage through the pore. iii. The DNA template continues to move through phi29. iv. Slippage of the DNA against the electrophoretic potential is compensated for by allowing nucleotides to rebind the DNA template, and the complex can again ratchet through phi29 (modified from Manrao et al., 2012; with permission).

Both the exonuclease method and the ratcheting method have been shown to miss a base anywhere from 10-25% of the time (Sampath, 2014). In order to circumvent this limitation, both systems can use several nanopores situated in tandem for redundant rechecking. If each nucleotide passes through 2-3 α-HL pores, the rate of loss can become as low as 0% (Sampath, 2014). If nanopores in tandem are used in conjunction with either the exonuclease or ratcheting methods, the only limit to DNA sequencing is the ability of the pore to distinguish among nucleotides. The specificity of the pore is currently therefore the most important part of a DNA-sequencing system.

The rate at which molecules interact with channel-forming proteins is normally controlled by the applied voltage and the concentration gradient of the molecule. To increase the rate of interaction, another method using the binding properties of DNA overhangs has been used (Rotem et al., 2012). In their study, Rotem et al. (2012) attached a DNA oligonucleotide to the opening of α-HL through a disulfide bond. Single stranded nucleic acid aptamers are created to be complementary to the α-HL-bound sequence, and through adoption of a three-dimensional

structure the aptamer is able to reversibly complex with an analyte (such as thrombin). This setup brings thrombin near to the opening of α-HL where it can disassociate from the aptamer and readily approach the vestibule. This method is both highly sensitive and specific to a single interaction, and can detect target substrates at very low concentrations or within large amounts of contaminant molecules.

Although modifying the substrate is one method to improve specificity, there are other means to improve peptide or DNA readings using α-HL. Modifying the pore-forming proteins directly can create low-affinity binding regions in the vestibule region, allowing for specific molecules to be read (Cheley et al., 2002). α-HL for example has been altered to preferentially bind both ATP and divalent metal cations. In 2002 researchers created a ring of 14 positively charged arginines which could specifically recognize inositol 1, 4, 5-triphosphate over the closely related analogs cAMP and ATP. They were able to detect inositol to concentrations as low as 10^{-9} M consistently across experiments.

DNA reading and substrate binding are not the only potential fields of nanopore analysis. The techniques have been used increasingly in the medical field for diagnostic purposes. Malignant tumours, for example, can be caused by methylation of the gene MS3 which results in disordered expression of MS3 and uncontrolled cell growth. Using a silicon-based solid-state nanopore, Mirsaidov et al. (2009) were able to detect translocation differences between the unmethylated, hemimethylated, and fully methylated states. Each DNA strand had different protein-pore interactions and the fragments could be distinguished from each other at low concentrations (10^{-6} M). Current methods of epigenetic testing couple methylated DNA immunoprecipitation (MeDIP) to either quantitative real-time PCR (qPCR) or HpaII tiny fragment enrichment ligation-mediated PCR (HELP). Both of these techniques are more complicated and difficult than solid-state analysis, assuming the solid-state pore is ready for use (Patsalis, 2012).

With recent advancements in creating solid-state pores via dielectric breakdown, the cost for determining DNA methylation using silicon oxide materials could also be considerably cheaper than materials required for MeDIP and HELP. The aforementioned diagnostic technique

is not limited to only epigenetic discrimination; it has been extended to single nucleotide polymorphisms (SNPs) and haplotype differentiation as well. Venkatesan and Bashir (2011) showed how nanopore sensors have been used in distinguishing between single-nucleotide mutations, and other groups have been able to distinguish pathogenic HIV-1/B and HIV-1/C on the basis of their genetic code (Singer et al., 2010).

Most of the 20 years of nanopore analysis has been focused on DNA. More and more, investigators are finding that α-HL also has uses in the field of protein and peptide research. In 2012, three peptide derivations of the amyloid-β peptide, two of which are implicated in the progression of Alzheimer's disease, were shown to have distinct event profiles and pore-molecule interaction times (Madampage et al., 2012). Given as little as 1 μg of material, researchers were able to distinguish each strain of amyloid-β from the others. The hope is that techniques using patch clamp can one day be used diagnostically to detect Alzheimer's disease in its early stages before symptoms manifest, which is currently not possible.

Nanopores can not only distinguish between different peptides, they can distinguish between different conformations of the same peptide. There are many methods to determine the conformational changes that drugs can have on their target effectors. Isothermal titration calorimetry, circular dichroism (CD), and nuclear magnetic resonance (NMR) are among such methods used to visualize these changes. It has recently been shown (Tavassoly et al., 2014) that biological pores such as α-HL are able to perform the same function. Although the level of detail is not as high as is possible with NMR, or as precise as calorimetry, the technique is simpler and quicker than either method.

To study conformational changes in a peptide's secondary structure, the peptide is initially added to a patch clamp apparatus and an event profile is established for the peptide in the absence of any binding partners. A second study is performed with the peptide in the presence of the drug or molecule of interest. If the same peaks and profiles are present in both experiments, it can be concluded that the peptide is not affected by its suspected binding partner. If the peaks change either their width or total blockade current, it is likely that the peptide and the added molecule are able to bind together as a complex and the altered events are caused by

the unique structure now present in solution. If there are more peaks present than what was seen in the initial peptide-only experiment, it is possible that the suspected binding partner is interacting with the pore. Another experiment can be done using only the suspect molecule without peptide to rule out the possibility of interactions with the pore. In all cases the results can be confirmed using any of the other aforementioned techniques if the findings are ever in doubt.

The size constraints of protein and peptide analysis continue to limit what kind of research is possible with nanopores (Meng et al., 2010). Until solid-state pores become simpler and more consistent to use, anything larger than a simple peptide is difficult to characterize due to the small constriction of α-HL and other biological channels.

1.2 Introduction to the Outer Membrane Protein GspD

1.2.1 Function of GspD and Its Role in the Type II Secretion System

The type II secretion system (T2SS) is the most widely-used pathway for Gram-negative bacteria to secrete proteins, such as exotoxins and lytic enzymes, into the extracellular space (Pugsley, 1993). The T2SS has a two-step process for protein secretion (Sandkvist, 2001). The first step transfers proteins with an N-terminal signal sequence from the cytoplasm into the periplasm. The second step passes the protein through the outer-membrane channel formed by the secretin. The T2SS pathway is encoded by 12-16 genes designated A-O and S, which together form an inner membrane platform, a pseudopilus, and an outer membrane pore (McLaughlin et al., 2012). The proteins produced from these genes are commonly referred to as general secretory pathway (Gsp) proteins, though when applied to a specific bacteria such as *Aeromonas hydrophila,* the pathway proteins are designated ExeA, ExeB, etc.

When a protein is destined for excretion, it leaves the cytosol and enters the periplasm via either the Sec or Tat pathways. The general secretion route (Sec) is responsible for enabling proteins to cross the inner membrane in their unfolded states before adopting their native structure in the periplasm. The twin-arginine translocation pathway (Tat) first folds the protein in the cytosol, and then moves secretory proteins across the inner membrane in their folded state.

The T2SS uses proteins entering the periplasm from either method, but as most proteins enter via the Sec pathway, the Sec system is the major contributor to T2SS secretion (Mori and Ito, 2001).

Regardless of how the protein enters the periplasm, the inner membrane platform is responsible for recognizing proteins ready to be secreted. The platform is believed to have a central role in the T2SS as it interacts with the other major elements of the system, communicating with both the outer membrane complex and the pseudopilus in the periplasm, and the secretion ATPase in the cytoplasm (Korotkov et al., 2012). The platform is formed by anchoring the proteins GspC, GspE, GspF, GspL, and GspM to the lipids of the inner membrane and providing a stable base for interactions. The stable platform allows the pseudopilus to form and extend outwards into the periplasm, and thus indirectly aids in the eventual secretion of the secretory protein (Filloux et al., 1998). It is thought that the platform may even be responsible for converting the activity of the secretory ATPase into the piston-like extension of the pseudopilus, and thereby directly links the actions of the former to the latter (Korotkov et al., 2012).

GspG-K comprises the entirety of the pseudopilus. The apparatus is first synthesized as short precursors of prepilins which await processing prior to assembly on the platform. A leader peptide having both a positively charged head of 6-7 residues and a hydrophobic domain of 20 residues is cleaved by the enzyme prepilin peptidase at a site immediately proximal to the hydrophobic region (McLaughlin et al., 2012). In the leader peptide, the new N-terminal region is methylated to help with platform binding, and a highly-conserved glutamate is left exposed in the hydrophobic region. Incoming psuedopilins retain their positive charge at their N-terminal and bind by forming a salt bridge with the leader peptide's glutamate residue. The assembly of the pseudopilus acts as a piston for protein extrusion by binding a target molecule, elongating its structure to direct the proteins towards the outer membrane pore, and then disassembling its fibrils upon completion. The T2SS setup therefore requires a pseudopilus for protein secretion, and movement of proteins through the outer membrane pore does not occur without its assembly.

The final part of the T2SS is the secretin. GspD is the only part of the T2SS that is bound to the outer membrane, and is the only point of the system from which proteins are able to leave

the cell (Filloux et al., 1998). The secretin native to *Aeromonas hydrophila* is ExeD, a homododecamer comprised of twelve monomeric subunits of 72,451 Da each (Ast et al., 2002). It is believed that the C-terminal domain has a series of β-strands designed to insert into the hydrophobic outer membrane and act as gateway to the extracellular milieu, though this has not been conclusively demonstrated. The N-terminal region extends into the periplasm and promotes interactions with substrate molecules attached to the pseudopilus and the platform-bound GspC (Korotkov et al., 2009). Studies have shown that assembly of the dodecamer depends upon the N-terminal region, and that even when amino acids are added to the C-terminal domain the function of the secretin can remain at wild-type levels (Chami et al., 2005). The C-terminal domain is primarily used for insertion into the lipid bilayer and has a highly-conserved 60 amino-acid sequence. An overview of the T2SS is shown in Figure 8.

The architecture of GspD from *Vibrio cholera* has been revealed by electron cryomicroscopy (Reichow et al., 2010). Lengthwise the channel is 200 Å, with approximately 125 Å belonging to the periplasmic regions. The width of the pore is 155 Å across and has a large periplasmic opening of 55 Å. Two constriction points are present in GspD: the first occurs at the two interior loops which can either block the pore entirely, or can be moved to pass large proteins through. The second constriction point is an extracellular cap which is capable of opening completely to accommodate fully folded proteins, but in its resting state remains partially closed at a 10 Å limiting dimension (Reichow et al., 2010). GspD as visualized by electron microscopy is shown in Figure 9.

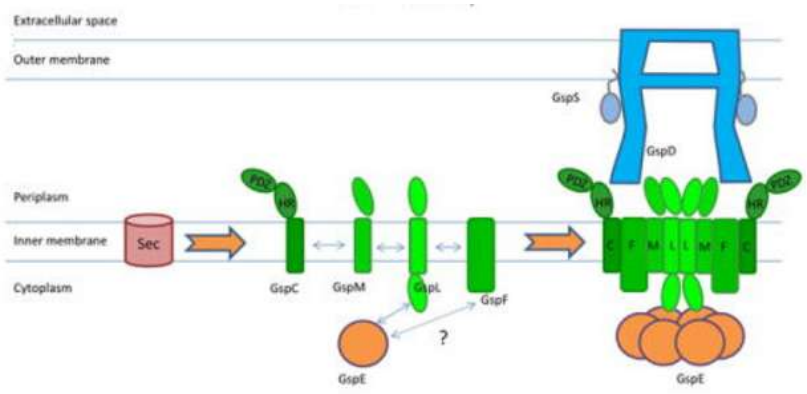

Figure 8: Overview of the Type 2 Secretion System. Exoproteins first enter the periplasm via either the Sec or Tat pathways. GspC, E, F, M, and L form the inner-membrane platform. G, H, J, K, and I subunits comprise the pseudopilus. GspD is the large, outer membrane form and point of exit for exoproteins. The lipid-bound GspS acts as a pilotin for the secretin (from Korotkov, Sandkvist, and Holl, 2012; with permission).

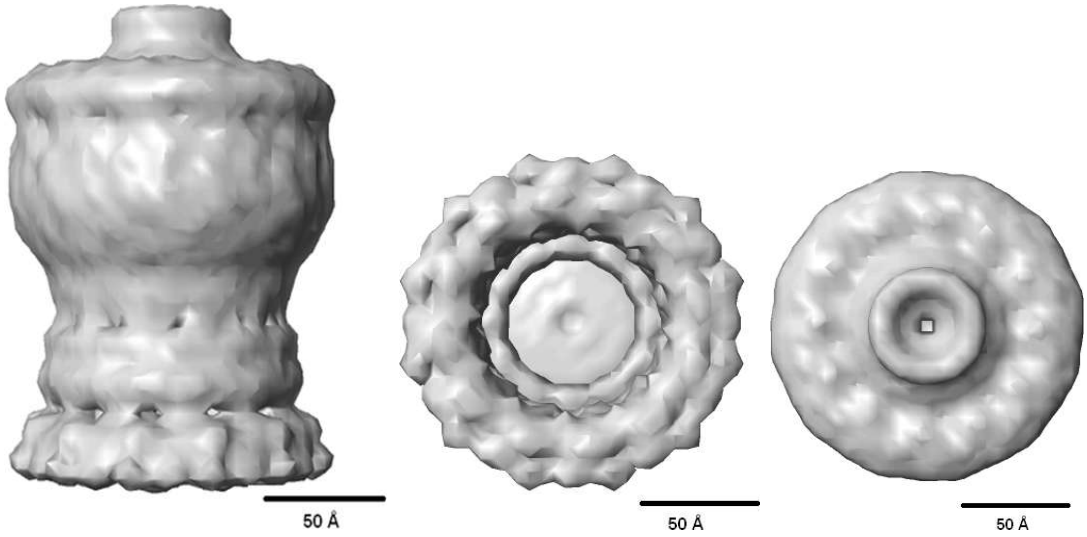

Figure 9: Electron Microscopy Structure of GspD. The structure of 12-subunit GspD as viewed from the side, bottom, and top (pictured left, middle, and right respectively). Note that the scale is set at 50 Å (modified from Reichow et al, 2010; with permission).

1.2.2 Formation, Structure, and Domains of GspD

Though GspC-O are highly conserved across all bacterial species which use the T2SS, the GspAB and GspS subunits are more variable between species. GspS for example is not present in *A. hydrophila*, though its role is believed to fulfilled by ExeAB (Ast et al., 2002). GspS is a small lipoprotein that targets GspD (ExeD in *Aeromonas hydrophila*) monomers for movement through the periplasm to the outer membrane, and functions as a chaperone for the protein's multimerization (Nouwen et al., 1999). The GspAB complex (ExeAB in *A. hydrophila*) is required for localizing ExeD into the outer membrane (Ast et al., 2002). ExeA utilizes an AAA ATPase activity in its cytosolic domain to form a complex with ExeB. When ExeAB is present, ExeD localizes to the outer membrane and assembles correctly. If either ExeA or ExeB is missing, the secretin is largely unable to enter the periplasm; it will instead localize primarily to the inner membrane and subsequently loses functionality.

The assembly model of ExeD uses ExeB as a scaffold to bring together ExeA and ExeD in a trimeric complex through the N-terminal region of ExeD (Vanderlinde et al., 2014). The scaffold appears to be required for correct multimerization in wild-type *A. hydrophila.* However, in mutants of *Aeromonas* lacking the AB complex, over-expression of ExeD has led to multimeric complexes appearing in both the inner and outer membranes (Ast et al., 2002). In these cases, high expression of the protein bypasses the need for a scaffold and the secretin multimerizes independently of ExeAB. A pilotin (GspS) is often required to help transport ExeD to the outer cell membrane. Interestingly, despite the absence of a pilotin in *A. hydrophila*, a very small amount of oligomeric ExeD still localizes to the outer membrane in these mutants.

GspD proteins have 3 distinct domains: the N-terminal region with 4 periplasmic subdomains and a signal peptide, the C-terminal domain which forms the transmembrane region, and an S-domain which is utilized by the pilotin to localize secretin components to the outer membrane (Korotkov et al., 2009).

The N-terminus contains both a signal peptide and 4 distinct subdomains (N0-N3; Vanderlinde et al., 2014). The N0-N3 regions were previously crystallized in enterotoxigenic

Escherichia coli (ETEC) and viewed using X-ray crystallography (Korotkov et al., 2011). The signal peptide's role is to target GspD to the periplasm. When finished, the signal is cleaved off by Sec-pathway machinery and the pore is able to form. The N0-N3 subdomains resemble toroid stacks as seen in Figure 10. The structure of N0 is circular in shape with several β strands residing on the top surface. N0 is structurally related to the signaling domain of TonB-dependent receptors, suggesting that this is the region where much of the substrate-protein interaction occurs (Wang et al., 2012). The β-2 strand of N0 is of particular importance as this strand is believed to interact with β-strands of secreted proteins or other T2SS components. These β-strand interactions facilitate translocation of proteins through GspD, and β-2 may be required to bind transiently to all proteins prior to their secretion (Korotkov et al., 2009). A secondary interaction between N0-N1 and GspC (a subunit associated with the inner membrane platform) allows GspD to bind to a highly conserved section of the GspC N-terminal called the homology region (HR). The interaction between HR and GspD suggests that the N0-N1 region is critical to GspD's function within the T2SS.

The N1-N3 subdomains have some degree of sequence homology within themselves, with N1 and N3 sharing 16% of the same amino acids and N2 and N3 sharing 17% (Korotkov et al., 2009). N1 and N2 contain a repeat of 166 amino acids in both of their two domains, a repeat which is also seen in the Type 3 Secretion System extracellular pore. These domains adopt a

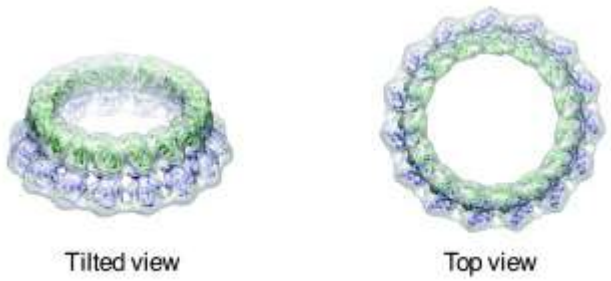

Figure 10: N0-N3 Terminal Domain of GspD. The N-terminal domain consists of 4 subdomains arranged in toroid stacks (modified from Korotkov, Gonen, and Hol, 2011; with permission).

KH-fold typically used for binding DNA or RNA (Grishin, 2001). However, to bind nucleic acids a series of positively charged amino acids needs to be embedded within this sequence repeat. In peri-GspD, these amino acids are absent. Although the secretin in T2SS does not associate with nucleic acids, the GspD homologue pIV has a role in DNA transport (Craig and Li, 2008). Research indicates that N1 and N2 provide a location for the exoprotein substrate to load in preparation to being excreted, and N3 acts as a signal point to verify the substrate has entered the periplasm (McLaughlin et al., 2012). N1-N3 are connected by flexible linkers which allows them to rearrange upon substrate binding. In the presence of trypsin, these sites can be cleaved from the secretin leaving only the C-terminal intact (Chami et al., 2005).

The beginning of the C-terminal region includes a series of amino acids which codes for a periplasmic ring-like structure (Chami et al, 2005). This is the only region of the C-terminal which exists outside the outer membrane and is the location of an interior plug that has been shown to act as an occlusion point for the multimeric pore (Nouwen et al., 2000). This plug, under the influence of the pseudopilus, moves aside to allow passage of large, fully folded proteins. The plug is comprised of two loops that extend into the C-terminal periplasmic ring. Evidence indicates that the opening and closing of the pore is governed by these loops, and as they respond to interactions with the pseudopilus, they either block or allow passage of secretory proteins (Chami et al., 2005). Researchers have found that mutations in this region produce a pore which is constitutively open and can continually extrude proteins to the outside of the cell (Spagnuolo et al., 2010).

There is a second C-terminal ring encoded for by 100 amino acids, starting at the midpoint of the GspD protein (Chami et al., 2005). Unlike the first C-terminal ring, this structure is completely embedded within the outer membrane of the cell. This is essentially the “core” of the protein as it codes for the outer membrane channel and transmembrane region. The 100 amino acid stretch in this region is theorized to primarily produce β-strands. When the dodecamer forms, the C-terminal ring is believed to give rise to a β-barrel structure which acts as a gateway to the cellular exterior. It is notable that even when the N-terminal domain is cleaved off, this region retains the ability to form a circular channel (Brok et al., 1999). This region also codes for the extracellular cap (also called the extracellular gate), the final constriction point of

the pore. The cap rests outside the cell and is the final passageway for proteins targeted for secretion. The cap is believed to be constitutively open with a width of 10 Å across. A cross-sectional diagram is shown in Figure 11 (Reichow et al., 2010).

At the extreme end of the C-terminal in GspD is the S-domain, a small area of about 50 amino acids which is responsible for binding the pilotin (Nickerson et al., 2011). Interestingly, some species such as Xcp of *Pseudomonas aeruginosa* can completely lack the S subunit in their type two secretion systems. Though the pilotin is not present in *A. hydrophila*, ExeAB has been suggested to fulfill the role of the piloting system to aid in multimer assembly (Ast et al., 2002). Consequently, if the S-domain or the pilotin is not present in a system that requires it, the multimer mislocalizes to the inner membrane. The interior plug of GspD is not large enough to completely prohibit the movement of protons and electrolytes, and insertion into the inner membrane is believed to cause loss of the proton motive force (PMF) needed for preprotein translocation (Arkowitz and Wickner, 1994). The cell responds to loss of its proton motive force via the phage shock response, wherein a large amount of the phage shock protein is produced in an attempt to maintain the electrochemical gradient across the inner membrane. It

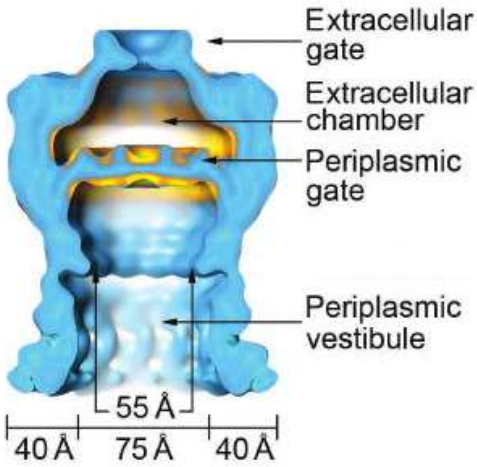

Figure 11: Cross-Sectional Diagram of PulD. The periplasmic vestibule, the periplasmic gate, and extracellular gate are all labelled and are the important points of constriction for pore control (modified from Reichow et al, 2010; with permission).

has been shown that when PulD is expressed without its pilotin, a massive amount of phage shock protein is produced to compensate (Jones et al., 2003). If the pore-forming protein levels continue to rise and the phage-shock response cannot compensate for the decrease of the PMF, the cell eventually dies (Guilvout et al., 2008).

As discussed, two biological pores have been extensively studied and utilized in nanopore analysis: α-hemolysin and MspA. Although ExeD is not the first biological pore to be used in these experiments, it has several advantages over either of these two pores. First, it is more stable than most other channels (Strozen et al., 2011) and would be less likely to unfold or dissociate during the course of the experiment. Specifically, the C-terminal region of GspD has been shown to be incredibly resilient. The detergent sodium dodecyl sulfate (SDS), commonly used for protein denaturation, has no immediate effect upon the quaternary structure of the pore. The dodecamer can be boiled in SDS without dissociation of the monomers from one another.

Secondly, its inner constriction point is almost four times larger than α-hemolysin (Reichow et al., 2010) and over 5 times larger than MspA. This size difference is important for the function of the T2SS secretin because its substrate exotoxins are often released fully-folded into the extracellular space. Conversely, α-HL is not able to pass such large molecules through its channel and this defines the size limitation of proteins in biological nanopore analysis (Meng et al, 2010). Note, however that GspD in its resting state has an extracellular cap which constricts to 1 nm at the C-terminal. How this cap operates is still not entirely understood, but evidence indicates that once a substrate enters into the vestibule of the pore, both the periplasmic gate and extracellular cap open spontaneously, even without the pseudopilus moving the substrate forward (McLaughlin et al., 2012). In its isolated state, ExeD may provide a way for molecules larger than DNA to be studied via nanopore analysis.

Third, ExeD can be subjected to point mutations while still retaining some function. Studies of GspD have shown that specific point mutations have a profound impact on the way the protein interacts with and transports substrates through its interior (Spagnuolo et al., 2010). The pore can vary its conductance from constitutively open to perpetually closed and/or malformed by modifying one or multiple amino acids in the C-terminal loops. The results

suggest that it in the future, it may be possible to control the size of the pore opening to suit the needs of the experiment.

1.2.3 Previous Work with Secretins and the Patch Clamp System

Studies of GspD homologues PulD and XcpQ have previously been investigated using patch clamp. The results from both experiments had a few common points of interest, but both also produced results significantly different from each other. These two studies are worth discussing.

Nouwen et al. (1999) studied PulD from *Klebsiella oxytoca* using a host *E. coli* strain with a PulD-encoding plasmid. The plasmid also contained a number of additional T2S proteins to ensure the pore was functional and able to secrete the exoprotein pullulanase. The *E. coli* vector did not confer a C-terminal *his*-tag, so purification was done using anion-exchange and size-exclusion chromatography. Researchers found that PulS copurified with PulD, and that the proteins were difficult to separate. The strong reducing agent dithiothreitol had no effect on the PulD-S complex, and only breaking apart the multimer with urea or boiling the complex in SDS could separate the two subunits. However, neither methods of separation yielded a usable PulD multimer. Consequently, all experiments done by Nouwen et al. used the PulD-S complex.

Insertion into the planar lipid bilayer was done by combining the purified PulD-PulS complex with solubilized L-α-phosphatidylcholine to create proteoliposomes. Detergents in the solution were removed by incubating the mixture with Bio-Beads for several hours. The proteoliposomes were separated from the buffer by ultracentrifugation and added directly to the perfusion cup. Researchers found that it was difficult to merge the planar lipid bilayer with the formed liposomes, so they used a salt gradient to drive the liposomes towards the bilayer. The *cis*-side of the perfusion cup contained 400 mM KCl and the *trans*-side contained 100 mM KCl.

Experiments showed that PulD had an open and a closed state, and that the pore inserts in the closed state. The closed state had periodic gating events that were detectable but uncommon. Although the pore was termed “closed”, ions were still capable of flowing through the channel.

Unfortunately, an open pore current was visible but never stated in their published works. When an 80 mV voltage was applied to the pore for 5-10 minutes, the pore entered its open state and the gating events became rapid and varied (Figure 12).

After the pore had opened, the PulD-PulS complex was subjected to a constant positive voltage and events were recorded. Researchers found that two kinds of gating events occurred simultaneously. The first gating event had a long duration (lasting for several seconds) and increased the open pore current 20-30 pA. Superimposed on these events was a secondary form of gating which was both shorter in duration and had a more varied amount of current change. These secondary events were on the order of milliseconds rather than seconds, and the detected change in amperage ranged from 5-60 pA. It was found that the secondary type of gating was independent of the first, and occurred regardless of whether the pore was in its open or closed state.

At low negative potentials, the researchers found that channel activity was more regular and defined, and had clear patterns of distribution. However, they found that the size of these

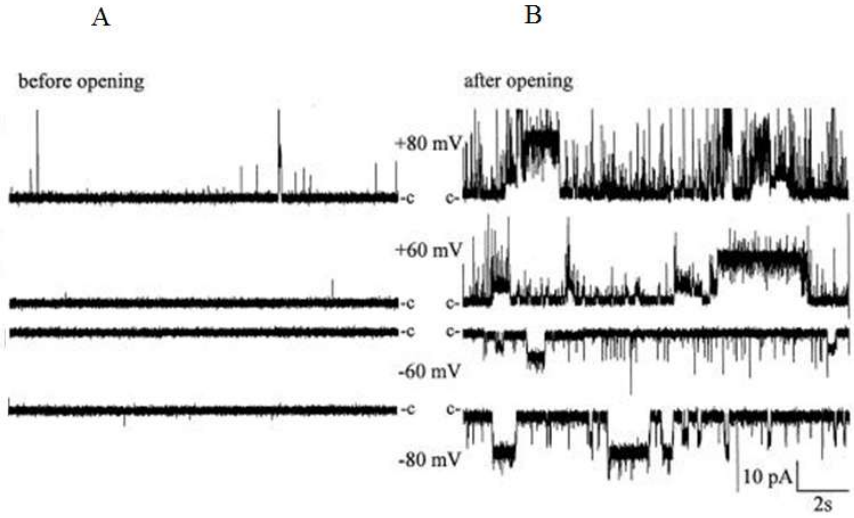

Figure 12: Gating of PulD-PulS Complex. Two states of the pore are visible. A- The closed state of PulD-PulS occurs shortly after a voltage is applied. B- Several minutes after the presence of a potential difference, the pore complex opens and rapid gating events are observed (from Nouwen et al, 1999; with permission).

events varied from one bilayer to another. Without consistent readings across experiments, it is not possible to establish an event histogram. Consequently, there is no event distribution data for their experiments at low negative potentials.

Nouwen et al. (1999) found that when they applied a voltage of approximately -20 mV, the measured current reversed. This indicated the channel was weakly selective for cations. Additionally, when the exoenzyme pullulanase was added to the perfusion cup, no change in channel activity was identified. Pullulanase is one of the enzymes the T2SS is capable of excreting, so a lack of channel activity indicates that the protein was not being secreted. Notably, there was no visible interaction between PulD and pullulanase.

One of the major limitations of the study was the size of the event threshold being used. In all nanopore experiments ranging from solid-state to α-HL, there is some amount of background noise due to current flowing through the nearby electrical machinery, ion charge of the air, and nearby movement of equipment or the observer. The contribution of the noise level is usually small, approximately 5-10 pA, so standard practice is to discard all events under 5-7 pA because it is very unlikely they are "true" nanopore interactions. In Nouwen et al.'s research done on PulD, the vast majority of recorded events fall around the 3 pA range as shown in Figure 13.

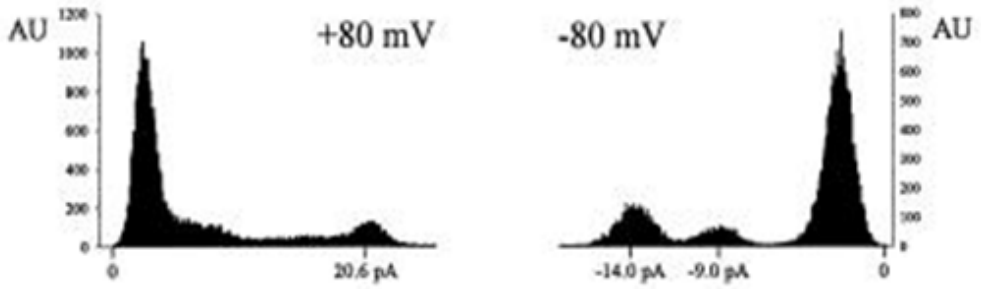

Figure 13: Distribution of Events from the PulD-PulS Complex. At an initial inspection, two peaks are present at +80 mV at ~ +3 pA and 20.6 pA. Standard practice is to disregard any events below a designated threshold, usually 10 pA. At -80 mV another peak at ~-2 pA is visible alongside -9 pA and -14 pA distributions (from Nouwen et al, 1999; with permission).

A second series of experiments was done with the C-terminal of the PulD homologue XcpQ in 1999 (Brok et al.). XpcQ is the T2SS secretin native to *Pseudomonas aeruginosa*. In attempting to isolate XpcQ from *P. aeruginosa* however, the researchers were unable to collect an appreciable amount of the protein. They found that when the C-terminal *xpcQ* genes were inserted into a high-expression plasmid, the host cells lysed when the oligomeric complex started to form. To circumvent the low amount of protein produced, Brok et al. used a mutant strain of the closely related species *Pseudomonas alcaligenes* which had been involved in a separate study to overexpress an exoprotein lipase. Inserting the *xpcQ* plasmid into this mutant *P. alcaligenes* strain allowed for a far greater level of protein expression than that seen in *P. aeruginosa*.

Isolation was done using a method similar to Nouwen et al. (1999) involving ion-exchange columns and solubilizing the protein in a zwitterionic detergent. The extract was added directly to the perfusion cup and the XpcQ oligomers spontaneously inserted into the bilayer.

When viewed using patch clamp, the C-terminal multimers had a large variance in their channel conductance, changing from between 4-10 nanosiemens (nS) as shown in Figure 14. This corresponds to a channel insertion variance roughly 5-10x those of other channels.

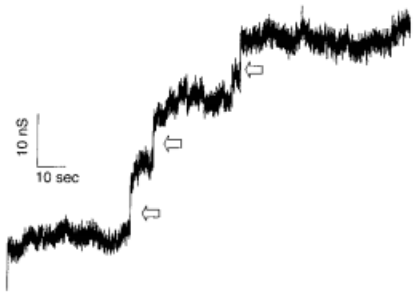

Figure 14: Variance of the C-Terminal Domain of XcpQ. The open pore current changed widely from one insertion to the next (pore insertions are marked by arrows). The conductivity of ions was also inconsistent and did not demonstrate the same linear baseline as those of other pores (cf. Figure 10). Figure is from Brok et al., 1999 with permission.

As a comparison, α-HL has an open pore current of 100 pA with a variance of +/-5 pA per pore insertion. If the same variability of XpcQ was applied to hemolysin, the open pore current would range from 50 pA to 150 pA. A second unusual event was observed with XpcQ in these experiments. After the pore was inserted, the pore conductivity would slowly increase by a few pA every few minutes. The cause of this was undetermined. Normally when pore conductivity increases at such a rapid rate, the experiment is terminated prematurely because either there is a problem with the membrane where ions are getting through, or buffer is being lost through another mechanism (usually an incorrect apparatus assembly). It is unusual to continue experiments with these issues (Stefureac et al., 2007).

The results of both studies showed that XpcQ and PulD had clear channel forming abilities due to the C-terminal region of the pore. Nouwen et al. (1999) found significant amounts of gating in PulD-PulS and attributed this to an internal plug in the pore's channel. Lastly, both studies found that gating at positive and negative voltages was asymmetrical and that the pore responds to these two types of voltages with different levels of conductance (i.e. -80 mV gating events were distinct from +80 mV gating events).

1.3 Purpose of This Work

The small internal β-barrel structure in α-hemolysin limits nanopore use in protein analysis and aggregation studies. Secretin ExeD is proposed as a more viable alternative. The ExeD pore has a significantly larger cavity which is capable of passing natively folded proteins through its structure (Reichow et al., 2010). It may be possible to use this secretin to study larger peptides and proteins which are otherwise unable to be studied using biological methods. Furthermore, the secretin conformation has a greater stability than that of α-HL (Strozen et al., 2011) and may make nanopore experiments easier to perform.

The objective of this study was to produce and isolate the ExeD pore and make it suitable for use in nanopore research. To accomplish this, *exeD* was inserted into the pET-30 (a) vector and then expressed in BL21 DE3 cells. The protein was isolated by a combination of detergent extraction, affinity and size-exclusion chromatography, after which it was incorporated into

liposomes and inserted into a lipid bilayer. Pore characteristics were analyzed using standard patch clamp techniques to determine gating events, the open pore current, and interactions with peptides and DNA.

2.0 Materials and Methods

Item	Supplier
Chemical and biological reagents	
1,2-diphytanoyl-sn-glycero-3-phosphocholine in $CHCl_3$	Avanti Polar Lipids
3-8% Tris-Tricine precast SDS-PAGE gel	Bio-Rad
Acetone	Sigma-Aldrich
Anti-*his* Antibody Selector Kit	Qiagen
Agar	Sigma-Aldrich
Agarose	Sigma-Aldrich
Argon (gaseous)	Praxair
BL21 DE3 Cells	New England Biolabs Inc.
Bromophenol blue	Bio-Rad
Cobalt chelate agarose resin	Pierce Scientific
Deoxynucleotides (dNTPs)	New England Biolabs Inc.
DNA Primers	Life Technologies
Ethidium Bromide	Bio-Rad
Ethylenediaminetetraacetic acid (EDTA)	Sigma-Aldrich
Fmoc-$D_2A_{10}K_2$ (A10)	Sigma-Genosys
Kanamycin Sulfate	Sigma-Aldrich
NdeI Restriction Enzyme	New England Biolabs Inc.
Nitrogen (gaseous)	Praxair
pET 30(a) Vector	Clontech
Potassium chloride (KCl)	Sigma-Aldrich
Protein molecular weight markers	Boehringer Mannheim, Promega
Potassium phosphate, dibasic (Na2HPO4)	Sigma-Aldrich
Potassium phosphate, monobasic (NaH2PO4)	Sigma-Aldrich
QIAquick PCR Purification Kit	Qiagen
Sephacryl S-500 HR	GE Lifesciences
Silver wire	Alfa Aesar
Sodium Acetate	Bio-Rad
Sodium dodecyl sulfate (SDS)	Sigma-Aldrich
Sodium Chloride	VWR
Sulfuric acid (H2SO4)	EMD
Taq DNA Ligase	New England Biolabs Inc.
n-Tetradecyl-N,N-dimethyl-3-ammonio-1-propanesulfonate (Zw 3-14)	Sigma-Aldrich
n-tris-hydroxymethyl-methyl glycine (Tricine)	Clontech
Tris-[hydroxymethyl] aminomethane (Tris)	Sigma-Aldrich
Tryptone	Sigma-Aldrich
XhoI Restriction Enzyme	Sigma-Aldrich
Yeast Extract	New England Biolabs Inc.
Equipment and Supplies	
Active-air floating table	Sigma-Aldrich
Automatic Pipettes and tips	Kinetic Systems
Axopatch 200B amplifier	Eppendorf , VWR

Basic pH meter	Axon Instruments
BC-535 amplifier	Fischer Scientific
Centrifuge Tubes (1L)	Beckman-Coulter
DigiData 1440A digitizer	Axon Instruments
Falcon tubes	Axon Instruments
Faraday cage	VWR
Filters (0.2 μm)	Warner Instruments
Glass vials and plastic caps	Sarstedt
Headstage model BC-535	Kimble-Kontes, VWR
Headstage model CV203BU	Warner Instruments
HP 8662A signal generator	Axon Instruments
LPF-8 eight-pole low pass Bessel filter	Hewlett Packard
Microcentrifuge tubes	Warner Instruments
Microliter syringes	VWR
Mini-PROTEAN® electrophoresis cells	Hamilton
Pierce Protein Concentrator (30K MWCO)	Thermo Scientific
Ultracentrifuge Tubes (10 mL)	BIO-RAD
Ultracentrifuge Tubes (25 mL)	Beckman-Coulter

2.1 Production and Isolation of the ExeD Protein

The *exeD* gene from *Aeromonas hydrophila* was obtained from cell strain C5.84 containing plasmid PRJ 100.1 (obtained from work previously done by Ast et al., 2002). The C5.84 cells were plated out and grown at 37°C overnight. A single colony was obtained and added to 250 μL of sterile H_2O in a microcentrifuge tube. The mixture was heated to 95 °C to separate the DNA strands and 0.5 μL was taken to use in PCR amplification, adding the NdeI and XhoI restriction sites. The ideal temperature for amplification was determined to be 67 °C using gradient PCR. Electrophoresis on a 1% agarose gel (10 μL loading buffer, 2 μL genetic material) for 30 minutes at 100 mV demonstrated the amplified gene was the correct size at ~2 kb. A QIAquick PCR Purification Kit (Qiagen) was used to purify the DNA from agarose using a spin column and to insert and ligate the *exeD* DNA into the pET 30(a) vector after restriction enzyme digestion. The DNA primers used in the procedure were (forward) GTA CCG CAT ATG ATA AAT AAA GGG AAG GGC TGG and (reverse) GAC TCC CTC GAG CTT GTT ACC CTG AAC GAA TGG. This put the gene for *exeD* under the control of the T7 promoter within the pET 30(a) vector, and made it capable of expression via addition of IPTG. The *exeD* sequence is shown in Appendix A with the accompanying *his* tag which was conferred by the pET 30(a) vector.

The vector was transformed into *E. coli* strain BL21 DE3 via electroporation at 1.7 kV and immediately added to 400 µL super optimal broth with catabolite repression medium (2% w/v tryptone, 0.5% w/v yeast extract, 10 mM NaCl, 2.5 mM KCl, 10 mM $MgCl_2$, 10 mM $MgSO_4$, 20 mM glucose). The electroporated cells were incubated in a cell shaker for 4 hours at 37 °C and plated on an agar medium containing 50 µg/mL kanamycin at 37 °C overnight. Kanamycin is the antibiotic resistance conferred by the expression plasmid, and enabled selection for only those cells possessing the vector. A miniprep was done on a single colony using a Qiagen Miniprep Kit (Qiagen). The isolated vector and gene were digested with the XhoI and NdeI restriction enzymes and electrophoresed in 1% agarose as described above to ensure *exeD* was properly inserted. The *exeD* gene from this procedure was sequenced to confirm the correct orientation and the full-length insertion of the gene.

Once the strain was confirmed to contain *exeD* in pET 30(a), the colony was streaked onto a kanamycin-containing agar plate (50 µg/mL) to allow the cells to grow and replicate. A stock was made by selecting and growing a colony overnight at 37 °C in 50 µg/mL kanamycin. Eight-hundred µL of the stock was added to 200 µL sterile glycerol for storage at -70 °C, and could be drawn from whenever cells were needed. For experiments, 2 µL of stored stock was removed and streaked out on an agar plate containing selectivity for kanamycin. This allowed us to obtain a colony from a single cell growing on the agar medium. A single colony was taken from the agar plate and incubated overnight in 100 mL of LB and 50 µg/mL kanamycin at 37 °C. This overnight stock was used to grow a much larger amount of cells from which the *exeD* gene could be induced and the protein harvested. The overnight stock was grown in 20L LB medium at 37°C in 50 µg/mL kanamycin at a 1:200 ratio and induced at 100 µM IPTG at OD_{600} 0.6. Immediately after induction the cells were transferred to a 15°C incubator and allowed to express ExeD overnight to maximize the amount of protein the cells could generate.

Cells were harvested and resuspended in 10 mM mM HEPES, 400 mM NaCl (pH 7.4) and lysed using a cell disruptor at 34 PSI. The solution was centrifuged at 18000 x *g* for 10 minutes to pellet out the unlysed cells, and the supernatant (representing all the disrupted cells and their interiors and membranes) was collected and ultracentrifuged at 160000 x *g* for 1 hour.

This separated the membrane envelope in the pellet from the cytoplasm which remained as a supernatant. The membrane envelope was resuspended in detergent (2% n-Tetradecyl-N,N-dimethyl-3-ammonio-1-propanesulfonate, aka Zw 3-14), 250 mM NaCl, 10 mM HEPES (pH 7.4), solubilized with the aid of a Dounce homogenizer, and ultracentrifuged again at 160000 x *g* for 1 hour. A 2% Zw 3-14 detergent does not solubilize ExeD but does solubilize many of the lipids and membrane proteins remaining in the envelope. As a result, after centrifugation the pellet becomes a relatively clear solid containing ExeD, and the supernatant contains many of the membrane proteins not needed in this experiment. The pellet was collected and resolubilized again with a Dounce homogenizer in 5% Zw 3-14, 250 mM NaCl, 10 mM HEPES (pH 7.4), at which point the ExeD protein was soluble. Ultracentrifugation at 160000 x *g* removed any insoluble cell remnants from the solution, and all available ExeD existed in the supernatant. The supernatant was loaded onto a cobalt-NTA column and the ExeD *his* tag enabled binding to the resin. This was incubated for 1 hour at room temperature to maximize binding, and washed with 10 column volumes of 10 mM imidazole, 0.6% Zw 3-14, 250 mM NaCl, 10 mM HEPES (pH 7.5). Washing removed many background proteins from solution. Elution of monomers was done using 10 column volumes of 100 mM imidazole, 0.6% Zw 3-14, 250 mM NaCl, 10 mM HEPES (pH 7.5). Multimer elution was done using 4 column volumes of 0.5 M imidazole, 0.6% Zw 3-14, 250 mM NaCl, 10 mM HEPES (pH 7.5). The difference in imidazole concentrations between the elution of the monomer and multimer presumably relates to the 12 histidine tags binding to the cobalt instead of only 1 in the monomer.

Cell lysis and removal of the supernatant was done at 4 °C. All remaining procedures were carried out at room temperature as Zw 3-14 precipitates out at temperatures colder than 4°C. DegP, the protease responsible for ExeD degradation, is not affected by most serine inhibitors (Jones et al., 2002), and as such all experiments were done in the absence of protease inhibitor mixtures.

Concentration of these protein fractions was done using a Pierce Concentrator (30K MWCO) so that the protein stock from the cobalt column could be loaded onto a Sephacryl S-500HR size-exclusion column. Elution was done using 0.6% Zw 3-14, 250 mM NaCl, 50 mM Tris-HCl, 1 mM EDTA (pH 7.4) and fractions containing ExeD were detected using Coomassie

staining in conjunction with a Western blot using anti-*his* antibodies (Qiagen) or anti-ExeD antibodies.

Multimeric ExeD does not migrate into most acrylamide gels, but it was previously found that the complete structure can enter into a 3-8% Criterion XT Tris-Acetate gel (Strozen et al., 2011). 5 µL of purified sample was added to 5 µL sample buffer (62.5 mM Tris-HCl, pH 6.8, 25% Glycerol, 1% Bromophenol Blue, 2% SDS) and injected into the loading wells of the gradient gel. The running buffer was composed of 25 mM Tris, 190 mM glycine, 0.1% SDS, pH 8.0 and the sample was separated on a Bio-Rad Criterion Cell for 3 ½ hours at 4 °C and 100 mV. Transfer of proteins onto a nitrocellulose membrane was done in transfer buffer (25 mM Tris, 190 mM glycine, 20% methanol, pH 8.0, 0.1% SDS) using a Criterion blotter at 130 mV for 1 hour, and the Western blot was performed using the Anti-His Antibody Selector Kit (Qiagen).

Samples containing ExeD were placed in microcentrifuge tubes and stored at -20°C for up to 3 months. After approximately 3 months we found that the multimer significantly degrades and does not produce reliable pores.

2.2 Nanopore Analysis Using ExeD

Purified samples of ExeD were either added to lipids to form proteoliposomes or they were acetone precipitated, resuspended in the perfusion cup buffer, and added directly to the perfusion cup. Experiments using either of these methods were found to be indistinguishable from each other.

Proteoliposomes were formed by addition of 10 µg of purified protein extract to 50 µg L-α phosphatidylcholine in 2% SDS. The mixture was kept on ice for 10 minutes, rapidly diluted with 400 mM KCl 10 mM HEPES (pH 7.4) to create proteoliposomes, and put back on ice for another 10 minutes. Bio-beads were added (0.2 g) to remove the SDS and Zw 3-14 detergent, and the solution was incubated at 4 °C for 5 hours. The bio-beads were removed and the protein-bound lipids containing ExeD were ultracentrifuged at 250 000 x *g* to pellet them out of solution. The pellet was resuspended in 1M KCl, 10 mM HEPES (pH 7.4) and added to the perfusion cup.

Later experiments used acetone precipitation for nanopore analysis. This was done by adding 800 µL of acetone at -20 °C to 200 µl ExeD. Acetone was used to bind and remove the detergent in solution, and to precipitate out the protein. The sample was shaken gently for 15 seconds and cooled for 1 hour at -20 °C. The solution was then centrifuged at 13000 x g for 15 minutes at 4 °C. The acetone layer was removed by pipetting and air-drying in a fume hood for 40 minutes while not disturbing the protein precipitate. The remaining protein pellet was resuspended in 1M KCl 10 mM HEPES (pH 7.4) with gentle pipetting and added to the perfusion cup.

The perfusion cups used for experimentation were filled with 1 mL of 1M KCl, 10 mM HEPES (pH 7.4), 1 M KCl, 50 mM sodium acetate (pH 5), or 1 M KCl, 50 mM CHES buffer (pH 9.5) depending on the required pH of the experiment. Data was recorded with Digidata 1440 Digitizer and for each experiment a minimum of 4000 events were recorded. More were obtained if the experiment was able to continue to for longer without spontaneous removal of the pore or breaking of the lipid bilayer. Data was collected and analyzed using the pCLAMP 10 software (Molecular Devices) to remove any events which would be considered non-pore interactions. This frequently included cell collapse (which generates a multitude of events as the pore attempts to re-open) and gating events below a certain threshold which are deemed to be from environmental fluctuations. As mentioned, this includes anything below approximately 7 pA as these events arise from nearby electrical circuitry, air ambience, vibrations, or loud sounds conducted through the air.

3.0 Results

3.1 Oligomerization State of ExeD as a Function of the Rate of Monomer Production

3.1.1 Isolation and Purification

Previous studies had found that ExeD will multimerize spontaneously in *Aeromonas hydrophila,* even in the absence of T2SS assembly machinery. In such cases the monomer is the dominant form of the protein, but an appreciable amount of the oligomer also forms. It was expected that the multimerization of ExeD in this system would be similar to previous work as ExeAB is not present in our system. Indeed, it was found that when ExeD was expressed using the pET 30(a) vector at 37 °C, the protein existed primarily as a monomer (Figure 15 – Lane 2).

Our work in patch clamp required only the multimer. Although monomeric ExeD can oligomerize spontaneously (Guilvout et al., 2008), working with the multimer directly was more ideal as it was already assembled, and could theoretically be purified easier due to tighter binding

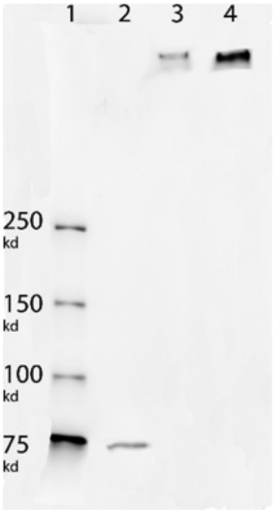

Figure 15: Western Blot of Whole Cell Extracts Showing ExeD Protein Generated at 3 Different Temperatures. Lane 1 – His-tagged protein standard. Lane 2- Whole cell fraction of BL21 cells containing *exeD* induced with 1 mM IPTG at 37 °C and left to grow overnight. Lane 3- Whole cell fraction of BL21 cells containing *exeD* induced with 1 mM IPTG at 26 °C and left to grow overnight. Lane 4- Whole cell fraction of BL21 cells containing *exeD* induced with 1 mM IPTG at 15 °C and left to grow overnight. Samples were resolved on a 3-8% gradient gel.

on the Co^{2+} column from an increased number of *his* tags. We wanted to decrease the amount of monomer and increase the amount of multimer in the purified product. We theorized that a slower rate of protein production would allow more time for oligomerization of the monomer in the cells. We undertook to test the amount of ExeD oligomer as function of temperature, IPTG concentration, and duration of expression.

Initial tests which examined the oligomerization of ExeD as a function of environmental temperature during the cell induction stage showed that there was a clear change in multimer formation with a decrease in temperature. When the temperature was decreased, the rate of multimer expression increased. Figure 15 shows that whole cell extracts, when expressed at 37 °C, produced almost no detectable levels of ExeD multimer. When the temperature was decreased to 26 °C and 15 °C, the amount of monomer produced decreased and the amount of multimer increased.

An unusual result was seen when the monomer produced at 37°C was purified. The initial expression conditions produced mostly monomeric ExeD. In the detergent-purified product, the oligomer was visible in appreciable amounts (Figure 16). It is unknown how much monomer was converted to multimer in the process, but the Western blot demonstrates that oligomer can be detected after solubilization in 5% zwitterionic detergent.

The temperature-dependent experiments supported our theory that amount of multimer can be controlled by changing the temperature of protein expression. Although we were able to increase our protein yield of ExeD by decreasing the temperature, the amount produced in our system was still extremely low. Attempts to visualize ExeD by Coomassie staining at this stage was not possible and the protein could only be identified by Western blot. Other groups have had this same issue producing the T2SS secretin (Brok et al., 1999; Nickerson et al., 2011), but circumvented the problem by using mutant strains designed to overexpress membrane proteins.

Unfortunately, we did not have access to these strains. To increase our amount of ExeD and to expand upon our findings of outer membrane expression, we tested the oligomerization of

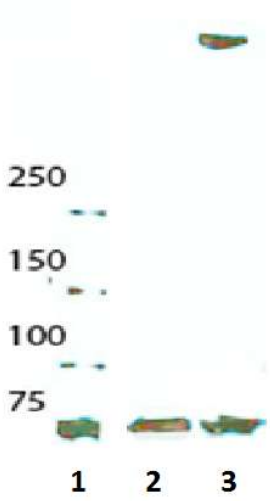

Figure 16: Western Blot of Whole Cell Extract Containing Monomeric ExeD Compared to Final Purified Product. Lane 1 – His-tagged protein standard. Lanes 2 – Whole cell extract of BL21 cells containing ExeD expressed at 37°C with 1 mM IPTG for 3 hours. Only the monomer is present at this stage. Lane 3 – Both the monomer and multimer are now present after detergent purification and solubilization in 5% Zw 3-14. Samples were 20x concentrated and resolved on a 3-8% gradient gel.

ExeD at different levels of IPTG and for different durations of expression (Figure 17). We found that longer durations of expression and lower levels of IPTG tended to increase the amount of multimer produced by the cells. The highest amount of protein produced from these tests was generated at 10-100 μM of IPTG when cells were allowed to express for 12 hours at 15 °C.

Increased generation of protein allowed us to visualize ExeD in a Coomassie stain as a purified product, shown in Figures 18 and 19. The ExeD multimer is unable to migrate into a standard 10% acrylamide gel, so visualization was done on a 3-8% gradient gel. It takes several hours to have ExeD enter into the 3-8% polyacrylamide, by which point smaller molecules have passed through the entirety of the gel. Another gel using 10% acrylamide was run using the same protein samples to show that no protein remains under the 150 kD marker after passing through the Sephacryl column.

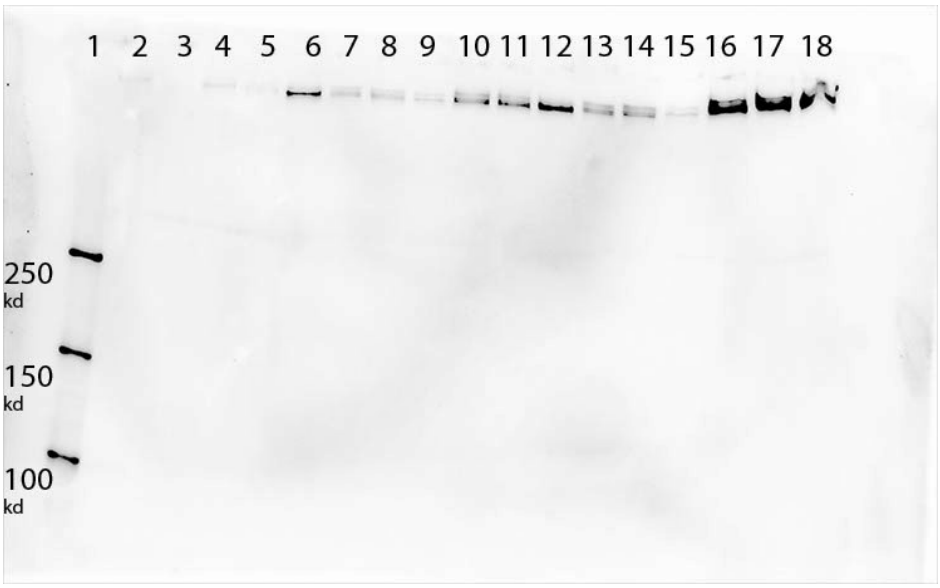

Figure 17: Western Blot of ExeD Protein Generated at 3 Different Temperatures and 3 Different IPTG Inductions. Lane 1 – His-tagged protein standard. Lane 2- Cells induced with 100 μM IPTG at 37 °C for 3 hours. Lane 3- Cells induced with 10 μM IPTG at 37 °C for 3 hours. Lane 4- Cells induced with 1 mM IPTG at 37 °C for 12 hours. Lane 5- Cells induced with 100 μM IPTG at 37 °C for 12 hours. Lane 6- Cells induced with 10 μM IPTG at 37 °C for 12 hours. Lane 7- Cells induced with 1 mM IPTG at 26 °C for 3 hours. Lane 8- Cells induced with 100 μM IPTG at 26 °C for 3 hours. Lane 9- Cells induced with 10 μM IPTG at 26 °C for 3 hours. Lane 10- Cells induced with 1 mM IPTG at 26 °C for 12 hours. Lane 11- Cells induced with 100 μM IPTG at 26 °C for 12 hours. Lane 12- Cells induced with 10 μM IPTG at 26 °C for 12 hours. Lane 13- Cells induced with 1 mM IPTG at 15 °C for 3 hours. Lane 14- Cells induced with 100 μM IPTG at 15 °C for 3 hours. Lane 15- Cells induced with 10 μM IPTG at 15 °C for 3 hours. Lane 16- Cells induced with 1 mM IPTG at 15 °C for 12 hours. Lane 17- Cells induced with 100 μM IPTG at 15 °C for 12 hours. Lane 18- Cells induced with 10 μM IPTG at 15 °C for 12 hours. A cell sample induced at 1 mM IPTG and grown for 3 hours at 37 °C is not shown here but is shown in Figure 16. All samples were taken from whole cell fractions and resolved on a 3-8% gradient gel.

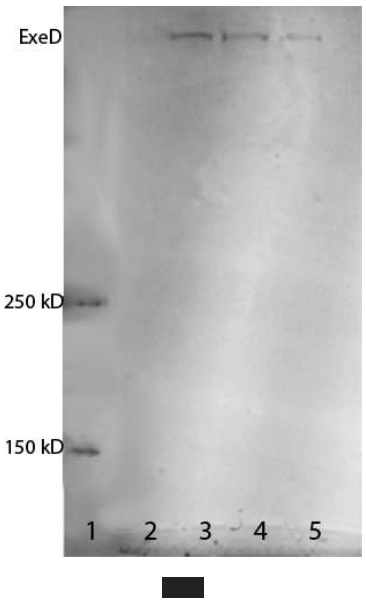

Figure 18: Purification of ExeD Visualized in a 3-8% Acrylamide Gel Using a Coomassie Stain. Lane 1- Protein standard. Lane 2: 100 mM imidazole elution from cobalt column. Lanes 3-4: 0.5 M imidazole elution. Lane 5: Isolated fraction from the Sephacryl S500 exclusion column. ExeD was expressed at 15 °C overnight with 100 mM IPTG.

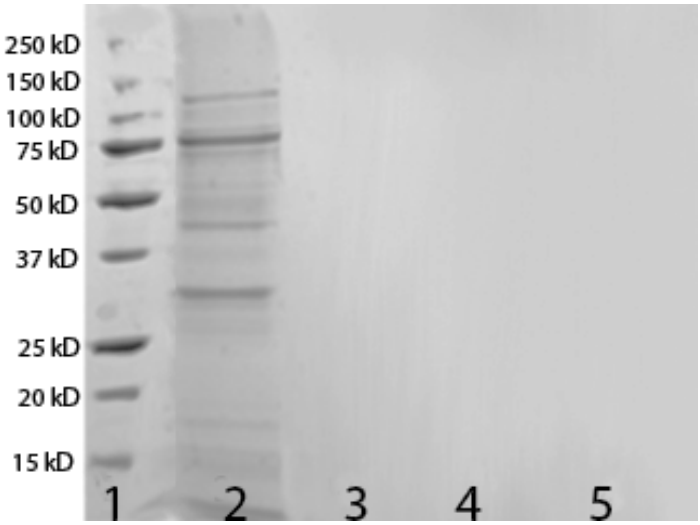

Figure 19: Purification of ExeD Visualized in a 10% Acrylamide Gel Using a Coomassie Stain. Lane 1- Protein standard. Lane 2: 100 mM imidazole elution from cobalt column. Lanes 3-4: 0.5 M imidazole elution. Lane 5: Isolated fraction from the Sephacryl S500 exclusion column. ExeD was expressed at 15 °C overnight with 100 mM IPTG.

3.1.2 Determining the Native Conformation of Multimeric ExeD and Its Corresponding Ion Conductivity

After expression and isolation at each of the three temperatures, we started work on determining the open pore current of ExeD. Although Nouwen et al. (1999) had used the homologue PulD in previous work, no information about the open pore current could be found in any published materials. We used four criteria for determining the correct open pore current for ExeD: 1) having a reproducible level of conductance 2) a patch clamp visualization that resembles that of other pores (Figure 20), 3) graphing the pore's conductivity as a function of voltage and comparing it to that expected from the literature (Meng et al., 2010**),** and 4) seeing multiple pores insert in similar increments (e.g. a 135 pA insertion going from 0 to 135 pA, and again from 135 pA to 270 pA, (Figure 21). Patch clamp displays of each of the commonly seen pores are shown in Figure 22, followed by a brief discussion of their characteristics. It is important to note that a small amount of variance is allowed between currents across individual pores, usually in the range of ±5 pA. Thus two ExeD multimers at 135 pA may have a total open pore current of 270 pA or slightly more or less. Figures 22 and 23 show the results of commonly occurring structures, including patch clamp displays and event histograms. Note that each block of time represents 0.5 seconds, as shown in Figure 21.

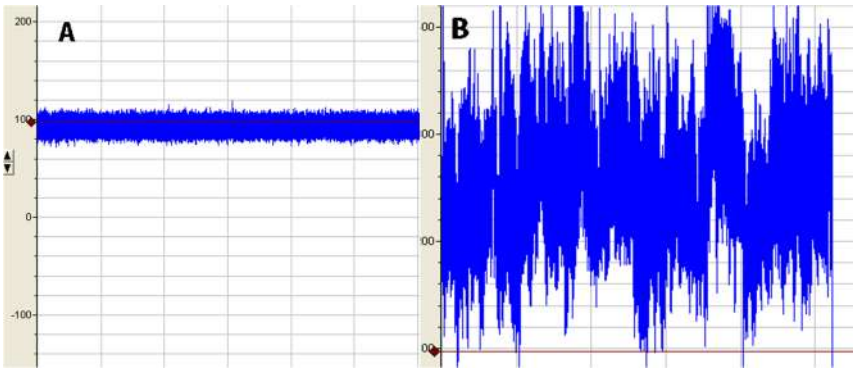

Figure 20: Patch Clamp Visualization of Pores Formed in Lipid Bilayer Experiments. A- A properly formed pore, in this case α-Hemolysin. B- A malformed pore that allows translocation of ions but does not appear to be properly formed. This example was taken from an experiment using ExeD.

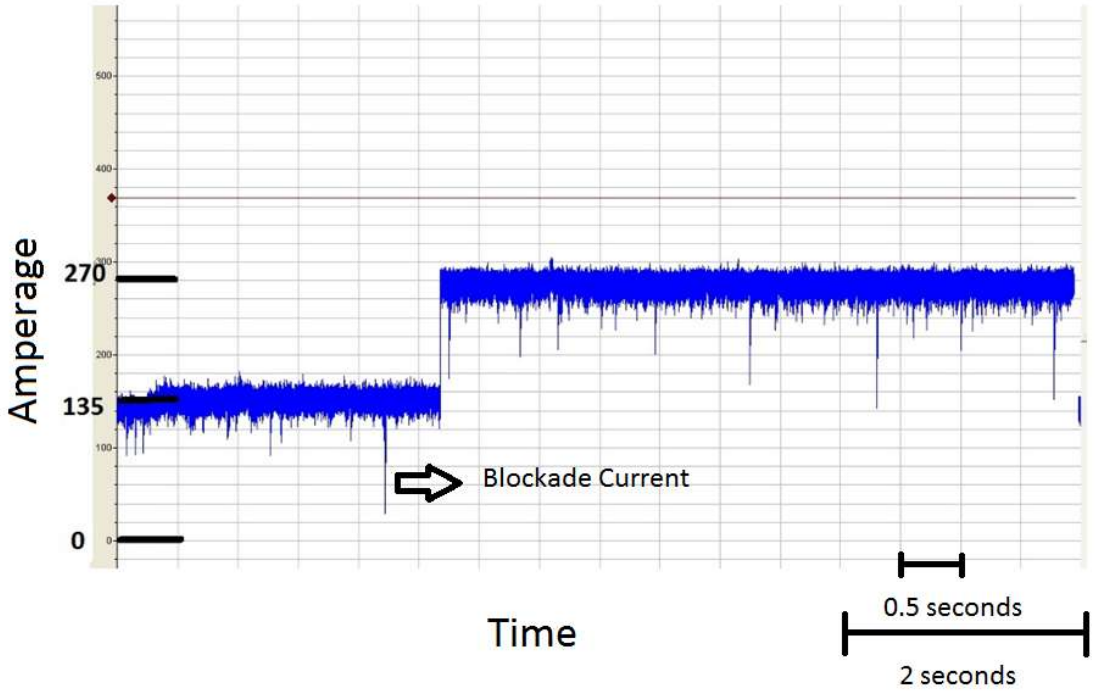

Figure 21: Single Pore Insertions. Evidence for the presence of a properly formed pore is provided by similar insertion events. Pictured is a single pore insertion of ExeD changing the open pore current from 135 pA to 270 pA, representative of a second 135 pA pore inserting into the lipid bilayer.

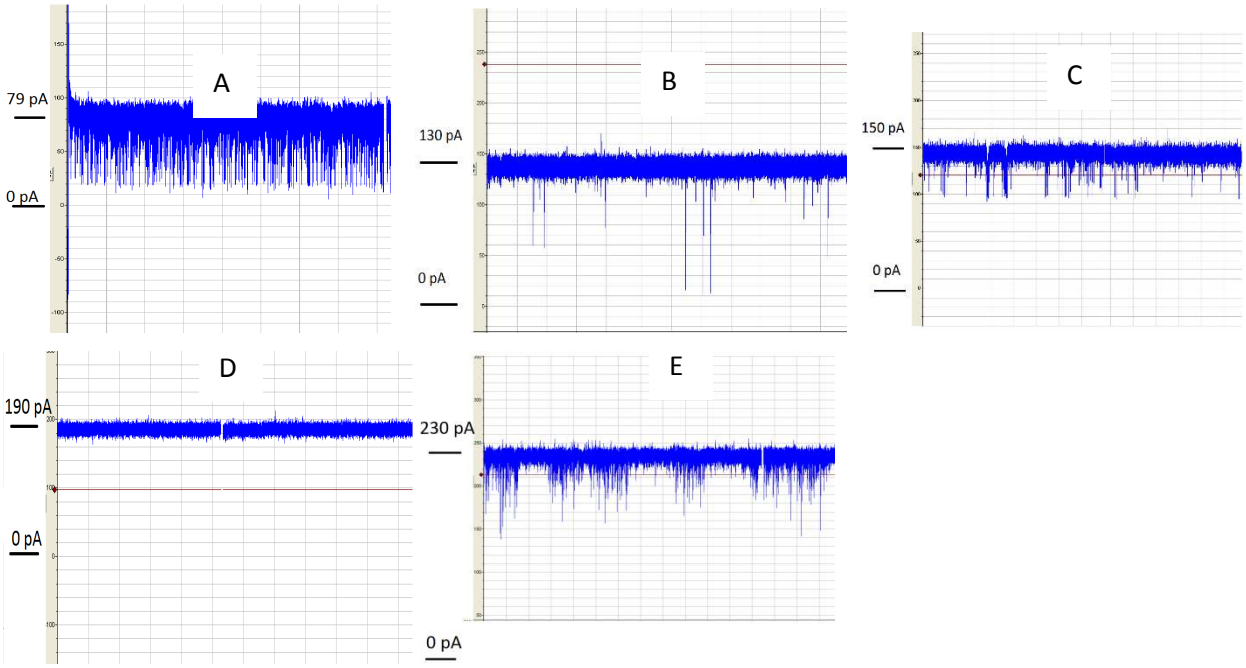

Figure 22: Patch Clamp Visualization of Commonly Formed Pores across a Range of Temperatures. A - Pore formed with a 79 pA current. B - Pore formed with a 135 pA current. C - Pore formed with a 150 pA current. D - Pore formed with a 190 pA current. E - Pore formed with a 220 pA current.

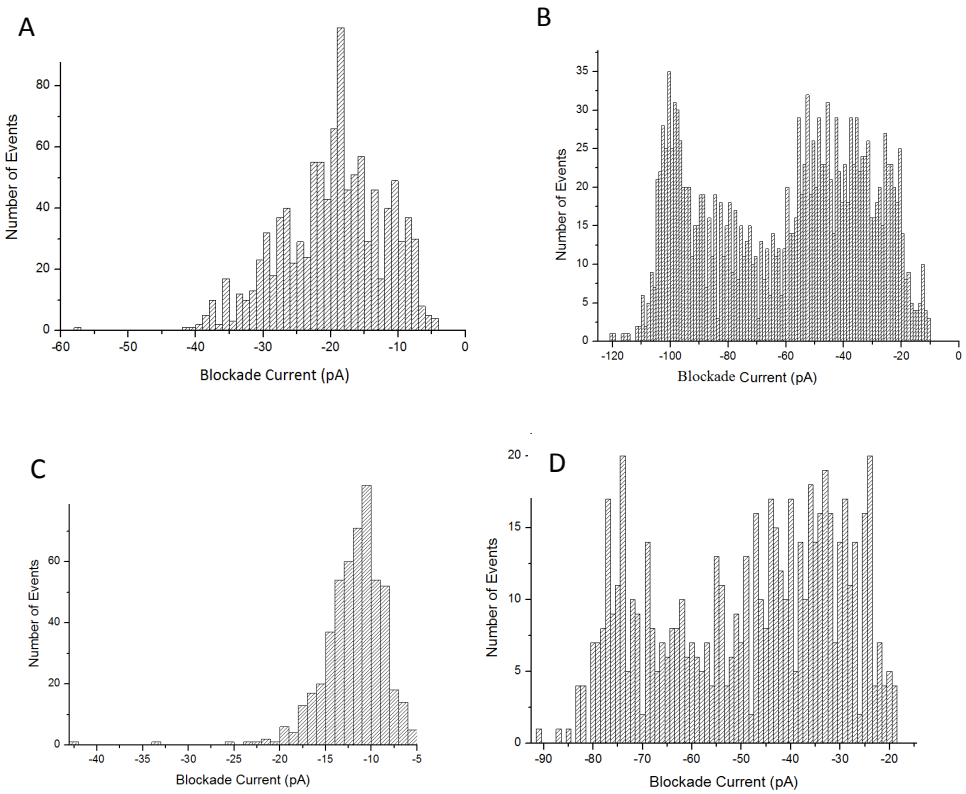

Figure 23: Distribution of Gating Events for Pores Formed Across a Range of Potentials at +100mV. A- Pore formed with a 79 pA current. The single gating peak centers around 20 pA. B- Pore formed with a 135 pA current. Dual peaks center at -100 pA and -40 pA. C- Pore formed with a 150 pA current. A single peak is evident at -12 pA. D- Pore formed with a 220 pA current. This pore produces dual peaks at -40 pA and -75 pA. Note that no distributions are available for the 190 pA pore as this pore gives no gating events.

At 37 °C the formation of the pore occurs with some variability. Part of the reason for discrepancies between ExeD multimers at this temperature likely relates to the transition from a monomer to a multimer over the course of the purification process, rather than forming multimers at the time of induction (as discussed previously and shown in Figure 16). The open pore currents (as measured at +100 mV) produced by expression at this temperature varied between 190 pA, 150 pA, and 135 pA (Figure 22 – D, C, B). Of these structures, insertions at 135 pA are most likely to occur, but it is not uncommon for a pore to insert at 150 pA, be ejected from the bilayer, and have a different pore reinsert at 135 pA. Pore structures for 135 and 150 pA show similarities to other pores in that they possess low background noise levels, have linear

current vs. voltage graphs (Figures 23 and 24), and gating events can be detected on the patch clamp apparatus. However, gating events at 135 pA tend to produce two visible Gaussian distributions**,** whereas a 150 pA pore produces only a single peak (Figure 23 - B, C). At 190 pA, the pore formed is able to conduct KCl but does not show gating events (Figure 22 - D). Voltage versus time graphs show that the trend for these pores are all nearly entirely linear (Figures 24-26) – note that we name the pore based on the measurement of the open pore current at +100 mV. Even upon addition of high amounts of DNA, very few if any interactions are observed (Figure 27). Evidence indicates that although a 190 pA pore looks like an ideal candidate for nanopore analysis, the formation prevents meaningful interactions from occurring.

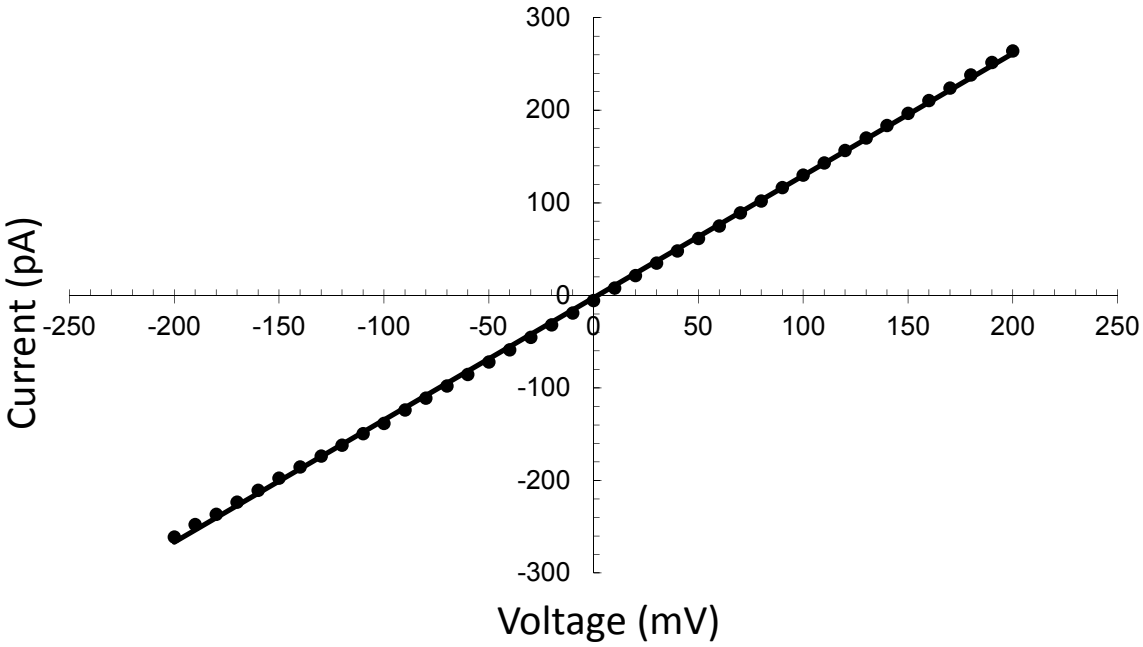

Figure 24: Voltage vs. Current Graph Using a 135 pA Pore at +100 mV. The graph is almost entirely linear with the exception of very small deviations at either extreme voltages (±200 mV).

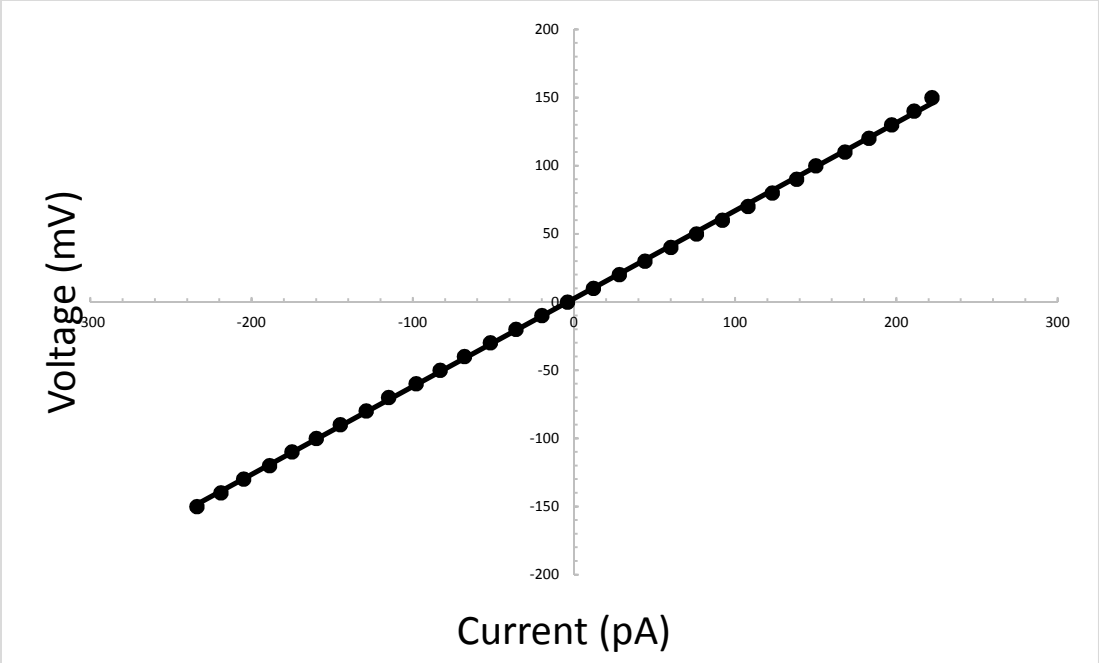

Figure 25: Voltage vs. Current Graph Using a 150 pA Pore at +100 mV. The graph is largely linear but bows slightly throughout.

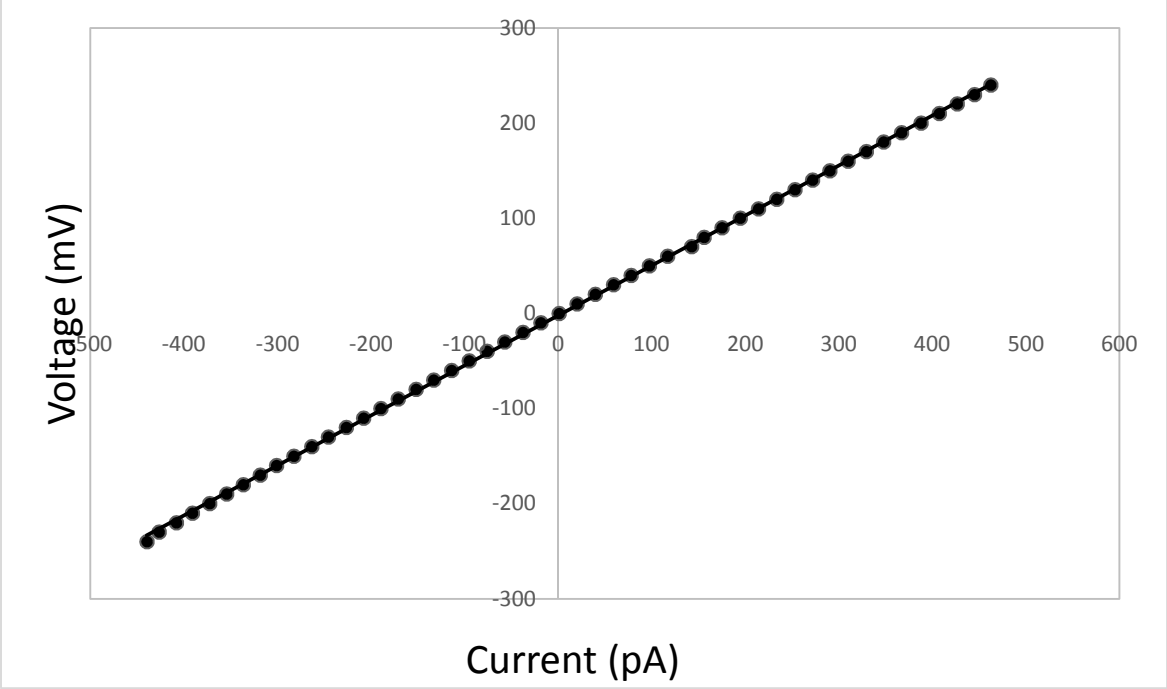

Figure 26: Voltage vs. Current Graph Using a 190 pA Pore at +100 mV. The graph is almost entirely linear but bows slightly throughout.

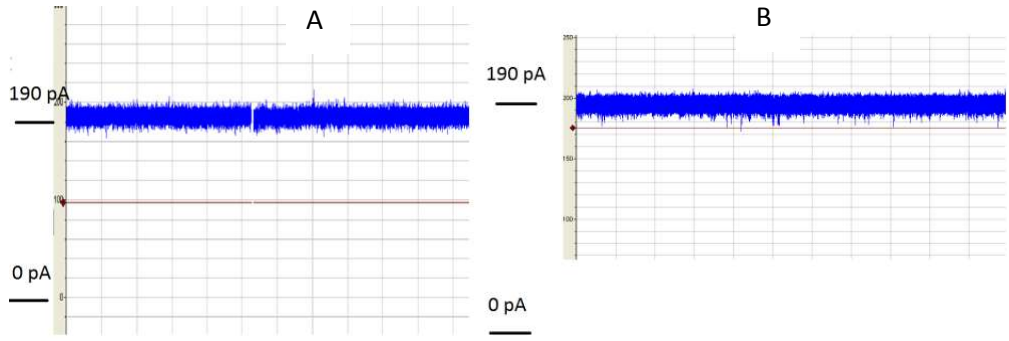

Figure 27: Patch Clamp Visualization of ExeD at 190 pA with and without DNA. A- Before addition of DNA. B- After addition of 150 µg of DNA. No changes are seen.

After expression at 26 °C, pores have a tendency to occur at 150 pA, 135 pA, 230 pA, and 80 pA (Figure 22 – C, B, E, A). However, of these four structures, the 150 and 135 pA are seen far more often. These two conformations still show the pore characteristics previously mentioned. At 80 pA, the ExeD structure shows extremely high levels of gating (Figure 22-A, Figure 23-A). These events produce a single peak around 20 pA, but the voltage vs. current graph provides evidence that the pore is malformed resulting in repeated and spontaneous collapse at various voltages (Figure 28). Problems also arise in the 220 pA pore, which shows large bursts of events for a few milliseconds and then closes for another few milliseconds, repeating this cycle throughout the experiment (Figure 22 - E, Figure 23 - D). Pores producing this current are short lived and difficult to analyze extensively, though the current vs. voltage graph shows only minor deviations from a linear line (Figure 29).

ExeD multimers formed at 15 °C occur almost exclusively at 135 pA (Figure 22 - B, Figure 23 - B). Gating events resemble those seen at the 26 °C and 37 °C formations. Very rarely a 150 pA multimer is inserted (Figure 22 – C, Figure 23 - C), possessing all the attributes previously mentioned. When pores have identical structures, they also have identical ion conductivity. Strong evidence for outer membrane pores having the same quaternary structure is provided when two or more pores insert in succession and they increase the open pore current in even increments (i.e. from 135 pA to 270 pA). The only dodecamer which was able to insert in

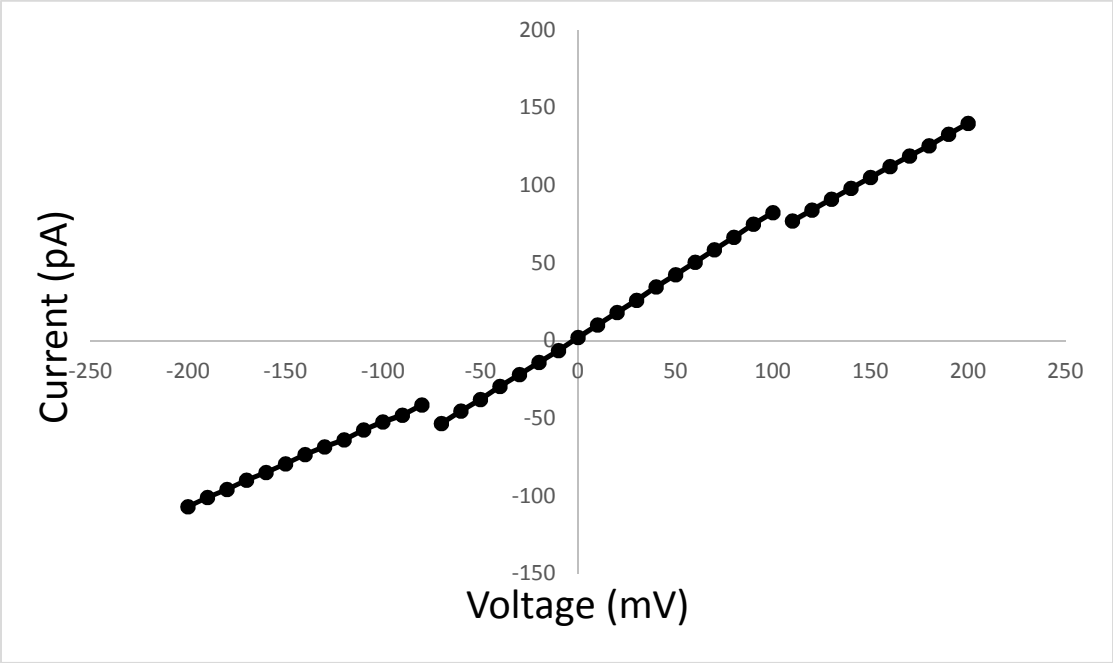

Figure 28: Voltage vs. Current Graph Using an 80 pA Pore at +100 mV. At -70 mV and +100 mV the pore rapidly opens and closes, stopping ion flow entirely and causing the observed breaks in the graph.

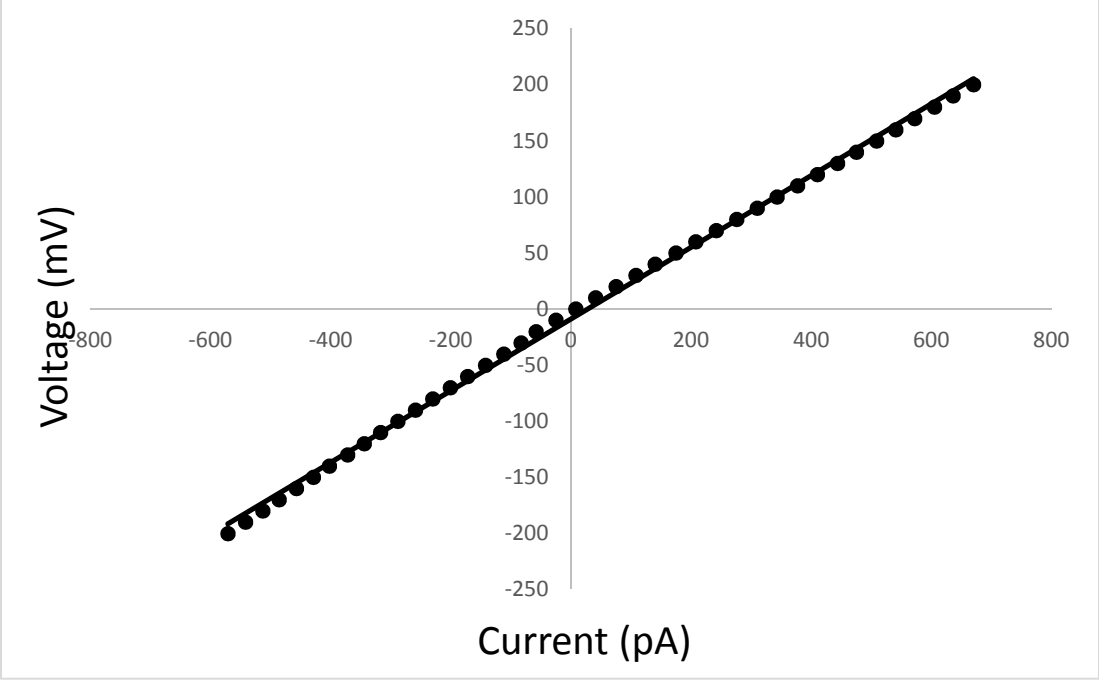

Figure 29: Voltage vs. Current Graph Using a 220 pA Pore at +100 mV. The graph is noticeably less linear than previous pores.

even increments was the 135 pA pore (Figure 21). Based on the common 135 pA insertions across a range of temperatures, the linear conductance graphs, its resemblance to other pores, and predictable incremental increases when a second pore is inserted, the most likely pore representing the native ExeD homododecamer is the 135 pA pore.

Our work gave evidence that there are different conformations of the multimer other than the native form. The 5 open pore currents described above indicate that the channel may form different sized openings within the lipid bilayer. We believe that the 135 pA OPC represents the native conformation, but how the other open pore currents are produced remained unclear. One theory is that the ExeD subunits may be associating rapidly after translation and misaligning to produce the dodecamer. Another transmembrane protein, *Escherichia coli* multidrug resistance protein (EmrE) has several multimeric forms depending on protein and detergent concentration (Bay et al., 2010), and human plasma paraoxonase has different conformations depending on the detergent used to solubilize it (Josse et al., 2002). An alternate explanation is that the pores produced are partial assemblies of ExeD not involving all of the 12 subunits. To delineate these two theories, we examined the sizes of the multimers used in our experiments as a function of the temperature in which they are produced. The Western blot shown in Figure 30 shows that the size of the ExeD multimer, after purification, is the same across all three temperature experiments. The native dodecamer is shown in Figure 31 and has the same molecular weight as those seen in Figure 30.

A caveat should be stated here however: small differences in sizes when working with structures nearing a million kD becomes quite difficult using only a 3-8% gel, and definitive results cannot be obtained. But this experiment does give evidence against significantly larger or smaller structures than the native dodecamer of ExeD being used for nanopore experiments, and it may be that the multimers formed are the same size as those found in *Aeromonas hydrophila*.

It should also be noted that the multimers produced in the 26 ºC and 37 ºC conditions are mostly the result of monomers oligomerizing during the purification process, and not during the expression phase. It is possible that the detergents used in the purification process are causing ExeD to multimerize incorrectly, but we have been unable to further test this theory.

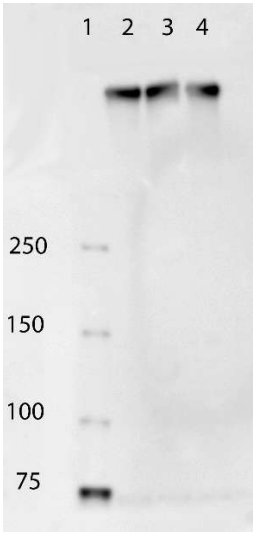

Figure 30: Western blot of Temperature-Dependent Multimeric Products. Lane 1 – His-tagged protein standard. Lane 2- Multimer from 37 °C at 100 mM IPTG expressed overnight and purified through detergent extraction, affinity, and size-exclusion chromatography. Disappearance of the monomer from this experiment may be related to how long the extract was allowed to incubate with detergents and lipid during the purification process. Lane 3- Multimer at 26 °C with the same conditions as in lane 2. Lane 4- Multimer at 15 °C with the same conditions as in lane 2. Samples are resolved on a 3-8% gradient gel.

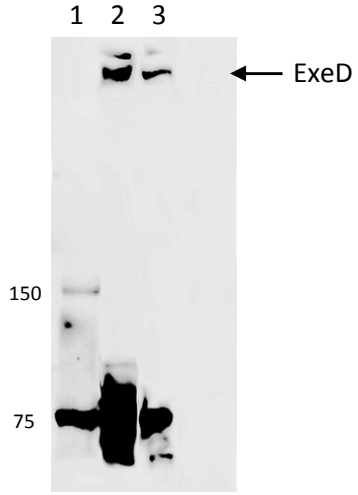

Figure 31: Comparison of Native ExeD in *A. hydrophila* to Recombinant ExeD in *E. coli*. Anti-ExeD antibody was used in a Western blot to detect the presence of ExeD in 2 cell fractions. Lane 1- protein standard. Lane 2 shows native protein production in *A. hydrophila* in a whole cell fraction, and lane 3 shows expression in *E. coli* under control of the pET-30(a) vector after isolation of the membrane fraction. Both the multimer and monomer recombinant were shown to be the correct size.

3.1.3 Pore Insertions Using Either Proteoliposomes or Acetone Precipitation

In previous work done by Nouwen et al. (1999), proteoliposomes were used to help the GspD pore merge with the lipid bilayer. The researchers used a chemical gradient of KCl (400mM in the *cis* chamber to 100mM *trans*) to facilitate movement of the proteoliposomes towards the micron hole within the Teflon wall. In their work, the applied voltage and chemical gradient were successful in helping the liposomes and bilayer to combine and produce a usable pore. Although this technique was successful, it is an unusual method for nanopore analysis. The difference in KCl concentrations between the *cis* and *trans* compartments leads to inconsistent Cl- ion flow as the salt concentrations change when chloride moves down its concentration gradient. This in turns results in inconsistent open pore currents being produced, higher levels of background noise, and DNA or peptide interactions being more difficult to interpret because the size of the blockade current depends upon salt concentrations in the chamber. Standard conditions require equal amounts of KCl on both the *cis* and *trans* side of the opening, and the concentrations of salts used are often much higher (1M KCl compared to 100 mM KCl; Smeets et al., 2006).

Initially we used the protocol established by Nouwen et al. (1999) for forming proteoliposomes and merging them with the bilayer. We were successfully able to replicate their work and produce multimers for our own experiments, though for the aforementioned reasons this protocol could not be used since we intended to investigate DNA and peptide interactions. Instead we wanted to create a simpler, quicker, and more direct method for working with ExeD in patch clamp. We turned our attention to ExeD's structural stability as a basis for an alternative protocol. We first expressed ExeD at 15 ºC, and purified it as discussed. We then took the purified extract from the size-exclusion column and added it directly to acetone in a 1:4 ratio. The precipitate was resuspended in buffer and added directly to the *cis* chamber, then the bilayer was thinned, broken, and reformed to facilitate insertion of the pore.

Figure 32 shows the patch clamp display of a pore formed using either proteoliposomes or an acetone precipitate. Across several experiments, evidence indicates the pores formed were identical. The conductance levels of both pores were found to consistently be 135 pA and the gating events had identical profiles.

It is unusual for an acetone precipitate to be able to maintain protein activity, though across dozens of experiments using both proteoliposomes and the acetone precipitate, we found the results reliable. Once we developed a consistent method for making and inserting the acetone-purified ExeD extracts, we switched from using proteoliposomes to using only the acetone protocol. Proteoliposomes were used for establishing the different open pore currents of ExeD, and for our initial tests in determining the A and B orientation of the pore (to be seen shortly). The remaining experiments, including some of the A and B pore orientations, were done using only the acetone protocol. At the point where we had started investigating the A and B insertions of the pore, we had already established the best ideal method for making pores which produced mostly 135 pA currents. Consequently, when the acetone precipitation was started, we did not repeat experiments looking at when multimers with different open pore currents were produced. There is still the possibility that an abundance of lipids in the proteoliposome protocol could have produced these OPC variabilities (see Discussion Section 4.1).

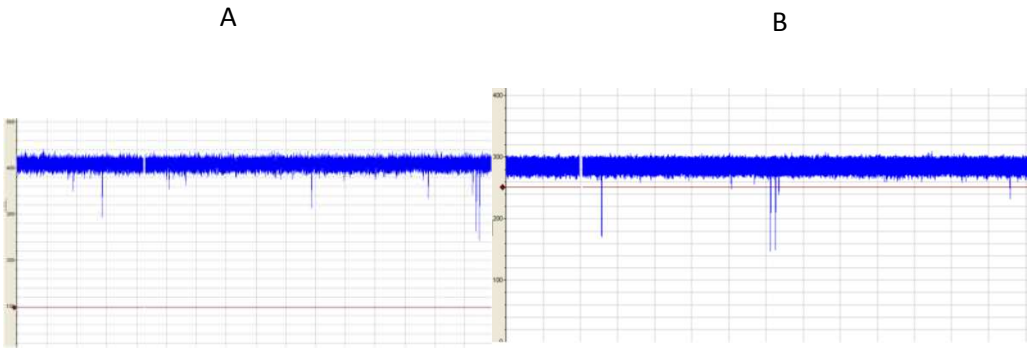

Figure 32: Patch Clamp Visualization of Pores Formed by both Proteoliposomes and Acetone Precipitation. A- Pore formed using proteoliposomes. B – Pore formed using acetone precipitate. Both openings occurred in increments of 135 pA.

3.2 Insertion of Multimeric ExeD into the Lipid Bilayer May Occur in One of Two Orientations

3.2.1 Introduction

In the absence of a chemical gradient to aid in the merging of ExeD with the lipid bilayer, pore formation relied upon continually breaking the bilayer and waiting for spontaneous insertion of the multimer when the bilayer reforms. This was done by applying a strong voltage to the membrane to first break it, then reforming the membrane using the suction of a syringe. The suction forces the pore towards the reforming bilayer and aids in insertion. An unexpected side-effect of this method was the pore orienting itself in one of two directions upon insertion. This is believed to arise because the bilayer reforms around the pore as it approaches, instead of the pore spontaneously inserting itself into the bilayer. These two orientations are not likely to occur in ExeD's native environment, but rather result because of the methods needed for insertion in the patch clamp system.

The two directions ExeD can face are either with the vestibule facing the *cis* chamber or with the stem facing the *cis* chamber. It has not been possible to determine which side the vestibule of ExeD faces when in the bilayer, so the orientations are termed A and B based upon their prevalence. Fortunately, the orientations can be distinguished based upon pore conductance at +/- 100 mV. +100 mV in the A direction has a different patch clamp display than +100 mV in the B direction and a cursory visualization can be done to identify which orientation the pore is inserted. We found that the A direction was more prevalent than the B direction in our setup.

3.2.2 The More Common "A" Orientation and Its Conductance Characteristics

ExeD primarily inserts into the bilayer in one direction under the influence of a positive potential. This insertion has been termed the "A" state due to its preferential formation. At positive voltages two gating events are seen, centering at -30 pA and -100 pA (Figure 33**)**. At negative potentials, the A state has mostly small blockade currents around +20 pA, but has large gating events scattered from +20 to +100 pA (Figure 34). Relative to the small blockade currents, larger events are significantly less common and make up only a small percentage of measured events.

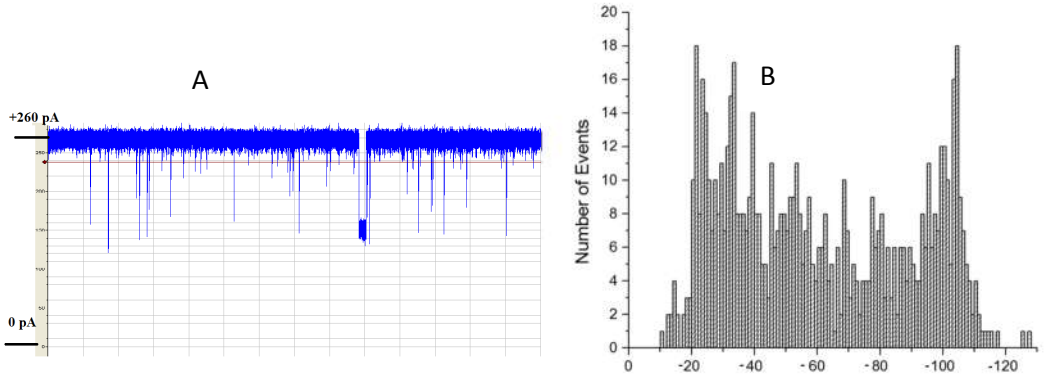

Figure 33: 135 pA ExeD at +100 mV Inserted in the A Direction. Left- Patch Clamp visualization of the pore. Right- Distribution of gating events as measured by brief changes in the pore current. Peaks center at -30 pA and -100 pA.

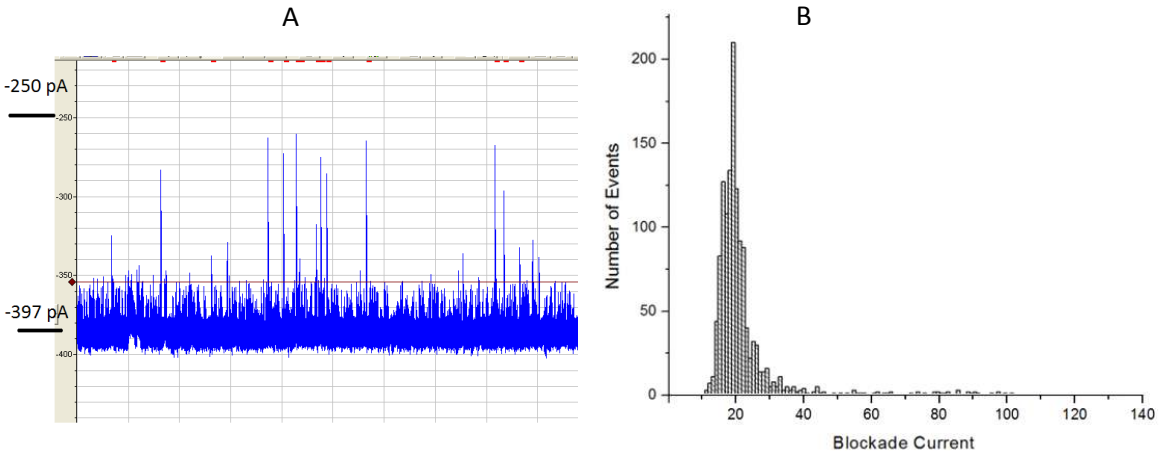

Figure 34: 135 pA ExeD at -100 mV Inserted in the A Direction. A- Patch clamp visualization of the pore. Three ExeD multimers are present during this experiment, bringing the open pore current up to approximately -397 pA. B- Distribution of gating events as measured by brief changes in the pore current. Blockade currents are mostly small at +20 pA, but have random large blockade events scattered up to +100 pA.

3.2.3 The Less Common "B" Orientation and Its Conductance Characteristics

Occasionally a second type of insertion is seen when precipitated ExeD is added to the *cis* chamber. This formation, termed the "B" state, is identical to the A state except that the pore is facing the other direction. Evidence for this is provided by measuring the gating events between the two insertions. In the A state, 2 blockade current peaks are found at positive voltages at -30 and -100 pA. Negative voltages produce a single peak at +20 pA. In the B state,

positive voltages produce a single peak at -20 pA and negative voltages produce a double peak at +100 and +40 pA (Figure 35, Figure 36). A patch clamp display of an experiment with a B orientation (shown in Figure 35 - A) has at least four pores inserted in the B direction simultaneously (the experiment measured a +520 pA current, representing four pores in the B orientation at 135 pA +/- 5 pA each).

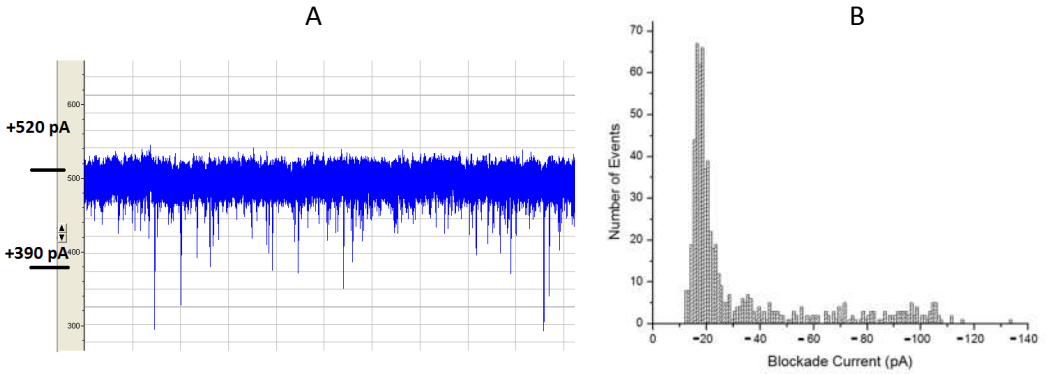

Figure 35: 135 pA ExeD at +100 mV Inserted in the B Direction. A- Patch clamp visualization of the pore. B- Distribution of gating events as measured by brief changes in the pore current. A single peak is visible at -20 pA. Four pores are evident in this experiment as shown by the patch clamp apparatus detecting a +520 pA open current.

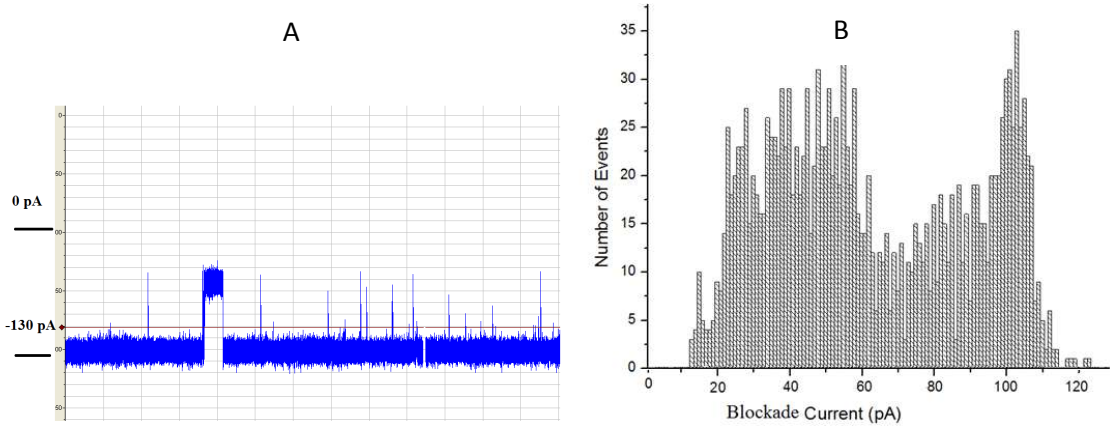

Figure 36: 135 pA ExeD at -100 mV Inserted in the B Direction. A- Patch clamp visualization of the pore. B- Distribution of gating events as measured by brief changes in the pore current. Peaks center at +100 pA and +40 pA.

3.3 ExeD Changes Its Conductance and Gating Depending upon Environmental pH

3.3.1 Introduction

A research paper published by Spagnuolo et al. (2010) showed that there are several specific regions in secretin pIV that control gating of the pore. We theorized that altering the environmental pH of the homologue ExeD would protonate or deprotonate key amino acids in these regions and that this would in turn affect the ability of the pore to open and close spontaneously.

For all work done hereafter, we wanted to only use the A orientation of the pore to promote consistency across experiments. However, inserting the secretin into the lipid bilayer is a difficult process that can at times take weeks to obtain. If a pore inserts in the B direction, it is possible to reverse the applied potential and obtain a pore that is essentially in the A direction. To compensate for the reversed potential, when a molecule is added to the perfusion cup, instead of being added to the *cis* chamber it is instead added to the *trans* chamber. This allows pores inserted in the B orientation to be compared to pores inserted in the A direction. This method was used only sparingly, and experiments done with this technique were considered only preliminary until the experiment could be repeated with the A orientation.

3.3.2 Patch Clamp Display, Measured Conductance, and Gating Levels at pH 5.0

We first examined pore conductivity at pH 5.0. This pH was used because it was still reasonably easy to obtain ExeD insertions within the bilayer and the lipids were able to remain stable for extended periods of time. We found that a single pore inserted at 135 pA and the spontaneous closing of the pore was frequent (Figure 37). The conductivity of the pore changed linearly with increasing voltage (Figure 38), with the trend line crossing the Y-axis at 3 pA. The majority of the gating events at pH 5.0 were small and centered around +15 pA (Figure 39).

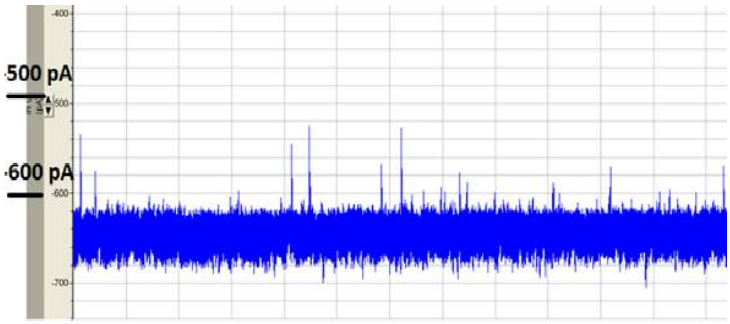

Figure 37: Patch Clamp Display of ExeD Gating Events at pH 5.0 and -100 mV. The patch clamp display shows intermittent large gating events of around -60 pA, but the majority of the events are small (< -20 pA) and brief.

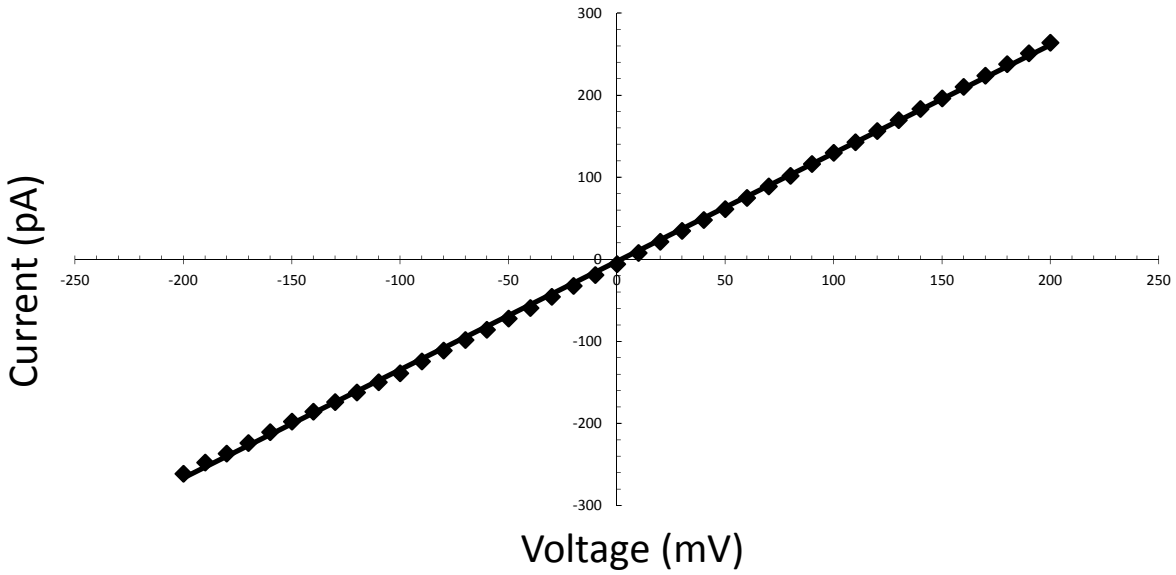

Figure 38: Voltage vs. Current Graph of ExeD at pH 5.0. The graph bows only slightly throughout the measured values. These results are nearly identical with the pore shown in Figure 24 measuring the conductivity of ExeD at pH 7.4.

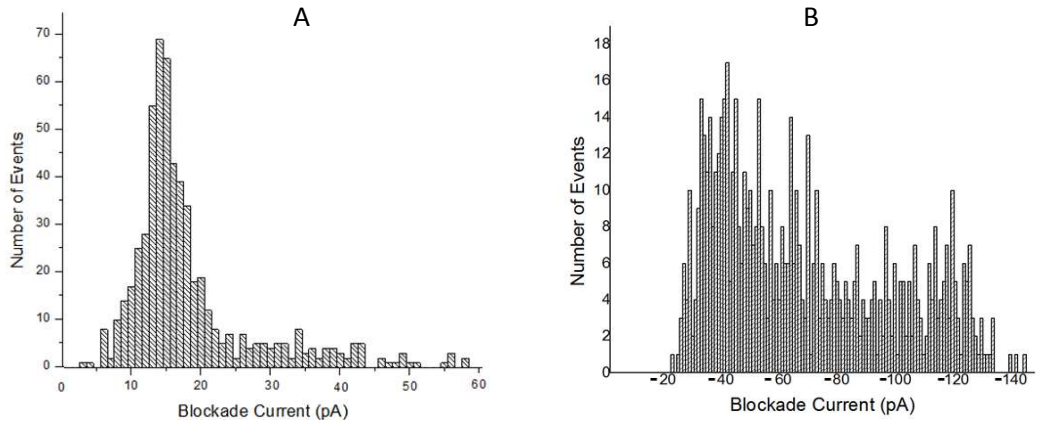

Figure 39: ExeD Gating at pH 5.0 Measured at -/+ 100 mV. A - A singular peak at approximately +15 pA is visible when the conductance is measured at -100 mV. B – Dual peaks at approximately -40 and -120 pA are visible at +100 mV, though the peak at -40 mV predominates.

3.3.3 Patch Clamp Display, Measured Conductance, and Gating Levels at pH 7.4

Most patch clamp experiments are done around pH 7.4 so as to mimic cellular conditions. We performed experiments at pH 7.4 to approximate some of the conditions that the outer membrane protein ExeD experiences in its native environment.

At this environmental pH, gating was frequent and resembled the events seen at pH 5.0. However, at pH 5.0 and -100 mV, large events reached a maximum of +60 pA (Figures 37 and 39 A). At pH 7.4, large uncommon events at the same voltage could reach upward of +100 pA (Figures 40 and 41 A). The level of conductance in response to applied voltage (Figure 42) was nearly identical to that seen at pH 5.0 (Figure 38), with the trend line crossing the Y-axis at a positive conductance of 3 pA. This indicates that the pore is weakly selective for cations. Distribution of events at pH 7.4 seemed to be more localized as +/- 100 mV peaks were narrower and less scattered than pH 5.0 as seen in Figure 39.

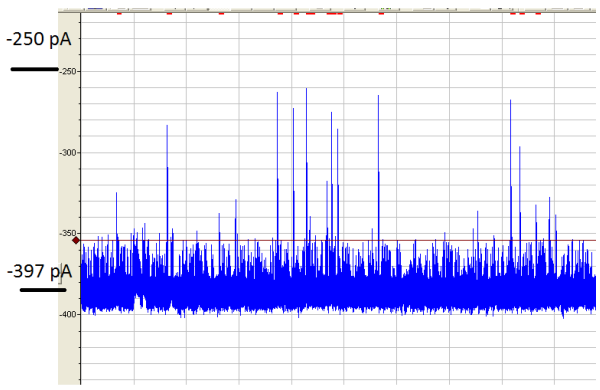

Figure 40: Patch Clamp Display of ExeD Gating Events at pH 7.4 and -100 mV. The patch clamp display shows that ExeD at pH 7.4 produces mostly small blockade events which are usually less than -18 pA, but large blockade events occur as well which can range up to -100 pA.

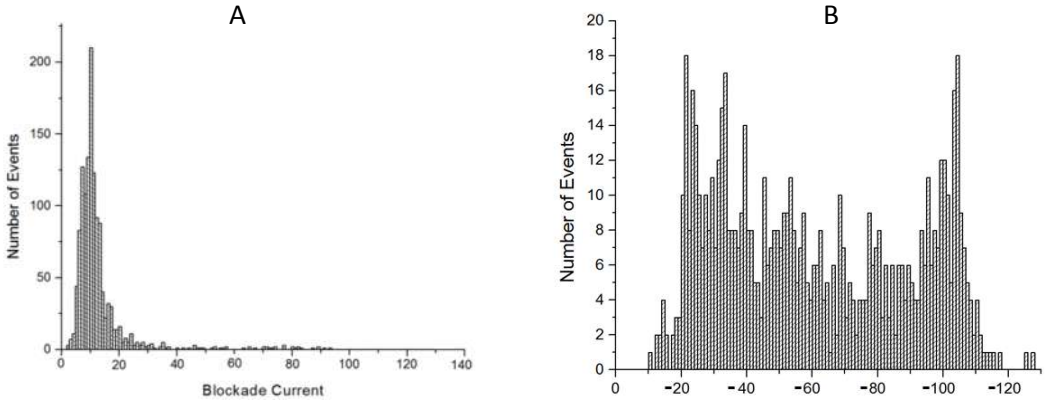

Figure 41: ExeD Gating at pH 7.4 Measured at -/+ 100 mV. A - A singular peak at approximately +18 pA is visible when the conductance is measured at -100 mV. B – Two peaks at -30 pA and -100 pA are visible at +100mV with the majority of events falling around the -30 pA area.

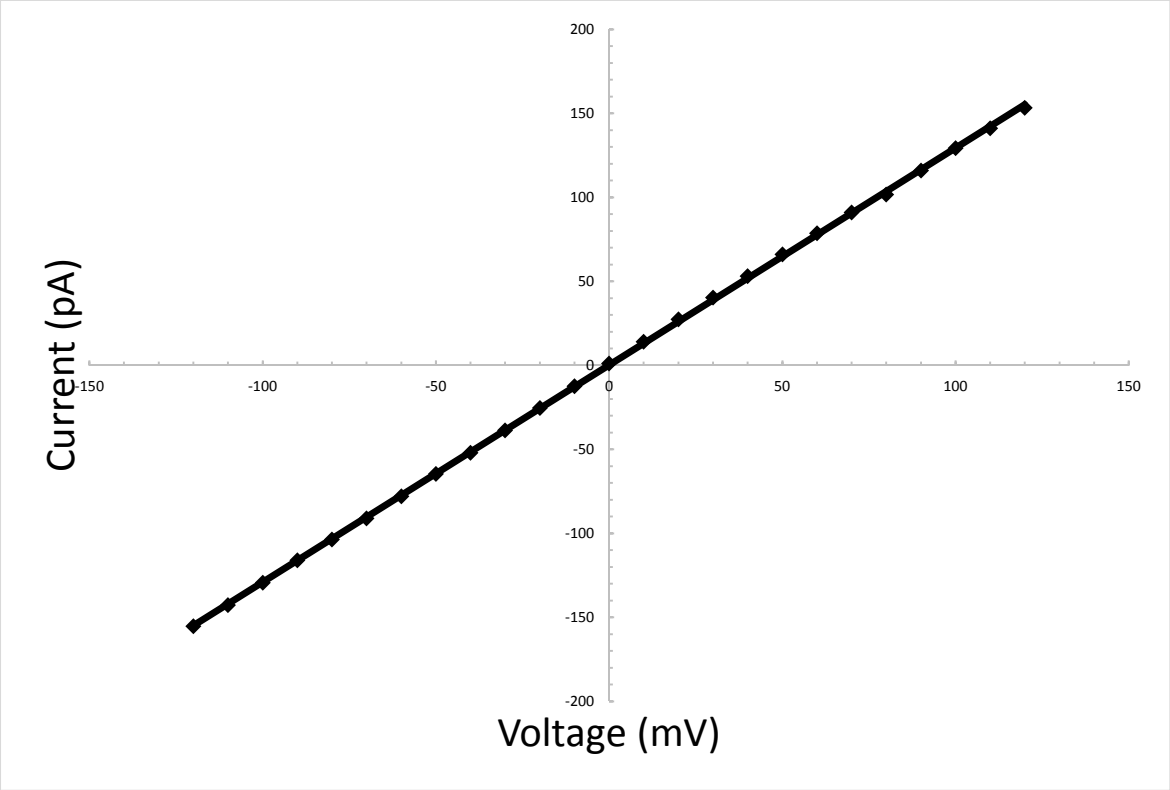

Figure 42: Voltage vs. Current Graph at pH 7.4. The graph is largely linear. Note that the trend line crosses the Y-axis at 3 pA, indicating that this pore is cationic selective.

3.3.4 Patch Clamp Display, Measured Conductance, and Gating Levels at pH 9.5

Our last set of pH experiments was done at a high pH level. We used pH 9.5 to investigate how the spontaneous opening and closing of the pore is affected by deprotonating any residues having a pKa in this range. Higher pH levels were attempted but the thin lipid bilayer was difficult to maintain over long periods as the pH approached 10.

We observed that the number of gating events at this pH decreased considerably. Measurements of these openings showed that at -100 mV they occurred almost exclusively in the range of 20 to 60 pA (Figures 43 and 44). At positive potentials, graphs no longer show dual peaks with different gating events (cf. Figure 41 B); instead only a single peak is evident at -40 pA. The open pore current also shifted noticeably at this pH (Figures 43 and 45). At +100 mV,

pores tended to have an OPC of 140 pA instead of the typical 135. Although there is always a +/- 5 pA difference between each individual pore in any patch clamp experiment, pH 9.5 experiments were almost exclusively 140 pA and varied +/-5 pA around this conductance.

Another interesting change we observed was ExeD's selectivity for charged molecules in the absence of an applied voltage. At pH 7.4 and pH 5, the conductance flow at 0 mV usually hovered around 3-4 pA. At pH 9.5, the conductivity dropped to -9 and -10 pA at 0 mV (Figure 45). This likely represents a complete reversal of the normal ionic selectivity from cationic to anionic.

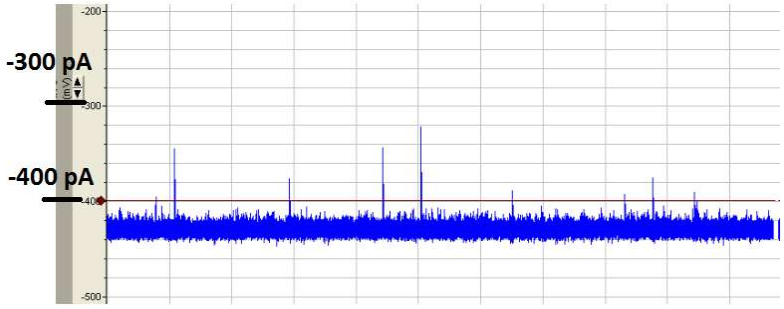

Figure 43: Patch Clamp Display of ExeD Gating Events at pH 9.5 and -100 mV. The patch clamp display shows that ExeD at pH 9.5 has far fewer background events than those seen at pH 5 or 7.4.

.

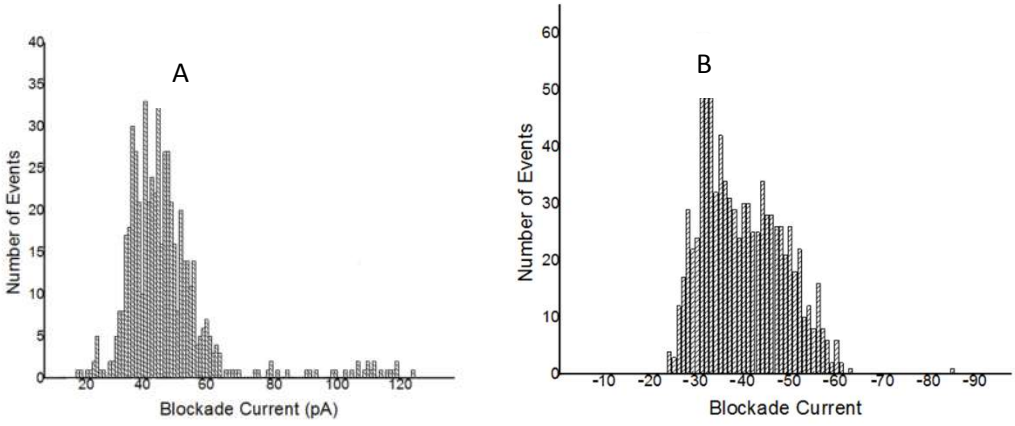

Figure 44: ExeD Gating at pH 9.5 Measured at -/+ 100 mV. A - A singular peak at approximately +45 pA is visible when the conductance is measured at -100 mV. B – A single distorted peak is found at -40 pA at +100 mV.

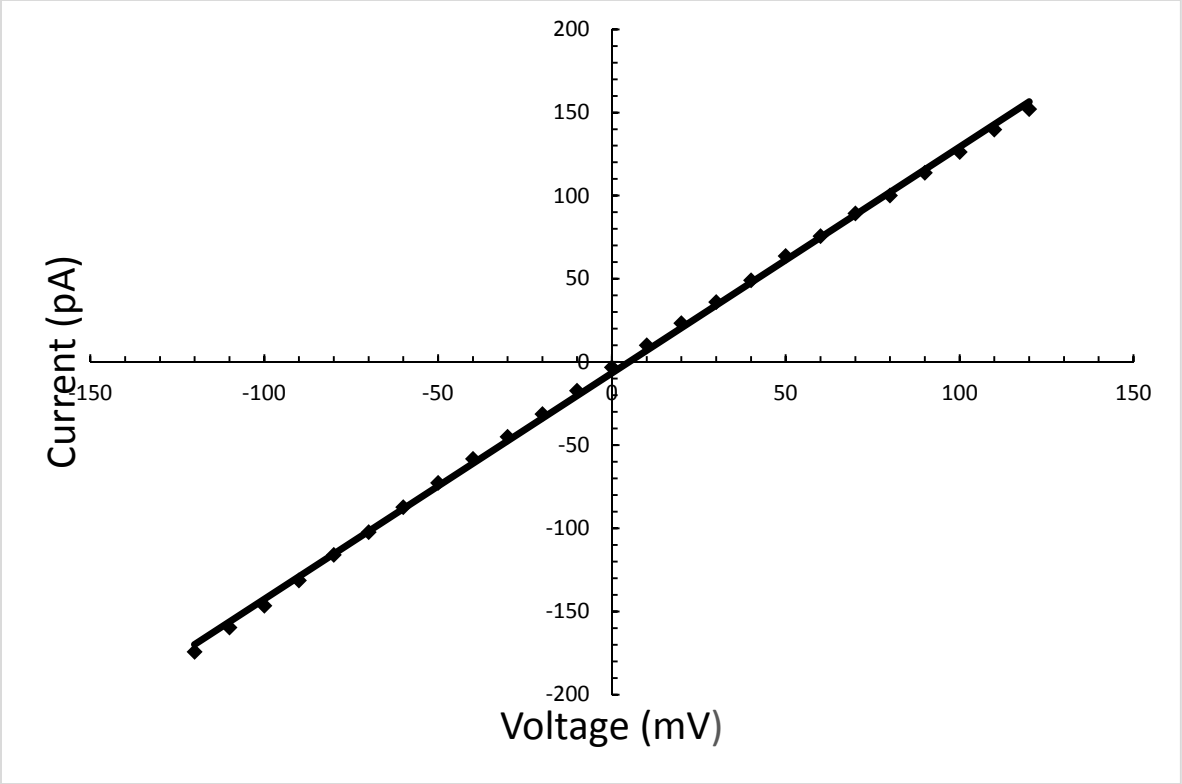

Figure 45: Voltage vs. Current Graph at pH 9.5. The graph is almost entirely linear. Note that the trend line crosses the Y-axis at -9 pA, indicating this pore is selective for anions.

We lowered the voltage during these experiments and noticed a unique trend (Figures 46-48). At positive voltages the gating of the secretin still occurred frequently (Figure 46 and Figure 48 B), but at negative voltages the spontaneous opening of the pore decreased considerably (Figure 47 and Figure 48 A). Background events remained present, but they were considerably less frequent than any other condition studied thus far.

It is important to note that in order to gather enough events to produce a graph at pH 9.5 +/- 50 mV, experiments are typically run for 3-4 hours. Conversely, at lower pH levels sufficient events can be gathered in approximately half an hour. This is an important difference when studying peptides and DNA. If the background events are too frequent, it becomes difficult to distinguish between the gating of the pore and pore-peptide interactions. The more infrequent background events are, the easier it is to establish event profiles for peptides or DNA.

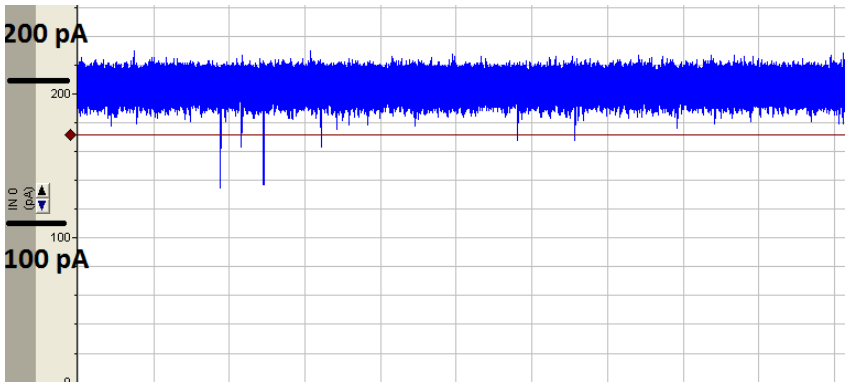

Figure 46: Patch Clamp Display of ExeD Gating Events at pH 9.5 and +50 mV. Despite the high pH value of the experiment and the low voltage, gating events still occur fairly frequently. The amount of baseline noise generated is comparable to that seen at higher voltages.

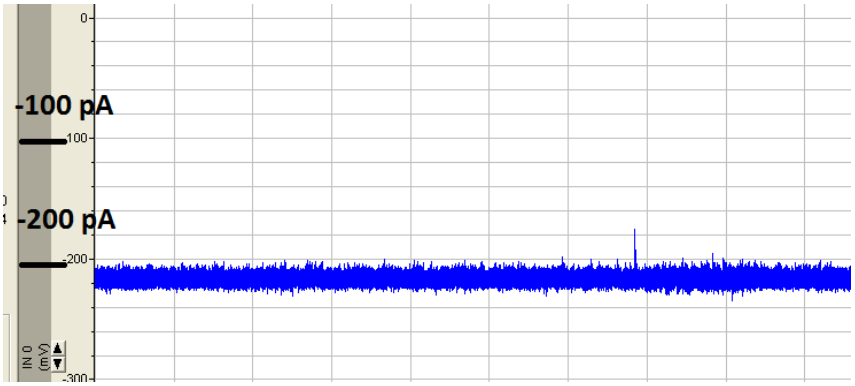

Figure 47: Patch Clamp Display of ExeD Gating Events at pH 9.5 and -50 mV. At high pH values and low voltages, gating of the pore drops to a negligible amount. Background noise is also extremely low.

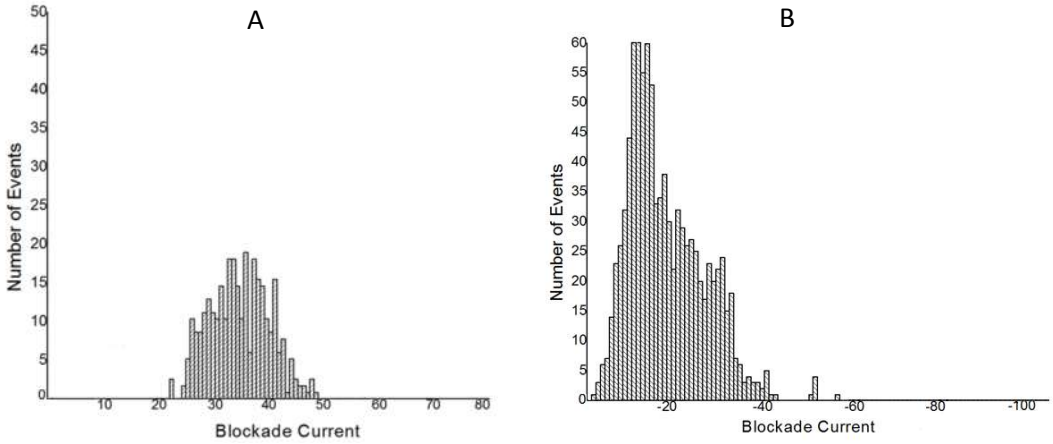

Figure 48: ExeD Gating at pH 9.5 Measured at -/+ 50 mV. A – At -50 mV, events tend to occur with low frequency and have a low average blockade current at approximately +35 pA. B– At +50 mV and high pH values, gating occurs much more often though the average blockade current is around -20 pA.

3.4 Rate of Gating Events

Our next series of experiments was performed to analyze the rate of gating events at different pH levels and voltages. We obtained pores at pH 5, 7.4, and 9.5 and counted gating events over the course of 1 minute at +/- 100, +/- 75, and +/- 50 mV. The results are shown in Figures 49 and 50.

The observed number of events declined with decreasing voltages. pH 7.4 and pH 5 follow similar trends at both negative and positive potentials, but pH 9.5 has an unusual distribution of gating events. Positive potentials yield more gating events at pH 9.5 than at either pH 7.4 of pH 5, but at negative potentials the trend disappears. Instead, at negative potentials the observed gating at pH 9.5 is far lower than at any other pH or condition, and remains low regardless of the amount of applied voltage. The low levels of gating at -50 mV became the basis for peptide and DNA analysis. Even though gating was still prevalent, we hoped that by running experiments at these low voltages the relative rate of DNA and peptide interactions would be high enough to detect amongst background events.

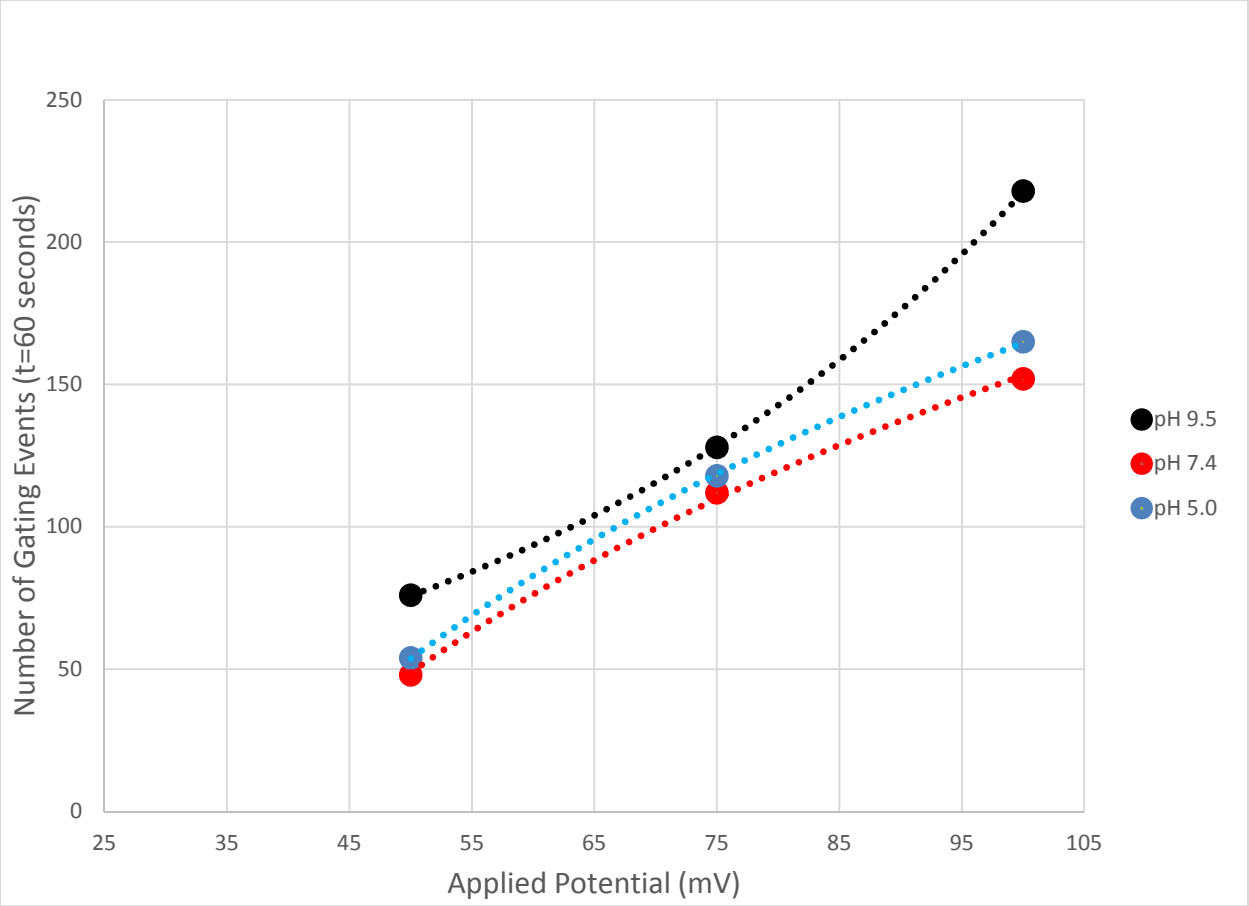

Figure 49: Gating Events as a Function of Positive Potential. Gating events for ExeD measured at positive potentials. The open pore current used was 135 pA +/- 5 pA. Three pH levels were tested at each of +50 mV, +75 mV, and +100 mV and the number of gating events were recorded over 60 seconds. Recordings at higher voltages were unable to be obtained due to the spontaneous closing of the pore.

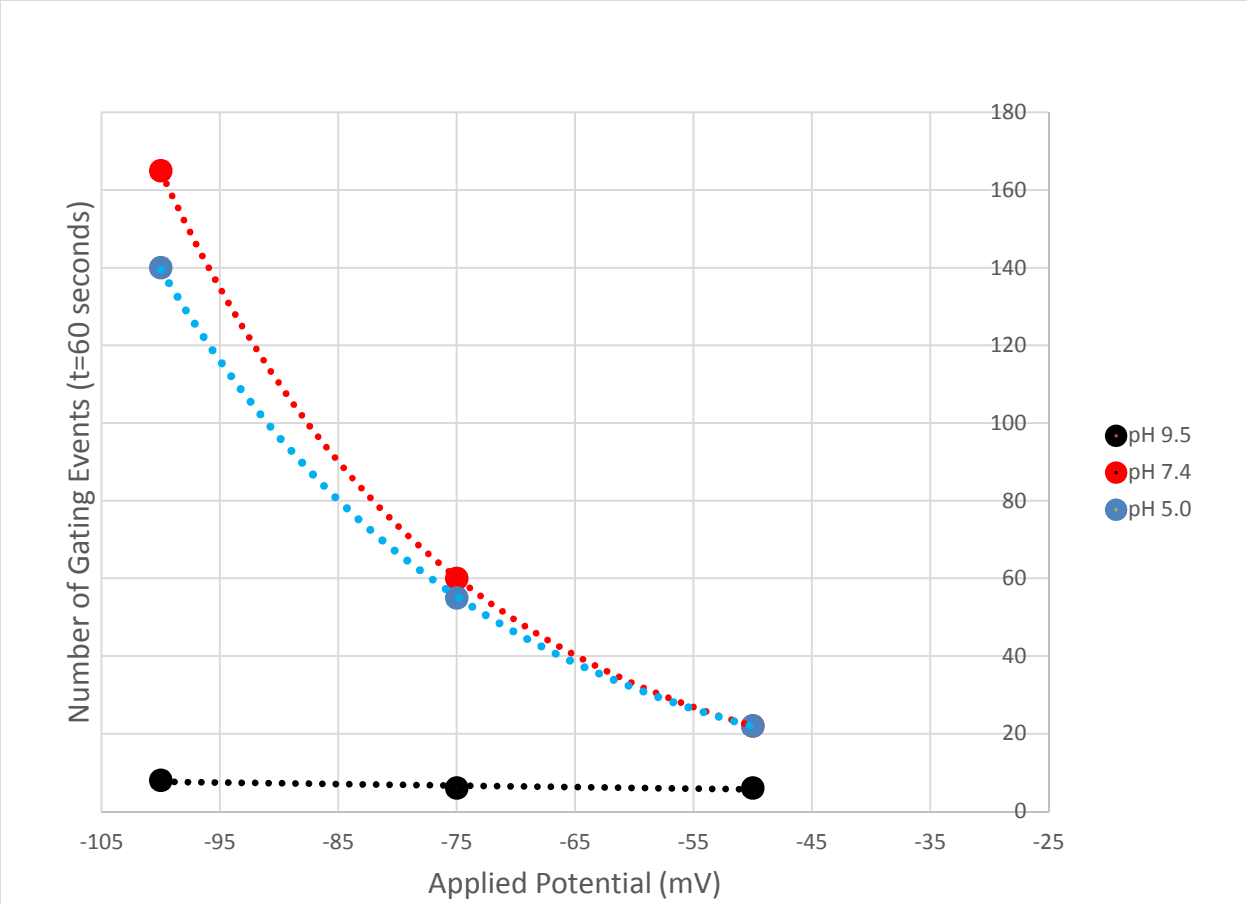

Figure 50: Gating Events as a Function of Negative Potential. Gating events for ExeD measured at negative potentials. The open pore current used was 135 pA +/- 5 pA. Three pH levels were tested at each of -50 mV, -75 mV, and -100 mV and the number of gating events were recorded over 60 seconds. Recordings at lower voltages were unable to be obtained due to the spontaneous closing of the pore.

3.5 ExeD Interactions with DNA at pH 7.4 and 9.5

The internal dimensions of the secretin range from 1-5 nm at its constriction point depending on whether the pore is in a relaxed or open state (Chami et al., 2005). ssDNA has a width of approximately 1 nm. We theorized that based upon the large open pore current of ExeD in the presence of an applied voltage, the inner constriction points of ExeD are not entirely closed while in the lipid bilayer, and that therefore the pore may be able to translocate ssDNA.

Although only the homologue secretin pIV has been shown to be involved with transport of DNA, the ExeD secretin is still large enough to accommodate the translocation of ssDNA. We added 10 µg/mL of ssDNA with a sequence of AAGGTCTCTC to the perfusion cup and observed the interactions with ExeD at pH 7.4 and pH 9.5. The DNA chosen was used as it was readily available from a previous experiment as excess primer. Both experiments were done at -50 mV as we believed this produces the lowest levels of background gating while also providing enough of an electrophoretic driving force to promote pore/DNA interactions. It was decided that the gating of ExeD at pH 5 was not significantly different enough from pH 7.4 to warrant further investigation.

When DNA is added to the perfusion cup at pH 7.4, only a single new peak is seen (Figure 51). The background gating events at +15 pA are visible, but a new peak is also seen at +22 pA. Figure 52 shows that at pH 9.5 two new peaks are now visible – the original gating events centered at +35 pA are still evident, but there are also peaks at +15 and +42 pA. When these two peaks are analyzed according to their time of interaction with ExeD (Figure 53), it is found that DNA interactions around +15 pA occur only briefly with the pore (0.02 ms), and the interactions around +42 pA spend slightly more time near ExeD at 0.07 ms. Note that Figure 52 A and Figure 48 A are the same graph as they are measuring the same conditions – gating of ExeD at pH 9.5 and -50 mV.

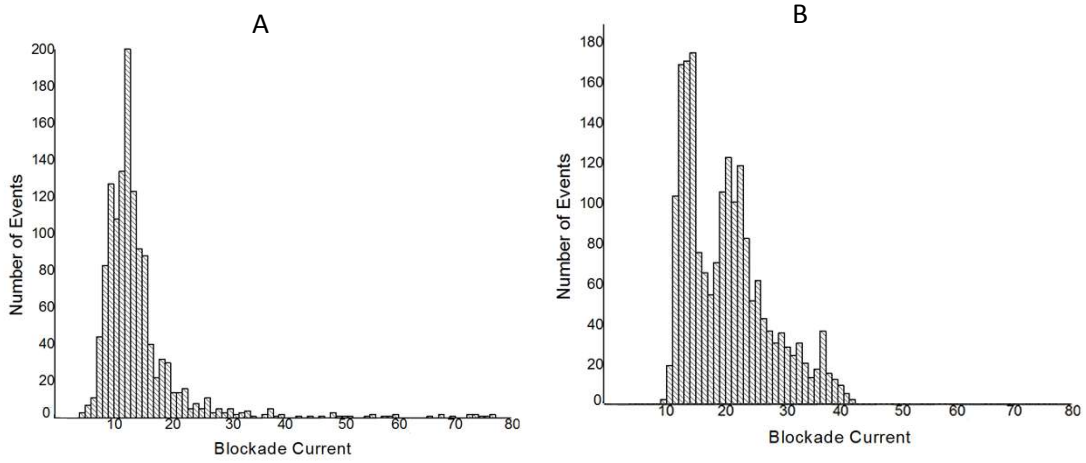

Figure 51: DNA Events at pH 7.4 and -50 mV. A – In the absence of DNA, gating events produce a single type of event at approximately +15 pA. B– When DNA is added at pH 7.4 the background peak is still visible but a second event also occurs at +22 pA.

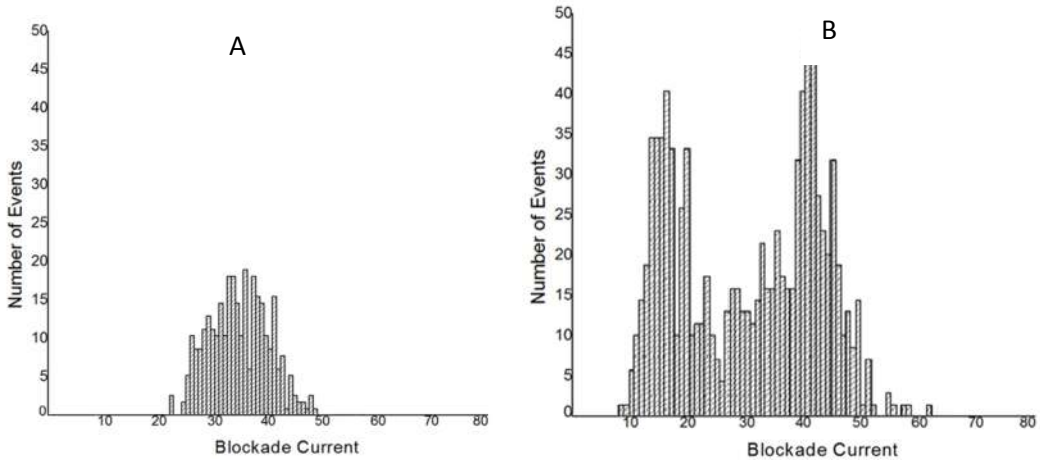

Figure 52: DNA Events at pH 9.5 and -50 mV. A – No DNA at pH 9.5. Events are observed centered at +35 pA. B - The same pore with DNA added. Two peaks are present at +15 and +42 pA. The background gating events are still visible at +35 pA.

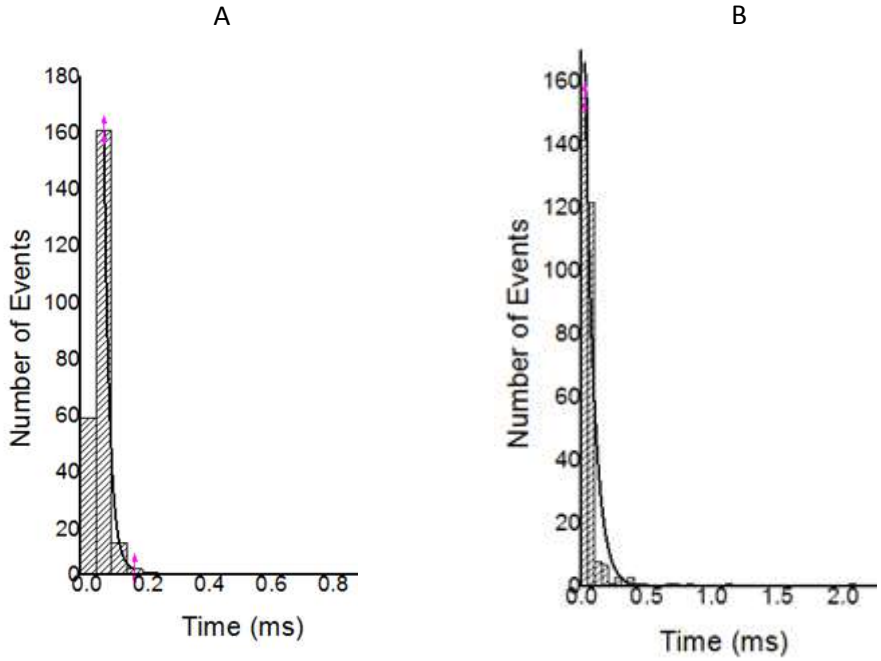

Figure 53: Time of Interaction for DNA Events at pH 9.5. A- The peak in Figure 52 B occurring at +15 pA (having a range between +30 pA and 0 pA) was calculated as having a time of interaction of 0.02 ms. B - The peak in Figure 52 B occurring at +42 pA (having a range between +80 pA and +30 pA) was calculated as having a time of interaction of 0.07 ms.

3.6 ExeD Interactions with α-helical A10 Peptide at pH 7.4 and pH 9.5

Fmoc-$D_2A_{10}K_2$ (A10) is a small, 14 amino acid peptide (DDAAAAAAAAAAKK) with a very stable α-helical secondary structure. The peptide contains a strong negative charge due to its Fmoc group, an aromatic complex having a chemical formula of N-(9-fluorenyl) methoxycarbonyl. Previous work done by Stefureac et al. (2007) found that with α-HL, A10 produces a single sharp peak corresponding to translocation (Figure 54). Based on those findings we believed that A10's ease of translocation would be useful for investigating ExeD's ability to translocate peptides in the absence of other T2SS machinery.

We formed pores at both pH 7.4 and pH 9.5 and added 10 μg of A10 peptide. Results were recorded on patch clamp and the results are shown in Figures 55 and 56. The presence of an additional interaction at pH 7.4 is clear based upon the new events at the +28 pA mark. In Figure 55 – A there is a singular peak representing background gating events. In 55 –B the same gating events are observed, but a secondary type of interaction is evident as a result of the added A10 peptide.

Results at higher pH levels are more difficult to determine (Figure 56). It is possible that a new type of interaction occurs at pH 9.5 after the addition of A10, but there is a large amount of overlap with the pore's gating events. Distinguishing between gating events and A10 events is difficult because the size of both interactions are roughly similar (Figures 56 A and B), so instead of seeing a new peak as appears in Figure 55 A and Figure 55 B, there is only a single distribution. A second experiment was performed recording gating events for 2 hours without A10 present, and then adding A10 peptide and again recording the results over 2 hours. The number of inserted pores was held consistent throughout the duration of the experiments so as to control the number of gating events that would occur pre-and-post addition of the peptide. The events recorded in the absence of the peptide were subtracted from the events which occurred in the presence of the peptide. This was believed to be the best approximation we could achieve of ExeD interactions with A10. The results are shown in Figure 57.

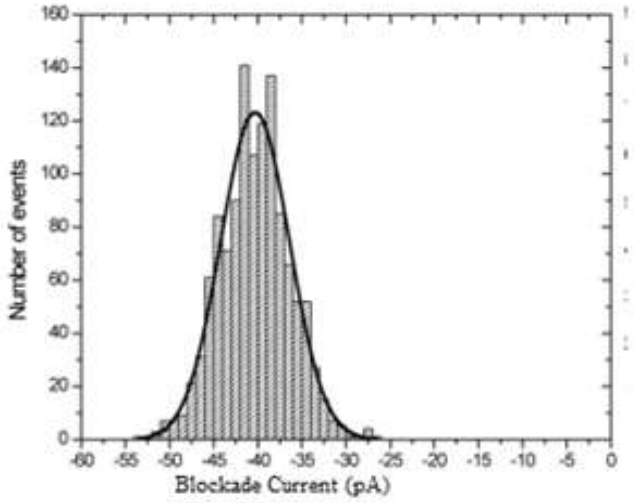

Figure 54: A10 Peptide as Measured by α-HL at +100 mV. A singular peak is evident. When further experiments were done with increasing voltages, the time of interaction of A10 with the pore decreased. This suggested that the single peak as shown here is evidence of translocation and not bumping.

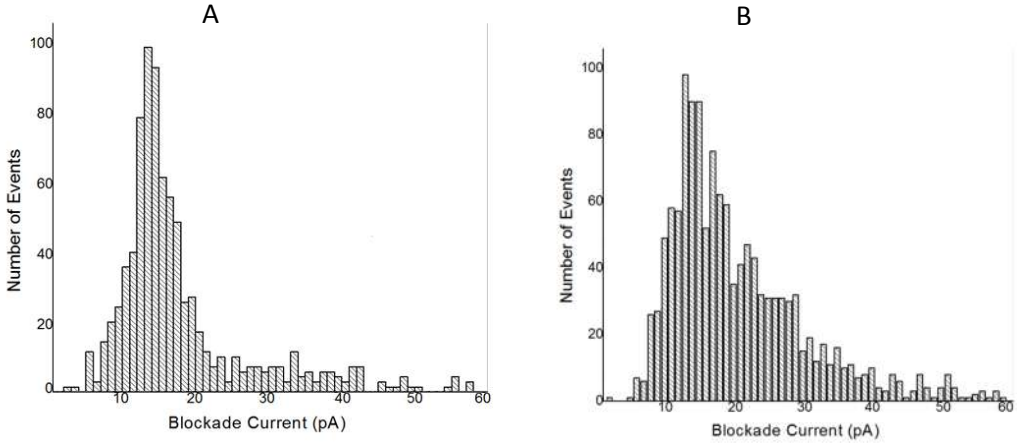

Figure 55: A10 Peptide at pH 7.4 and -50 mV. A– No A10 peptide present. The same peak previously seen as background gating events is at approximately +15 pA. B –ExeD with A10 peptide. The same +15 pA events are observed but additional events around +28 pA are now able to be seen.

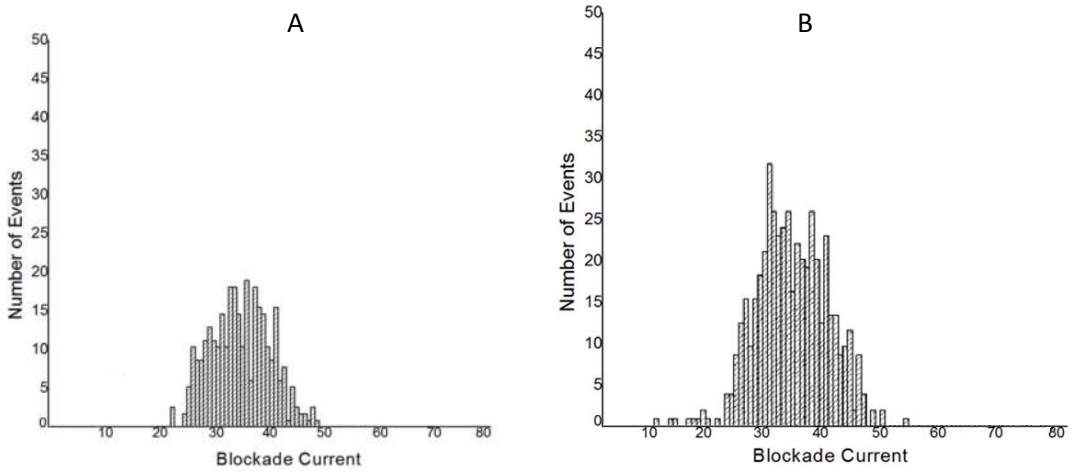

Figure 56: A10 Peptide at pH 9.5 and -50 mV. A – The background gating events are at approximately +35 pA as in Figures 48 A and 52 A. B – When A10 peptide has been added to the perfusion cup, the peak retains its same approximate shape.

A unique graph was produced which represented only those interactions we believed to be A10 peptide. It had a strong resemblance to the previously displayed graph representing only gating interactions at similar conditions (Figure 56 A). Notably, the central peak remained at approximately +35 pA. To further clarify the results between gating-only and A10-only, the time of interaction for each event type was calculated and the findings were compared. A greater time profile means that the current was interrupted for a longer duration. The results are shown in Figure 58. The standard time of interaction for gating functions alone was 0.061 ms and the time of interaction for the A10 graph was 0.036 ms.

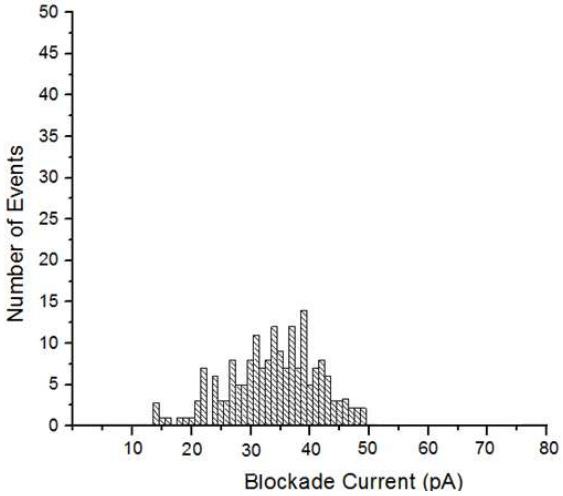

Figure 57: A10 Peptide without Suspected Gating Events at pH 9.5 and -50 mV. Gating events were recorded and subtracted from events representing both A10 and gating interactions. The remaining channel activity is the most accurate way of showing only A10-ExeD interactions.

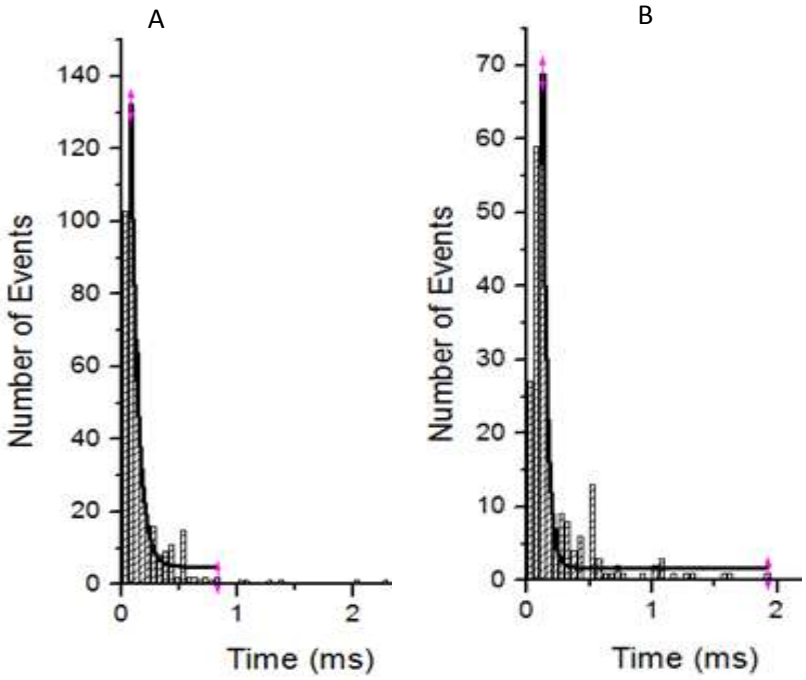

Figure 58: Time of Event Occurrence without A10 and with A10. A- Time of gating events before peptide was added was calculated to be 0.061 ms. B- Time of A10 interactions alone was calculated to be 0.036 ms.

4.0 Discussion

Experiments using the secretin ExeD native to *Aeromonas hydrophila* were done using the patch clamp apparatus. We tested for reproducibility of the pore, different methods to facilitate inserting ExeD into the lipid bilayer, gating events under variable pH and voltage conditions, and the ability of ExeD to translocate DNA and small peptides. Each experiment was done a minimum of two times. Our results have produced a more detailed mechanistic view of the secretin and have given insights into the capabilities of the pore in the absence of other T2SS proteins.

There were several obstacles that needed to be overcome before ExeD could be used in nanopore analysis. The major problem with using ExeD in nanopore experiments was the internal gating mechanism of the pore. The two interior loops are pushed aside by the T2SS pseudopilus *in vivo*, though it is hopefully possible that exoproteins can move through the channel spontaneously after passing through the N3 constriction (McLaughlin et al., 2012). GspD occlusions from the septum-like plug have been partially controlled via mutation (Reichow et al., 2010), but it was unknown to what extent the plug's ability to occlude the opening was modified or how viable for growth such mutations were after expression. In our experiments, instead of attempting to control the loops through mutations, the environmental pH of the loops were changed by altering the pH of the buffer solution.

Another problem was the difficulty in obtaining a large amount of purified ExeD material. When the gene for GspD was expressed using a common vector such as pET30 in a host *E. coli* strain, the high rate of protein production stopped cell growth and gave low protein yields (data not shown). This has been seen twice previously by Guilvout et al. (2008) and Nickerson et al. (2011), presumably due to overwhelming the aforementioned phage shock response. We compensated for this by using a very large volume of cells (20L) and by changing the temperature and rate at which ExeD was produced. Chami et al. (2005) found that *his*-tags on the C-terminal do not interfere with the function of GspD, and so we used a similar approach in purifying the monomers. We decided that expressing the protein in *E. coli* with a C-terminal *his*-

tag was preferential to obtaining ExeD from its native *A. hydrophila*, though we found that protein yield was always extremely low.

4.1 Purification of the Monomer and Multimer

Initially we expressed *exeD* at 37ºC and 1 M IPTG. Under these conditions we found that the lysed cells contained much more of the monomer than the multimer. However, after taking samples from the cobalt column, we found that ExeD had largely oligomerized into the homododecamer (Figure 16). We believe that some aspect of the purification process facilitated oligomerization of ExeD. The purification process involves incubating monomers with their outer membrane extracts for extended periods of time. After the membrane fraction is isolated by ultracentrifugation, it is exposed to 2% and 5% (w/v) zwitterionic detergent for 1 hour. Our results show that during these steps much of the available monomer converts into multimer.

There are two possible explanations for this result. The first possibility is that the amount of available lipids increases in the purification steps as membrane proteins are removed, allowing monomeric ExeD to use the free lipids for multimerization. Previous work done by Chami et al. (2005) found that PulD can be solubilized at concentrations of Zw 3-14 between 3-5%. In their work, they were able to take the cell membrane fraction remaining after ultracentrifugation, solubilize it in 3% Zw 3-14, and add it directly to a nickel column. However, we required a very large amount of cells to produce a sufficient amount of ExeD for use in our analysis. Simply solubilizing the cell membranes and adding them to an affinity column blocked buffer flow through the beads. We instead solubilized some of the membrane proteins in 2% Zw 3-14 and centrifuged out the fraction containing ExeD. We then took the resulting pellet containing ExeD and the large amount of waxy insoluble material (presumed to be insoluble membrane lipids) and suspended it in 5% Zw 3-14 detergent before adding it to the column. We found that this process removed much of the unneeded proteins and we lost little of the secretin. A side-effect of these steps was that monomeric ExeD was allowed to incubate alongside large amounts of concentrated lipids at room temperature for several hours during the centrifugation process (as Zw 3-14 is insoluble at lower temperatures). The presence of lipids has previously been shown to

increase the rate of formation of ion-channels (Betaneli et al., 2012) and it is possible that these steps promote oligomerization of the secretin.

Another explanation for the formation of the homododecamer is that Zw 3-14 has a tendency to form micelles at high concentrations. It is possible that the detergent micelles help facilitate a lipid-protein complex that brings the monomers in closer proximity to one another. It is difficult to distinguish whether the increased rate of oligomerization comes from increased lipid concentrations (as discussed in the preceding paragraph) or from the presence of the zwitterionic micelles since both variables occur in the same step. We did not investigate this attribute of the secretin in-depth because for our intents, clarifying the mechanism of oligomerization was not needed after we started expressing ExeD at 15 ºC. Under these colder conditions, the multimer was the primary product.

Purification of the multimer was found to be easier than purification of the monomer. Our work found that after ExeD is extracted with detergents and added to the cobalt column, elution of the monomer occurs at 100 mM imidazole (not shown) and elution of the multimer occurs at 0.5 M imidazole (Figure 18). When elution is done in 3 steps using a 10 mM imidazole wash, a 100 mM imidazole elution, and a 0.5 M imidazole elution the 0.5 M imidazole fraction containing multimeric ExeD has far fewer non-secretin proteins than the 100 mM elution. Separation on a size-exclusion column produces a peak that is distinctly isolated and can be directly subject to acetone precipitation. When the monomer is eluted at 100 mM imidazole, many other proteins elute alongside it and are run concurrently down the size-exclusion column (Figures 18 and 19). Isolation of the monomer is more difficult because little of it remains at this stage and it has a low concentration relative to that of other membrane proteins in the eluted fraction. These background proteins exist in only small quantities in the imidazole extract, but compared to the low amount of monomeric ExeD this is still problematic. When the elution is run down a size-exclusion column the monomeric peak is hence difficult to identify and use. Isolating only the multimer is therefore more appropriate.

4.2 Conductance Levels of Different ExeD Conformers

Due to the low amount of protein obtained from these experiments, Coomassie blue stains showing background proteins separate from ExeD might be unreliable. We cannot be absolutely certain there are any non-ExeD proteins remaining in our purified extract at the final step, even though none were detectable. Indeed, Reichow et al. (2010) found that even when GspD was purified using binding affinity and size-exclusion columns, some cholera toxin remained in the vestibule of the pore. Unfortunately, no other readily available method for protein purification can be done beyond what is outlined herein. As a result, we must entertain the possibility that there may be more than 1 oligomeric form of the ExeD protein under these conditions. Given that there may be more than one conformation of the protein, there is a great degree of difficulty in determining the conditions under which these conformations arise.

Guilvout et al. (2008) showed that when *E. coli* is used to express the homologue PulD at 30 ˚C using 50 μM of IPTG, very little multimer is produced. The initial product is largely monomeric. We found similar results, but we also learned that if this extract is purified, the process converts most of the monomer into the oligomeric form. When the membrane fraction is separated from the cytoplasm and resuspended in 5% SB 3-14, the amount of remaining monomer decreases and the amount of multimer increases. When these multimers are isolated and used with patch clamp, several different conductance levels are seen. Coomassie stains and spectrophotometry of the size-exclusion column shows that no other detectable proteins are present in the final extract, though it should again be noted that differentiating small molecular size differences amongst large complexes on a 3-8% gel gradient Coomassie stain is not reliable. There is also the possibility that these multimers undergo minor degradation from the length of time they spend at room temperature during purification, though this is unlikely due to the stability of the pore when boiled in SDS (Strozen et al., 2011).

Our results showed that if both the temperature is kept low and IPTG levels are in the 10μM range, more multimer than monomer is produced. Furthermore, these multimers are far more likely to produce 135 pA conductance levels than the multimers produced under higher temperatures and concentrations of IPTG. This was a major breakthrough in our work, as it represented the stage at which we stopped getting variable oligomeric products and could instead focus all our efforts on studying a pore with a specific and common amplitude. The variations of

ExeD at 220, 190, 79, and 150 pA were no longer present in the final extract and nearly every time a pore was inserted, it was only the 135 pA native conformation. Why the rate of expression affects the final conformation of ExeD is unknown, but there are at least two explanations for how this is possible.

The first explanation is that the rate of expression of ExeD in the pET-30 vector is so rapid that the individual subunits become misaligned when assembling the quaternary structure. This has been seen previously in both membrane proteins (Bay et al., 2010) and non-membrane proteins (Josse et al., 2002). When the temperature is 37 ˚C and a 1 M IPTG concentration is used, protein expression is extremely fast. The rapid production of the monomer leads to a high local concentration of the protein in the cytosol. It is possible that such a high concentration of the protein results in assembly of a channel in a non-native conformation as ExeD monomers converge in an attempt to assemble without the ExeAB scaffold. It is however unlikely that alternate channel formation occurs during the expression stage because the amount of multimer spontaneously assembled at 37 ˚C accounts for only a small amount of ExeD present in the final extract (as most protein initially exists as monomer and assembles only through the detergent solubilization - Figure 16). These channels would therefore be less likely to insert due to their low prevalence in the concentrated product.

The second possibility of improper pore assembly may be the result of the high concentration of detergent being used in the isolation process. During the purification steps, the monomers are exposed to up to 5% (w/v) of micelle-forming detergents, in conjunction with excess lipids. Lipids are a known factor for assembly of other channels (Betaneli et al., 2012), and combining free lipids with large amounts of detergents may have implications in how the secretin oligomerizes. An alternate explanation, such as an incomplete homododecamer being used for experiments, was unlikely because all visible multimers were the same molecular weight (Figure 30). We eventually circumvented these problems by expressing the protein at 15 ˚C, so no further attempt to resolve the issues was made.

Concerning the open pore current for ExeD, it is difficult to predict the expected OPC but 135 pA is reasonable. In 1M KCl solution, a perfect cylinder has a conductance according to the equation:

$$G = \sigma \frac{\pi d^2}{4l}$$

where l is the thickness of the membrane, d is the diameter of the pore, σ is the bulk conductivity of the solution, and G is the conductance (Kowalczyk et al, 2011).

This formula holds true for α-HL because of its near-perfect cylindrical shape wherein ions are free to pass through the channel without impedance (Figure 3). In ExeD the internal gates and extracellular cap provide constriction points for ion movement and the interior cavity is decidedly not cylindrical (Figure 11). We found that the open pore current for ExeD is 35% higher than it is for α-HL (135 pA vs. 100 pA), which could indicate either the gate regions have a wider diameter across their openings in ExeD than the vestibule opening has for hemolysin.

Assuming the equation is suitable for ExeD, it helps to explain our observations that at pH 9.5, the open pore current increases to 140 pA. When the radius of the opening slightly increases due to a pH change in the gate regions, the transversing current will increase proportional to the square of the change in radius. Whether the increase in the OPC is due to changes in the internal gates or extracellular cap is not clear, though there are likely changes to the lysines present at the internal gates (see Discussion 4.5). Our work indicates that at pH 9.5 the pore may have a slightly less obstructed opening than at lower pH levels.

4.3 Bilayer Insertions using Proteoliposomes Versus Acetone Precipitation

One of the most difficult parts of working with transmembrane proteins in patch clamp experiments is getting the pore to insert into the lipids painted on the perfusion cup. Even with self-inserting pores such as α-HL, the process can be difficult and time-consuming. Presumably this is because the experimental setup is not an accurate mimic of the cellular conditions in which these pores naturally exist. Past protocols using secretins in patch clamp have focused on two methods to aid in incorporating the transmembrane proteins into the lipid bilayer.

The first method is to create proteoliposomes using the purified protein and lipids dissolved in detergent. Nouwen et al. (1999) created a protocol to have PulD multimerize in the presence L-α-phosphatidylcholine by combing them in a 1:200 ratio. The product is rapidly diluted with buffer and gently shaken in the presence of Bio-Beads to remove detergent. The proteoliposomes are denser than the lipid micelles remaining in solution, and by centrifuging the solution at 250 000 *x g* for 1 hour the proteoliposomes pellet out of the surrounding lipids. The extracted protein-lipid complex is merged with the lipid bilayer in the patch clamp apparatus using a gradient of KCl buffer (100 mM KCl on the *trans* side of the perfusion cup, 400 mM KCl on the *cis* side) and the pore is established.

Several problems with this method made it difficult to perform this with our setup. Firstly, a gradient of KCl from *cis* to *trans* is not ideal in nanopore analysis (as previously discussed in Results 3.1.1). When a concentration gradient of ions is present, the measured open pore current will vary because a continually decreasing amount of ions are passing through the channel. To perform consistent, reliable experiments we would have to wait until the amount of KCl had equilibrated on both sides of the channel. The time it would take for 1 mL of 400 mM KCl and 1 mL of 100 mM KCl to equilibrate would be longer than the time the experiment is capable of running before the membrane breaks.

Secondly, our patch clamp system is optimized for the lipid 1,2-diphytanoyl-sn-glycero-3-phosphocholine (DGCP) instead of the L-α-phosphatidylcholine used by Nouwen et al. (1999). In most nanopore experiments, DGCP is applied over the micron opening in the perfusion cup and forms the lipid bilayer used for pore insertion. DGCP has a higher molecular weight than L-α-phosphatidylcholine and does not possess a lipophilic side-chain kink. The conditions for drying DGCP on the perfusion cup, the amount of chloroform required to dissolve the lipid, and minimum capacitance of the membrane required for pore insertion have all been previously determined over years of work (Stefureac et al., 2007). We found that the success rate for merging the two different lipids, the L-α-phosphatidylcholine proteoliposomes and the DGCP bilayer, was extremely low and cost us a great deal of time and materials in the process. This is presumably due to the unusually kinked shape of phosphatidylcholine compared to the straight

formation of DGCP. Instead of reconfiguring the patch clamp machine for L-α-phosphatidylcholine, we decided to attempt to form proteoliposomes using a modified form of Nouwen et al.'s protocol. Unfortunately separating the micelles from the proteoliposomes proved difficult when we used DGCP. We changed both the centrifugal force being applied on the tube and the concentration of salt in the buffer, but the proteoliposomes either would not pellet out of solution or would simply remain alongside the remaining lipids if they did pellet out.

The second common method for inserting pores into the planar lipid bilayer is to repeatedly break and reform the bilayer while forcing the pore towards the perfusion cup opening. In this technique, the membrane is first thinned using a paintbrush and then repeatedly broken using either mechanical force or by a large surge of voltage from the electrodes. 1M KCl is present in both the *cis* and *trans* sides of the cup, so there is no chemical driving force for a pore to insert. Instead, the bilayer is reformed using a small hand-operated syringe which draws the buffer and suspended lipids through the perfusion hole, making contact with lipids which have been previously painted on. Small amounts of the hydrophobic ExeD multimer move towards the broken bilayer and interact with the unbound lipids. Occasionally the bilayer will spontaneously reform around the hydrophobic pore and produce a correctly structured channel. In the past with α-HL this has proven to be a highly effective method of facilitating pore insertion, but to our knowledge this has never been attempted with pores that were pre-assembled.

Another issue with this method was the presence of detergents in the purified extract. Normally the detergent is removed using Bio-Beads and the lipids assemble around the insoluble proteins. We use a very low amount of protein in these experiments, a concentration typically around 50 µL of 100 ng/mL. If lipids are not present at this stage, it becomes extremely difficult to pellet out the low amount of protein remaining and to separate it from the 200 mg of Bio-Beads used. For some time, it therefore appeared that proteoliposomes were required to have functional pores for use in patch clamp because lipids needed to be present to aid in binding the protein and separating it from the Bio-Beads.

We theorized that because ExeD is such a robust protein in its multimeric form, if we used acetone to precipitate the protein it may still produce a useable pore. We combined the protein with acetone in a 1:4 ratio, cooled it in a -20 ˚C freezer for 1 hour, and centrifuged the protein out at 13000 *x g* for 15 minutes. The detergent was found to remain in solution and a small pellet containing multimeric ExeD was produced. Experiments using both proteoliposomes and acetone precipitation products were compared, and in both cases the level of conductance and background noise were similar (Figure 32). From then on, all nanopore experiments were done using acetone precipitated ExeD as it was faster and simpler than the creation of proteoliposomes.

Why an acetone precipitated protein, which should exist as a single soluble aggregate, was able to form properly structured openings is difficult to explain. We note however that across dozens of experiments, the observed pores were always equal to each other regardless of either a proteoliposome or an acetone extract being used. It is thought that although the majority of the protein aggregates into an insoluble mass upon addition of acetone, there are still some single multimers present which do not adhere to the general mass. When the precipitate is reintroduced into solution these single units can navigate to the membrane. It is also possible that individual subunits break off from the general aggregate in the 1M KCl solution, though this is presumably less likely due to the difficulty in separating such hydrophobic proteins from each other.

Regardless, acetone precipitation has been easier to use in many cases as it avoids the problem of adding excess lipid into the perfusion cup. During our initial experiments using proteoliposomes, experiments would often end prematurely because the excess lipids would eventually cause the bilayer to thicken and eject the pore. An acetone precipitate allowed us to use far less lipids as we no longer needed liposomes, and this in turn allowed for longer-lasting experiments.

4.4 Different Orientations of ExeD Upon Insertion into the Bilayer

An unforeseen consequence of abandoning ExeD insertions using proteoliposomes was that the pore was observed to insert in one of two possible orientations. When proteoliposomes were used, the liposomes facilitate fusion with the planar lipid bilayer and the pore orients with a single direction as shown in Figures 33 and 34, which we termed the "A" direction. In our modified method, the lipid membrane within the perfusion cup is continually broken and reformed to assist in inserting the pore. This method has been very useful in getting pores which are not self-inserting to enter into the bilayer. However, this process allows ExeD to insert with either the N-terminal or C-terminal side facing the *cis* side of the perfusion cup (Figures 33-36). The direction ExeD faces appears to have a preference for what we termed the A orientation, appearing about 75% of the time. The B orientation occurs the remaining 25% of the time.

The A and B orientations have effects upon the recorded events. At positive voltages and pH 7.4 the A orientation produces two separate peaks with a high number of events at both points (Figure 33 B). Orientation B in the same conditions (Figure 35 B) has only a single peak but with an even number of random events scattered from 0-130 pA. At negative voltages the effects are reversed: orientation A has a single peak and orientation B produces 2. These results are shown in Figures 34 B and 36 B respectively.

To establish consistency between experiments, only pores having the A orientation are shown herein for pH, DNA, and peptide analysis. Fortunately, the A and B directions can be distinguished from each other prior to recording data by visual inspection. This involves looking at the frequency and size of the displayed events when ExeD inserts into the bilayer and determining which orientation is currently being used. Events from pores in the A orientation have a large amount of variability in their size and occur intermittently. Pores in the B orientation have events which are far more frequent and are predominantly small and short. Before each recorded experiment involving DNA, α-helical peptide, or pH it was first determined that the pore was facing the A direction. Although data does not need to be recorded to ensure the pore was in the A direction, we still recorded approximately 1000 events before DNA or peptide was added so that we could confirm the pore was in the A direction by event processing in addition to visual inspection. In this way we always controlled the background events of ExeD.

4.5 Gating of ExeD at Different pH Levels and Voltages

Closing and opening of the pore occurs *in vivo* in the course of exoprotein secretion. It was previously discussed how Nouwen et al. (1999) found that PulD-PulS forms a structure that has varying levels of gating depending upon the amount of applied voltage, the length of time the pore has been opened, and differences in bilayers. Our research was able to develop a more stable and consistent method for using these pores for *in vitro* experiments involving patch clamp. We found that across experiments, each of these conditions were highly reproducible. Each patch clamp recording represents a minimum of 3 experiments whose results are overlaid on top of each other. Variation between experiments was found to occur, but the difference between peaks from one experiment to the next was between 0-4 pA. Gaussian distribution of the events would have a y-axis range between 0-10% of the total number of recorded interactions, with most experiments showing only a 3-5% change in event occurrence at a specific blockade current. The most notable of these was seen at pH 5.0, which was the only experiment to approach a 10% variance. All other conditions had less than a 6% difference between event numbers.

Figures 49 and 50 show several drastic changes in gating events as a result of modifying the environmental pH and applied voltage. Voltage has a strong effect on how the pore opens and the duration of the events observed. Whether the applied voltage is positive or negative, decreasing the voltage consistently leads to less observable events. The correlation is slightly exponential at positive potentials and pH 9.5, and slightly logarithmic at pH 7.4 and 5.0. At pH 9.5 and 100 mV, the number of events occurring over 1 minute averages out to ~220 instances of pore opening and closing. At 50 mV there are only about 80 events occurring over the same time period. pH 7.4 and 5.0 have similar trends with about 155 and 165 events at 100 mV and ~50 events at 50 mV. The general trend that less voltage produces less gating is not surprising since there is a smaller electrical force being applied on the interior loops, but the significantly different levels of gating at pH 9.5 are unexpected. The changes in events may have something to do with the change in buffer used at pH 7.4 (HEPES) and pH 9.5 (CHES), but the sodium acetate

buffer used for pH 5.0 did not change the number of gating events significantly compared to HEPES.

The major discrepancies between low/neutral pHs (5.0 and 7.4) and high pH levels (9.5) occur at negative voltages. At pH 5.0 and 7.4 the number of events decreases exponentially as the voltage drops, dipping to a general minimum of approximately 20 events per minute. At pH 9.5 the rate of gating stays constant at 5-8 events per minute, regardless of the applied voltage.

The asymmetric gating between positive and negative voltages is consistent with the current model of the pore. One of the key features of ExeD and GspD protein in general is the presence of the charged cap near the first C-terminal domain. Depending on the mobility of the charged cap, the residues would flip away under an electric potential in one direction, but upon reversing the potential in the other direction the cap would be repeatedly thrust towards the inside of the pore. Another explanation comes from work done by Spagnuolo et al. (2010) regarding the interior of the pore. They determined that amino acids in the Gate 1 and Gate 2 regions, representing the interior plugs of the pore in the C-terminal domain, are rich in charged amino acids. At pH 7.4 the interior of secretin pIV contains mostly negatively charged amino acids, but there are also 6 lysine groups in the secretin family domain (situated around the C-1 terminal domain) and a histidine in the same region. We aligned the sequences of ExeD and pIV to find the corresponding gate regions in the ExeD protein and to determine which amino acids were likely to be affected by increasing the pH from 7.4 to 9.5 (Figure 59). Similarly to Spagnuolo et al. (2010), we found that the Gate 1 (red) and Gate 2 (blue) regions in ExeD contain sequences rich in lysine, which are amino acids likely to be affected by deprotonation at pH 9.5. These appear to be the most important functional groups in the interior gating region, and so we designated high pH levels (pH 9.5) where lysine is deprotonated as the gates being negatively charged, and low and neutral pH levels (5 and 7.4) as the gates having a more positive charge. We can therefore account for alterations at higher pH levels as the plug regions deprotonate and the charges are altered.

Changes in gating at lower pH levels are somewhat difficult to explain. One theory we are currently working with depends upon the direction the plug is facing relative to the applied

```
ExeD  325        TNALVITAQPDVMAELEQVVAKLDIRRAQVLVEAIIVEIADGDGLNLGVQ     375
                 :|.||::|..|::..|.|.::.:|:...|:|:|.:|.|:..||.|:....
PIV   169        SNLLVVSAPKDILDNLPQFLSTVDLPTDQILIEGLIFEVQQGDALDFSFA     219

ExeD  375        WANTNGGGTQFTNAGPGIGSVAIAAKDYKDNGTTTGLAKLAENFNGMAAG     425
                             ||...|:||        .|..|.......:..|.:.|
PIV   219        -------------AGSQRGTVA--------GGVNTDRLTSVLSSAGGSFG     248

ExeD  425        FYQGN-WAMLVTALSTNTKSDILSTPSIVTMDNKEASFNVGQEVPVQTG-    473
                 .:.|: ..:.|.||.||:.|.|||.|.|:|:..::.|.:|||.||..||
PIV   248        IFNGDVLGLSVRALKTNSHSKILSVPRILTLSGQKGSISVGQNVPFITGR    298

ExeD  473        -TQNSTSGDTTFSTIERKTVGTKLVVTPQINEGDSVLLTIEQEVSSVGKQ    522
                  |..|.:.:..|.||||:.||..:.|.|....|.:::|.|..:..|:...
PIV   298        VTGESANVNNPFQTIERQNVGISMSVFPVAMAGGNIVLDITSKADSLSSS    348

ExeD  522        ATGTDGLGPTFDTRTVKNAVLVKSGETVVLGGLMDEQTKEEVSKVPLLGD    572
                 ...:|.:   .:.|::...|.::.|:|::||||.|.:...:.|.||.|..
PIV   348        TQASDVI---TNQRSIATTVNLRDGQTLLLGGLTDYKNTSQDSGVPFLSK    395

ExeD  572        IPVLGYLFRSTSNNTSKRNLMVFIRPTILR    602
                 ||::|.||.|.|::..:..|.|.::.||:|
PIV   395        IPLIGLLFSSRSDSNEESTLYVLVKATIVR    425
```

Figure 59: Alignment of the Interior Plug Regions between pIV and ExeD. Amino acid sequences along the C-terminal plugs in ExeD and PIV were aligned. The Gate 1 region, corresponding to the first internal loop comprising a plug, is shown in red. The Gate 2 region for the second plug is shown in blue. EMBLOSUM62 was used for calculating sequence similarity, with a more comprehensive report detailed in Appendix A.

voltage. When the gating region is more positively charged at pH 5 and 7.4 and a positive voltage is flowing through the pore, the voltage will cause the gate regions to be "pushed" towards the constriction point. The interior loops are still relatively free to oscillate in the interior of the pore, but the tendency is for the plug to flow with the applied voltage and interact with the C-terminal constriction. This applied force results in a decrease of gating events at low pH values when a positive potential is used because the plug is not as free to move around in the interior. When the potential is increased to the point of excess, the gate region is permanently forced against the constriction point and the pore closes completely. In support of this theory, complete pore closings are often seen at voltages of 250 mV or higher, where the pore can no longer be used for experiments (results not shown).

Similarly, when the pore is exposed to negative voltages at pH 5 and 7.4, the positively charged gates will be "pulled" towards the N-terminal opening but then repelled by the some of the positive interior charges of the pore. The gate regions becomes the focal point of a balancing of charges where the voltage is forcing the plug one direction but the interior charges are causing it to be repelled when the loops get too close to the surrounding β-sheets. When an excess of voltage is applied (approximately 250 mV) the pore seals completely until the potential is dropped, similar to the results discussed above. We found that when the negative gate is exposed to a positive voltage, a similar result was seen wherein the gating events were rapid. This would again be attributed to a balancing of forces between the repelling voltage pushing the negative loops one direction, and the negative interior charges forcing the loops back in the other direction.

It may stand to follow that if gating is very frequent with negative voltages and a positively charged gate (i.e. pH 5 and 7.4) then gating should be less frequent with negative voltages and a negatively charged gate (i.e. pH 9.5). We found this to be the case. The most interesting phenomena with ExeD are the number of gating events at high pH values and at low negative potentials where under these conditions gating events are almost entirely lost. Presumably this is where the more negative plug is continually repelled by the negative voltage, forcing the gate open almost permanently. The low amount of gating events seen under these conditions are nearly ideal for nanopore experiments and the following DNA and peptide work was done using this setup. Interestingly, the amount of voltage applied had little effect on the amount of gating seen; whether we used 50 mV or 150 mV the frequency of pore closure was approximately the same.

Graphs displaying the distribution of events for both negative and positive voltages as a function of pH have shown conclusively that gating is asymmetrical and changes as a result of the surrounding pH. More information about the plug can be obtained from graphs showing the number of events versus blockade current (Figures 39 and 41). When blockade current is measured, the size of the blockade corresponds to how much of the pore becomes occluded (Kasianowicz et al., 1996). If the open pore current is 100 pA, and the blockade current is 100,

the pore is being 100% blocked. In ExeD the open pore current is 135 pA, and for pH 7.4 at positive voltage blockade of the gates range from 10 pA all the way to 135 pA. This means that the interior plug is capable of blocking either a very small amount of the opening or the entire cavity. At negative voltages at pH 7.4 however, the amount of space the plug is capable of taking up is quite small – only 15 pA out of 135 is effectively occluded. The results suggest that the loop is much less able to block the pore at lower pH levels than higher ones.

At +100 mV, pH 9.5 gating is more centralized than the results from pH 7.4 (Figures 43 and 44, cf. Figures 40 and 41). At positive voltages and pH 7.4, the plug was able to block anywhere from 5% to 100% of the available pore space as evidenced by range of events occurring from 10 to 135 pA. However, at pH 9.5, positive voltages result in the cavity being less than 50% blocked (pA changes range from 20-65 pA as shown in Figure 44 B). This is significantly smaller than the 5-100% gating events of pH 7.4 and 100 mV. Negative voltage for the pH 9.5 experiments produced a much wider range for current blockades, ranging from about 15% to 93% of the OPC (i.e. a current blockade of 20/135 pA and 125/135 pA as shown in Figure 44 A). These results may suggest that changing the charge of amino acids within the interior loop changes the loop's ability to occlude the opening.

4.6 DNA Interactions at pH 7.4 and 9.5

Type IV pili are polymers of a 15-20 kDa subunit which multimerizes and displays upon the surface many of gram negative bacteria. Upon assembly, the multimer allows for bacterial adhesion, motility, secretion of proteases, and translocation of DNA. This secretin is an outer membrane protein with a cytoplasmic N-terminal domain and a membrane-spanning C-terminal region. While the T2SS extrudes enzymes and toxins, the type IV pili extrudes filamentous phages responsible for bacterial infection. Unlike the GspD secretin, pIV is capable of translocating DNA across the lipid bilayer (Craig and Li, 2008).

The highly-variable N-terminal domain of secretins contains the binding sites used by proteins to enable their passage through the membrane channel (McLaughlin et al., 2012). Bacterial secretins like PulD from *Klebsiella oxytoca* contain 77% sequence similarity to pIV in

the C-terminal region. It is possible that the reason DNA translocates through pIV but not through PulD is because the bacterial homologue does not contain the sites in the N-terminal region to allow DNA binding. In this case the C-terminal domain would be structurally able to move DNA through its interior channel if it could remain open.

Our experiments used small lengths of single-stranded DNA (ssDNA) to measure interactions with ExeD. We recorded ExeD interactions with DNA at both pH 7.4 and pH 9.5, representing both a cellular pH level and the conditions under which ExeD gates the least frequently.

At pH 7.4 there is a standard amount of background gating which occurs and represents the opening and closing of the pore at this pH, but with the addition of DNA a new peak at -22 pA occurs (Figure 51 A and B). Usually when a molecule is added for analysis to a nanopore, there are 2 peaks visible in any given experiment – bumping and translocation. This is not always the case however, as occasionally only bumping or only translocation will be observed. But in the majority of instances two novel events are produced (Stefureac et al., 2007). In our experiments with DNA at pH 7.4, we observed only a single new peak in addition to standard gating. This peak may be evidence of DNA moving through the pore, or it may be only transient interactions with the vestibule of ExeD. To delineate these results several more tests need to be done, including interaction time as a function of voltages at +/- 50, +/- 100, and +/- 150 mV and qPCR using samples taken from the *trans* compartment to verify the presence of DNA in the chamber. This was deemed beyond the scope of our work as similar experiments by Krasniqi (2013) took several years to obtain decisive results.

At pH 9.5, DNA interactions with ExeD are more predictable as shown in Figure 52. Background gating events at -35 pA are present in both experiments, but when DNA is added, 2 new peaks at -15 pA and -42 pA are observed. The -15 pA events likely correspond to bumping events as they occupy a small percentage of the pore and have rapid event profiles (Figure 53 A; 0.02 ms). The events at -42 pA may correspond to translocation interactions as they occupy a larger percentage of the pore and their time of interaction is slightly longer (Figure 53 B; 0.07 ms). The times of pore-molecule interaction are not only longer, they are also observed at a

higher pA. These two kinds of interactions are the expected event types when a molecule is added in appreciable quantities to a patch clamp experiment, though to verify that DNA is indeed passing through the channel further studies using time trials at varying voltages need to be done. Our results indicate that it may indeed be possible for DNA to translocate through the interior of ExeD, and it is either the lack of an N-terminal binding site or the gating mechanism of the pore which are preventing this from occurring.

4.7 Fmoc-$D_2A_{10}K_2$ (A10) Interactions at pH 7.4 and 9.5

The α-helical peptide A10 was chosen for our experiments because of its narrow, elongated structure. The peptide has only 10 amino acids and is small enough that it can pass through the smaller α-hemolysin pore. In experiments by Stefureac et al. (2007) the A10 peptide gave very distinct peaks at a predictable voltage, and the graphical display with α-hemolysin was visually unique in patch clamp because of the large, narrow events that were produced.

Our experiments were done at both pH 7.4 and pH 9.5 with the A10 peptide using ExeD. In α-HL, events center at -40 pA. Figure 54 shows the findings from A10 experiments with α-HL at pH 7.4. The histogram only vaguely resembles that seen at pH 7.4 with ExeD (Figure 55 A). However, because the open pore current and channel structure are very different from ExeD, direct comparisons between the histograms should not be made.

At pH 7.4 a unique event type is formed after the A10 peptide is added to an experiment with the ExeD pore (Figure 55). These events are distinct and lie outside the gating events of the pore at this pH (Figure 55 A cf. Figure 55 B). As mentioned previously however, when only one novel peak is seen after addition of a molecule into the patch clamp setup, it is difficult to determine whether it is a translocation or bumping interaction. Further studies comparing the rate of A10 interaction with ExeD as a function of voltage need to be done to clarify these findings. Samples taken from the *trans* chamber would also need to be analyzed to determine if A10 had passed through the bilayer channel. It is clear however that A10 is directly interacting with ExeD under these conditions, though in what regard is unknown.

Our findings for pH 9.5 in Figure 56 were also difficult results from which to draw conclusions. The relative prevalence of gating events, even though the gating was significantly lower at this low pH and voltage, made it challenging to distinguish the native events of ExeD from those of the A10. We compared native gating events before A10 was added to events after the addition of the peptide, and found that there was a unique distribution that arose for the peptide. The overall shape of the graph was somewhat different from that of spontaneous pore closures (Figure 57 cf. Figure 56 A), with the former having a more varied distribution and not centralizing so closely to a sharp peak. Standard practice is to compare the duration of the interaction between the gating events (Figure 56 A) and the peptide-only events (Figure 57) to determine if there is a significant time difference between them. This would indicate that they are in fact different events entirely. When these were calculated in Figure 58 it was found that peptide-only events were almost twice as fast as those of spontaneous pore closure, suggesting that the A10 peptide may approach the pore but is rapidly repelled away from the entrance.

4.8 Comparison with Other Studied Secretins

Two other outer membrane pores were previously studied using patch clamp with some similarities and discrepancies between each set of results. Nouwen et al. (1999) were able to insert PulD in a consistent, repeatable fashion but each pore was tightly bound to the chaperone PulS. Brok et al. (1999) isolated XpcQ without the concomitant pilotin, but patch clamp visualization of the pore was inconsistent and gating events were difficult to determine. Our work was able to establish consistent pores across a wide range of conditions, develop a histogram of gating events, and we were able to do so without the bound pilotin.

Our experiments had similar difficulties to XpcQ studies because of the inability of host cells to express large amounts of XpcQ or ExeD protein. Brok et al. (1999) were able to use a previously studied mutant of a closely related species as a host cell. The mutant had been selected for its ability to express large amounts of a T4SS exoprotein, and this attribute prevented the cells from easily lysing when XcpQ was overexpressed. Unfortunately we did not have the luxury of having mutant host cells to assist in production of ExeD. Instead we grew very large quantities of host *E. coli* cells and expressed them with low levels of IPTG, at low temperatures,

and for long periods of time. We found that these conditions yielded amounts of ExeD that could be extracted, concentrated, and purified for use in patch clamp.

Both our work and Nouwen et al.'s (1999) produced similar patch clamp results (Figure 12A cf. Figure 33, 34). We had pores insert in discrete steps in predictable increments (Figure 21), and these insertions were repeatable across a large number of experiments. Although the work done by Nouwen et al. (1999) did not provide a single channel conductance for PulD, they do provide the size of several gating events in their data. Direct comparisons are however difficult to make because of their experimental conditions. In most patch clamp experiments, the concentration of KCl on both the cis and trans side of the perfusion cup is the same. If the concentrations are different, a chemical gradient exists between the two chambers which will influence the flow of ions across the opening of the pore. Instead of Cl- being correlated only with voltage, it is now dependent on both an electrical and chemical gradient. Consequently, there is no direct way to calculate event sizes between our work and theirs. This is further complicated by the presence of PulS which still has unclear effects on the ability of the pore to gate.

It was previously discussed how nanopore events below a certain threshold are immediately discarded due to background noise from the instruments and temperature. Discarding of events occurs regardless of the KCl concentration or voltages because these influences are consistently 5-7 pA regardless of experimental conditions. If the background peaks shown by Nouwen et al. (1999) are removed from the event profiles seen in Figure 13, the distribution of events becomes similar to ours: a single peak at one voltage and two peaks when the potential is reversed (Figure 13, cf. Figure 41).

In contrast, much like Nouwen et al. (1999) our findings did not closely resemble those of Brok et al. (1999). However, this is mostly easily explained by the latter researchers being unable to establish a uniform single channel conductance for the C-terminal domain of XcpQ. They were able to detect discrete increases in conductance, but could not identify specific gating events. They also acknowledge that while most bacterial pores have a linear increase in conductance when the applied voltage is increased, XcpQ has a non-linear increase.

We believe our work has overcome the limitations of both studies done using secretins in patch clamp, and that we discovered several new and exciting findings relating to the gating of secretins in different experimental conditions. We have simplified the protocol of secretin isolation and insertion into planar lipid bilayers by using acetone precipitation. We have established standard conditions for ExeD experiments in patch clamp including the open pore current, rate of gating, and conditions for proper multimer assembly. We have also taken the first steps in being able to analyze DNA and small proteins by determining the setup necessary to facilitate identification of these molecules by ExeD, though as the secretin now exists it is not suitable for molecular analysis.

5.0 Future Directions

This project still contains several questions which have yet to be answered and are worth investigating. Among these are:

1. Identifying the exact cause of the multimer malformation. Our evidence suggests that this is largely an *in vitro* issue due to the high concentration of lipids and/or detergents, but the precise reason why we were able to see different multimer conformations is unknown. It could also be the remains of unfiltered background proteins residing in our sample, though at levels beyond common detection methods.

2. Expanding the field of our studies to include positively charged proteins or protein aggregates, with the eventual end-goal of studying biologically relevant oligomeric plaques such as the amyloid β peptide. Seeing how this molecule behaves in the earliest stages of aggregation is not possible in α-HL, but may be possible in ExeD. This could tell us much about the earliest stages of protein aggregation and the Alzheimer's disease.

3. We determined that it was likely the charges in the lysine region of Gate 1 or Gate 2 which cause changes in the gating events of the pore. Mutations of those amino acids and investigation of the resulting multimer could allow ExeD to be used without the recurring background events.

6.0 References

Almers, W., Stanfield, P. R. & Stuhmer, W. (1983). Lateral distribution of sodium and potassium channels in frog skeletal muscle: measurements with a patch clamp method. J. Physiol., 336, 261-284.

Arkowitz, R., & Wickner, W. (1994). SecD and SecF are required for the proton electrochemical gradient stimulation of preprotein translocation. EMBO J., 15(13), 954-63

Ashkenasy, N., Sánchez-Quesada, J., & Ghadiri, M. (2005). Recognizing a single base in an individual DNA strand: A step toward nanopore DNA sequencing. Chem. Int. Ed. Engl., 44(9), 1401-1404.

Ast, V., Schoenhofen, I., Langen, G., Stratilo, G., Chamberlain, M., & Howard, S. (2002). Expression of the ExeAB complex of *Aeromonas hydrophila* is required for the localization and assembly of the ExeD secretion port multimer. Mol. Micro., 44(1), 217-231.

Astier, Y., Braha, O., & Bayley, H. (2006). Toward single molecule DNA sequencing: Direct identification of ribonucleoside and deoxyribonucleoside 5'-monophosphates by using an engineered protein nanopore equipped with a molecular adapter. J. Am. Chem. Soc., 128(5), 1705-1710.

Bay, D., Budiman, R., Nieh., M., & Turner, R. (2010). Multimeric forms of the small multidrug resistance protein EmrE in anionic detergent. Biochim. Biophys. Acta. 1798 (3), 526-535.

Benowitz, S. (2014, July 3). Nanopore DNA sequencing: New approaches to an old challenge. Retrieved July 21, 2015, from https://www.genome.gov/27555651

Berman, A., Kamtekar, S., Goodman, J., Lázaro, J., De Vega, M., Blanco, L., . . . Steitz, T. (2007). Structures of phi29 DNA polymerase complexed with substrate: The mechanism of translocation in B-family polymerases. EMBO J., 26(14), 3494–3505.

Betaneli, V., Petrov, E., & Schwille, P. (2012). The role of lipids in vdac oligomerization. Biophys. J., 102, 523-531.

Briggs, K., Kwok, H., & Tabard-Cossa, V. (2014). Automated fabrication of 2-nm solid-state nanopores for nucleic acid analysis. Small, 10(10), 2077–2086.

Brok, R., Van Gelder, P., Winterhalter, M., Ziese, U., Koster, A., De Cock, H., . . . Bitter, W. (1999). The C-terminal domain of the *Pseudomonas secretin* XcpQ forms oligomeric rings with pore activity. J. Mol. Biol., 294(5), 1169–1179.

Butler, T.Z., Pavlenok, M., Derrington, I.M., Niederweis, M., Gundlach, J.H. (2008) Single-molecule DNA detection with an engineered MspA protein nanopore. Proc. Natl. Acad. Sci., 105(52), 20647–20652.

Chami, M., Guilvout, I., Gregorini, M., Rémigy, H., Müller, S., Valerio, M., . . . Bayan, N. (2005). Structural insights into the secretin PulD and its trypsin-resistant core. J. Biol. Chem., 280(45), 37732-37741.

Cheley, S., Gu, L., & Bayley, H. (2002). Stochastic sensing of nanomolar inositol 1,4,5-trisphosphate with an engineered pore. Chem. and Biol., 9(7), 829–838.

Cherf, G., Lieberman, K., Rashid, H., Lam, C., Karplus, K., & Akeson, M. (2012). Automated forward and reverse ratcheting of DNA in a nanopore at 5-Å precision. Nat. Biotechnol., 14(30), 344-348.

Christensen C, Baran C, Krasniqi B, Stefureac RI, Nokhrin S, Lee JS. (2011) Effect of charge, topology and orientation of the electric field on the interaction of peptides with the α-hemolysin pore. J. Pept. Sci, 17(11), 726-734.

Craig, L., & Li, J. (2008). Type IV pili: Paradoxes in form and function. Curr. Opin. Struct. Biol., 18(2), 267-277.

Dekker, C. (2007). Solid-state nanopores. Nature Nano., 2, 209-215.

Feng, Y., Zhang, Y., Ying, C., Wang, D., & Du, C. (2015). Nanopore-based fourth-generation DNA Sequencing Technology. Gen. Prot. Bioinf., 13(1), 4-16.

Filloux, A., Michel, G., & Bally, M. (1998). GSP-dependent protein secretion in Gram-negative bacteria: The Xcp system of *Pseudomonas aeruginosa*. FEMS Micro., 22, 177-198.

Grishin, N. (2001). KH domain: One motif, two folds. Nucleic Acids Res., 29(3), 638-643.

Guilvout, I., Chami, M., Berrier, C., Ghazi, A., Engel, A., Pugsley, A., & Bayan, N. (2008). In vitro multimerization and membrane insertion of bacterial outer membrane secretin PulD. J. Mol. Biol., 1(26), 13-23.

Guilvout, I., Chami, M., Engel, A., Pugsley, A., & Bayan, N. (2006). Bacterial outer membrane secretin PulD assembles and inserts into the inner membrane in the absence of its pilotin. EMBO J., 25(22), 5241–5249.

Hamill, O., Marty, A., Neher, E., Sakmann, B., & Sigworth, F. (1981). Improved patch-clamp techniques for high-resolution current recording from cells and cell-free membrane patches. Eu. J. Physiol., 391(2), 85-100.

Heinz, C., Engelhardt, H., & Niederweis, M. (2003). The core of the tetrameric mycobacterial porin MspA is an extremely stable β-sheet domain. J. Biol. Chem., 278, 8678-8685.

Japrung, D., Henricus, M., Li, Q., Maglia, G., & Bayley, H. (2010). Urea facilitates the translocation of single-stranded DNA and RNA through the α-hemolysin nanopore. Biophys J., 98(9), 1856-1863.

Jetha, N., Wiggin, M., & Marziali, A. (2009). Forming an alpha-hemolysin nanopore for single-molecule analysis. Methods Mol. Biol., (544), 113-127.

Jones, C., Dexter, P., Evans, A., Liu, C., Hultgren, S., & Hruby, D. (2002). *Escherichia coli* DegP protease cleaves between paired hydrophobic residues in a natural substrate: the PapA pilin. J. Bacteriol., 184(20): 5762-5771.

Jones, S., Lloyd, L., Tan, K., & Buck, M. (2003). Secretion defects that activate the phage shock response of *Escherichia coli*. J. Bacteriol., 185(22), 6707–6711.

Josse, D., Ebel, C., Stroebel, D., Fontaine, A., Borges, F., Echalier, A., Baud., D., Renault, F., le Maire, M., Chabrieres, E., & Masson, P. (2002). Oligomeric states of the detergent-solubilized human serum paraoxonase. J. Biol. Chem., 277, 33386-33397 .

Kasianowicz, J., Brandin, E., Branton, D., & Deamer, D. (1996). Characterization of individual polynucleotide molecules using a membrane channel. Proc. Natl. Acad. Sci., 93, 13770–13773.

Korman, C., Megens, M., Ajo-Franklin, C., & Horsley, D. (2013). Nanopore-spanning lipid bilayers on silicon nitride membranes that seal and selectively transport ions. Langmuir, 19(14), 4421–4425.

Korotkov, K., Gonen, T., & Hol, W. (2011). Secretins: dynamic channels for protein transport across membranes. Trends in Bioc., Sci. 36 (8), 433-443.

Korotkov, K., Johnson, T., Jobling, M., Pruneda, J., Pardon, E., Héroux, A., . . . Hol, W. (2011). Structural and functional studies on the interaction of GspC and GspD in the type II secretion system. PLoS Pathog., 7(9).

Korotkov, K., Pardon, E., Steyaert, J., & Hol, W. (2009). Crystal structure of the N-terminal domain of the secretin GspD from ETEC determined with the assistance of a nanobody. Structure, 17(2), 255-265.

Korotkov, K., Sandkvist, M., & Hol, W. (2012). The type II secretion system: biogenesis, molecular architecture and mechanism. Nat. Rev. Microbiol., 10(5), 336-351.

Kowalcyzk, S., Grosberg, A., Rabin, Y., & Dekker, C. (2011). Modeling the conductance and DNA blockade of solid-state nanopores. Nanotech. 22, 315101.

Krasniqi, B. (2013). Nanopore sensing of peptides and proteins. Dissertation.

Li, J., Stein, D., McMullan, C., Branton, D., Aziz, M., & Golovchenko, J. (2001). Ion-beam sculpting at nanometre length scales. Nature, 412(6843), 166-169.

Ma, L., & Cockroft, S. (2010). Biological nanopores for single-molecule biophysics. Chem. Bio. Chem., 11(1), 25-34.

Madampage, C., Andrievskaia, O., & Lee, J. (2010). Nanopore detection of antibody prion interactions. Anal. Biochem., 396(1), 36-41.

Madampage, C., Tavassoly, O., Christensen, C., Kumari, M., & Lee, J. (2012). Nanopore analysis: An emerging technique for studying the folding and misfolding of proteins. Prion, 6(2), 116-123.

Manara, R., Tomasio, S., & Khalid, S. (2015). The nucleotide capture region of alpha hemolysin: Insights into nanopore design for DNA sequencing from molecular dynamics simulations. Nanomaterials, 5, 144-153.

Manrao, E., Derrington, I., Laszlo, A., Langford, K., Hopper, M., Gillgren, N., . . . Gundlach, J. (2012). Reading DNA at single-nucleotide resolution with a mutant MspA nanopore and phi29 DNA polymerase. Nature Biotech., 30, 349-353.

McLaughlin, L., Haft, R., & Forest, K. (2012). Structural insights into the type II secretion nanomachine. Curr. Opin. Struct. Biol., 22(2), 208-216.

Meller, A., Nivon, L., Brandin, E., Golovchenko, J., & Branton, D. (2000). Rapid nanopore discrimination between single polynucleotide molecules. Proc. Natl. Acad. Sci. USA, 97(3), 1079-1084.

Menestrina, G., Pederzolli, C., Dalla-Serra, M., Bregante, M., & Gambale, F. (1996). Permeability increase induced by *Escherichia coli* hemolysin A in human macrophages is due to the formation of ionic pores: A patch clamp characterization. J. Membr. Biol., 149(2), 113-121.

Meng, H., Detillieux, D., Baran, C., Krasniqi, B., Christensen, C., Madampage, C., Stefureac, R., Lee, J. (2010). Nanopore analysis of tethered peptides. J. Pept. Sci., 16(12), 701-708.

Mirsaidov, U., Timp, W., Dimitrov, V., Schulten, K., Feinberg, A., & Timp, G. (2009). Nanoelectromechanics of methylated DNA in a synthetic nanopore. Biophys. J., 18(96), 32-34.

Mori, H., & Ito, K. (2001). The Sec protein-translocation pathway. Trends in Micro., 9(10), 494-500.

Nam, S., Choi, I., Fu, C., Kim, K., Hong, S., Choi, Y., . . . Lee, L. (2014). Graphene nanopore with a self-integrated optical antenna. Nano. Letters, 14(10), 5584-5589.

Nickerson, N., Tosi, T., Dessen, A., Baron, B., Raynal, B., England, P., & Pugsley, A. (2011). Outer membrane targeting of secretin PulD protein relies on disordered domain recognition by a dedicated chaperone. J. Biol. Chem., 286, 38833-38843.

Nouwen, N., Ranson, N., Saibil, H., Wolpensinger, B., Engel, A., Ghazi, A., & Pugsley, A. P. (1999). Secretin PulD: association with pilotin PulS, structure, and ion-conducting channel formation. Proc. Natl. Acad. Sci. U.S.A., 96(14), 8173-8177.

Nouwen, N., Stahlberg, H., Pugsley, A., & Engel, A. (2000). Domain structure of secretin PulD revealed by limited proteolysis and electron microscopy. EMBO J., 19(10), 2229–2236.

Patsalis, P. (2012). A new method for non-invasive prenatal diagnosis of Down syndrome using MeDIP real time qPCR. Applied & Translational Genomics, 1(1), 3-8.

Perera, A., Wang, H., Shrestha, T., Troyer, D., & Bossmann, S. (2013). Nanoscopic surfactant behavior of the porin MspA in aqueous media. J. Nanotechnol., 4, 278-284.

Pugsley, A. (1993). The complete general secretory pathway in gram-negative bacteria. Microbiol. Rev., 57(1), 50-108.

Reichow, S., Korotkov, K., Hol, W., & Gonen, T. (2010). Structure of the cholera toxin secretion channel in its closed state. Nat. Struct. Mol. Biol., 17(10), 1226-1232.

Rotem, D., Jayasinghe, L., Salichou, M., & Bayley, H. (2012). Protein detection by nanopores equipped with aptamers. J. Am. Chem. Soc, 134(5), 2781–2787.

Sampath, G. (2014). A Tandem Cell for Nanopore-based DNA sequencing with an exonuclease enzyme. BioRxiv. http://dx.doi.org/10.1101/005934

Singer, A., Rapireddy, S., Ly, D., & Meller, A. (2012). Electronic barcoding of a viral gene at the single-molecule level. Nano. Letters, 14(12), 1722-1728.

Schneider, G. F., & Dekker, C. (2012). DNA sequencing with nanopores. Nat. Biotechnol. 30, 326–328.

Shu, Y., Shu, D., Haque, F., & Guo, P. (2013). Fabrication of pRNA nanoparticles to deliver therapeutic RNAs and bioactive compounds into tumor cells. Nat. Prot., 8, 1635-1659.

Smeets, R., Keyser, U., Krapf, D., Wu, M., Dekker, N., & Dekker, C. (2006). Salt dependence of iIon transport and DNA translocation through solid-state nanopores. Nano. Letters, 6(1), 89-95.

Song, L., Hobaugh, M., Shustak, C., Cheley, S., Bayley, H., & Gouaux, J. (1996). Structure of *staphylococcal* alpha-hemolysin, a heptameric transmembrane pore. Science, 274(5294), 1859-1866.

Spagnuolo, J., Opalka, N., Wen, W., Gagic, D., Chabaud, E., Bellini, P., . . . Rakonjac, J. (2010). Identification of the gate regions in the primary structure of the secretin pIV. Mol. Microbiol., 76(1), 133-150.

Strozen, T., Stanley, H., Gu, Y., Boyd, J., Bagdasarian, M., Sandkvist, M., & Howard, S.P. (2011). Involvement of the GspAB complex in assembly of the type II secretion system secretin of *Aeromonas* and *Vibrio* species. J. Bacteriol., 193(9):2322-2331.

Storm, A., Chen, J., Ling, X., Zandbergen, H., & Dekker, C. (2003). Fabrication of solid-state nanopores with single-nanometre precision. Nature Matter, 2(8), 537-540.

Takale, B., Bao, M., & Yamamoto, Y. (2014). Gold nanoparticle (AuNPs) and gold nanopore (AuNPore) catalysts in organic synthesis. Org. Biomol. Chem, 12, 2005-2027.

Tavassoly, O., & Lee, J. (2012). Methamphetamine binds to α-synuclein and causes a conformational change which can be detected by nanopore analysis. FEBS Lett., 586(19), 3222-3228.

Vandenberg, J., & Waxman, S. (2012). Hodgkin and Huxley and the basis for electrical signalling: A remarkable legacy still going strong. J. Physiol., 590(11), 2569–2570.

Vanderlinde E.M., Zhong, S., Li, G., Martynowski, D., Grochulski, P., et al. (2014) Assembly of the type two secretion system in *Aeromonas hydrophila* involves direct interaction between the periplasmic domains of the assembly factor ExeB and the secretin ExeD. PLoS ONE 9(7): e102038.

Venkatesan, B., & Bashir, R. (2011). Nanopore sensors for nucleic acid analysis. Nature Nanotech., 6, 615–624.

Venkatesan, B., Shah, A., Zuo, J., & Bashir, R. (2010). DNA sensing using nanocrystalline surface-enhanced Al2O3 nanopore sensors. Adv. Fun. Mat., 20(8), 1266–1275.

Vercoutere, W., Winters-Hilt, S., DeGuzman, V., Deamer, D., Ridino, S., Rodgers, J., . . . Akeson, M. (2003). Discrimination among individual Watson–Crick base pairs at the termini of single DNA hairpin molecules. Nucl. Acids Res., 31(4), 1311-1318.

Wang, X., Pineau, C., Gu, S., Guschinskaya, N., Pickersgill, R., & Shevchik, V. (2012). Cysteine scanning mutagenesis and disulfide mapping analysis of arrangement of GspC and GspD protomers within the type 2 secretion system. J. Biol. Chem., 287, 19082-19093.

Wanunu, M., & Meller, A. (2007). Chemically modified solid-state nanopores. Nano. Letters, 7(6), 1580-1585.

Wendell, D., Jing, P., Geng, J., Subramaniam, V., Lee, T., Montemagno, C., & Guo, P. (2009). Translocation of double-stranded DNA through membrane-adapted phi29 motor protein nanopores. Nature Nanotech., 4(11), 765-772.

Xiao, F., Moll, W., Guo, S., & Guo, P. (2005). Binding of pRNA to the N-terminal 14 amino acids of connector protein of bacteriophage phi29. Nucl. Acids Res., 33(8), 2640-2649.

7.0 Appendix

Gene Sequence of ExeD, including restriction sites, with *his* tag at the C-terminal
The portion of the gene sequence which is bolded represents the *his* tag added in the cloning process. NdeI and XhoI restriction sites reside at the N-terminal and near the C-terminal, respectively.

gtaccgcat atgataaataaa gggaagggct ggcgtctggc cacggttgcg gcggcgctga tgatggcggg ctccgcctgg gccaccgagt attctgccag cttcaagaat gccgacatcg aagagttcat caacacggtc ggcaagaacc tgagcaagac catcatcata gagccttcgg tgcgcggcaa gatcaacgtc cgcagttacg acctgctcaa cgaggagcag tactaccagt tcttcctgag cgtgctcgac gtctatggct tcgccgtggt gcccatggat aacggtgtgc tcaaggtggt gcgctccaag gacgccaaga cctcggccat cccggtggtg gatgagacca acccgggcat aggcgacgag atggtgaccc gggtggtgcc tgtgcgcaac gtctcggtgc gcgaactggc gcctctgctg cgccagctca atgacaacgc cggtggcggc aacgtggtcc attacgatcc ctccaacgtg ctgctcatca cgggccgtgc cgctgtggtc aaccgtctgg tggaagtggt tcgccgggtc gacaaggcag gggatcagga agtggacatc atcaagctga aatatgcctc cgccggcgag atggtgcggc tggtgaccaa cctcaacaag gatggcaaca gtcagggcgg caacacctcc ctgctgctgg ctcccaaggt ggtggccgac gagcgtacca actctgtggt ggtcagtggc gaacccaagg cgcgggcccg catcatacag atggtgcgcc agctcgatcg ggatctgcag agccagggca acacccgggt cttctacctg aaatacggca aggccaagga tatggtggag gtgctcaagg gcgtcagctc cagcatagaa gcggacaaga agggcggcgg cacagctacg acagcgggtg gcggcgccag catagggggt ggcaagctgg ccatctccgc cgacgagacc accaatgcct tggtcatcac ggcccagccg gatgtgatgg ccgagctgga gcaggtggtc gccaagctgg atatccgccg cgcccaggta ctggttgagg cgatcatagt cgagatcgcc gacggcgacg gcctcaacct cggggtgcag tgggccaata ccaacggcgg cggcacccag tttaccaatg ccggtccagg tataggttct gtggccattg ccgccaagga ttacaaggat aacggtacca ctacgggtct tgccaagctg gctgagaatt ttaacggcat ggcggccggt ttctatcaag gtaactgggc catgttggtg acggcactgt cgaccaacac caagagcgat attctctcca ccccgagtat cgtcaccatg gataacaagg aagcctcctt caacgtcggt caggaagtgc cggtgcagac gggcacccag aactccacct ccggtgacac cacctttagc accatagagc gcaagactgt gggcaccaag ctggtggtga cgccgcagat caacgaaggg gactcggtgc tgctgaccat agagcaggag gtctccagcg tgggcaaaca agcgacaggt acggacggtc tgggccccac cttcgatacc cgtacagtca agaacgccgt gctggtgaaa agcggtgaga ctgtggtgct gggtggcctg atggatgagc agaccaagga agaggtttcc aaggtgccgc tgctcgggga tatccctgta ctcggctatc tgttccgttc cacttccaat aacacttcca agcgcaacct gatggtcttt atccggccca ccatattgcg ggatgcaaac gtctactcag gcatttccag caacaagtac accctgttcc gtgctcaaca gctagatgct gttgctcaag aaggatatgc cacctcaccg gatcgtcagg

tgctgcctga atatggccag gatgtgacca tgtctcccga ggcgcagaag cagatcgagc tgatgaaaac acaccagcag gcgacggccg acggagtgca accattcgtt cagggtaaca agctcgaggga gtc **caccaccaccaccaccac**

Criteria and report for sequence alignment, as performed by EMBOSS Water

```
#=======================================
#
# Aligned_sequences: 2
# 1: ExeD
# 2: PIV
# Matrix: EBLOSUM62
# Gap_penalty: 10.0
# Extend_penalty: 0.5
#
# Length: 280
# Identity:      87/280 (31.1%)
# Similarity:   142/280 (50.7%)
# Gaps:          27/280 ( 9.6%)
# Score: 351.0
#
#
#=======================================
```